Ocean Ambient Noise Field Modelling and the Optimized Noise Term

By

Lt(N) Nikita Kovaloff, RCN

Submitted in partial fulfillment of the requirements for the degree of
Master of Science

at

Dalhousie University

Halifax, Nova Scotia

December 2022

A bloody war or a sickly season.

For Sasha, Uncle David, Dad

и моей семье в России

Table of Contents

List of Tables

List of Figures

List of Abbreviations and Symbols Used

Symbols and Terms

A – Area of computational domain in m^2

AG – AG is array gain in dB

AIS – Automatic Identification System (vessel tracking system)

AMAR – Autonomous Multichannel Acoustic Recorder

ASW – Anti-submarine warfare

c – Propagation speed of acoustical wave in m/s

Charnock or Char – Dimensionless Charnock parameter

C_P – Phase speed of acoustic wave spectral peak in m/s

CTD instrument – Instrument used to measure the electrical conductivity (a proxy for salinity), temperature, and pressure of seawater (a proxy for depth)

dB – Decibel

DI – Directivity index in dB

DT – Detection threshold in dB

Exponential or Exp – Exponential math function

FFT – Fast Fourier transform

f_r – Bubble resonant frequency

H – RMS wave height from crest to trough in m

h – Vertical distance between upper and lower boundaries of water column in m

Hz – Hertz

I – Acoustical intensity watts / m^2

I – Intensity of the acoustical wave 1 m from the receiver in watts / m^2

I_0 – Intensity of the acoustical wave 1 m from the source in watts / m^2

I_i – Incident intensity at 1 metre from the source transducer in watts / m^2

I_r – Intensity of return at 1 metre from the target in watts / m²

k – Wave number; number of acoustical waves per m length

kHz – Kilohertz

Kts – Knots. A nautical unit of speed where 1 kt = 1.852 km/h or 10 kts = 18.52 km/h

log – Logarithm math function

n – I_0 / I; acoustical intensity 1 m from source / acoustical intensity 1 m from receiver

NL or N – Noise level in dB re 1 µPa

   NLself – Self noise level (equipment noise) in dB re 1 µPa

   NLambient – Ambient noise level in dB re 1 µPa

NSL/A – Noise source level in dB / unit area in m²

P – RMS pressure measured by a pressure-sensitive hydrophone in Pa

P_0 – Hydrostatic pressure

PSD – Power spectral density in dB re 1 µPa²/Hz

R – Rayleigh parameter

r – Radius in m

RL or R – Received level in dB re 1 µPa

   RL_N – Regression modelled received level in dB re 1 µPa

RMS – Root mean square

R^2 – A statistical parameter which provides information about the goodness of fit of a model

SL or S – Signal level in dB re 1 µPa

   SL_N – Noise source level in dB re 1 µPa

SL – Slope station (deep water)

SH – Shelf station (shallow water)

SNR – Signal to noise ratio

SPL – Sound pressure level in dB re 1 µPa

SSP – Sound speed profile; also SVP in m/s

Station or Stn – AMAR hydrophone station

SVP – Sound velocity profile; also SSP in m/s

SWH – Significant wave height parameter in m

TL – Transmission loss in dB re 1 μPa

   TL_N – Integrated noise transmission loss in dB re 1 μPa

U_{10} – Horizontal wind speed magnitude 10 m above sea level

U_{10N} – Neutral wind speed magnitude 10 m above sea level

$\vec{U}$ – Vector component of wind in m/s

u^* – Friction velocity in m/s

$\vec{V}$ – Vector component of wind in m/s

Wave age or Edson wave age – Cp/u*; phase speed of the wave spectral peak (Cp) in m/s divided by the wind friction velocity (u*) in m/s. Conventional wave age units are dimensionless; however, this study used a linear neutral wind speed approximation with units of slowness in s/m per Lin and Sheng (2020)

WW – Wind wave parameter in m

Greek Symbols

α – Weight afforded to Parameter 1 during iterated model regressions

$(1-\alpha)$ – Weight afforded to Parameter 2 during iterated model regressions

γ – Ratio of specific heats of the gas in a bubble

ρ – Fluid density in kg / m^3

ρc – Acoustic impedance in kg / m^{2}s

σ^2 – Statistical variance

θ – Acoustical wave grazing angle in degrees

μPa – Micropascal

Organizations, Websites

C3S – Copernicus Climate Change Service

CER – Canada Energy Regulator

CNLOPB – Canada / Newfoundland and Labrador Offshore Petroleum Board

DFO – Department of Fisheries and Oceans Canada

DOSITS – Discovery of Sound in the Sea (website)

ECMWF – European Centre for Medium Range Weather Forecasts

ERA5 – ECMWF 5th generation weather forecast model

ESRF – Environment Studies Research Fund

GEBCO – General Bathymetric Chart of the Oceans

IOC – Intergovernmental Oceanographic Commission

JASCO – Company providing consulting and research services for assessing and mitigating underwater noise

WOD – World Ocean Database

Experiments

FASINEX – Frontal Air-Sea Interaction Experiment

WOTAN – Wind Observations Through Ambient Noise Experiment

Software

MATLAB – Matrix Laboratory programming software

PAMGuide – Passive Acoustic Monitoring Guide software

Definitions

AIS Cull – Process of culling undesired acoustical noise and effects related to the presence of shipping and traffic from an acoustical recording

Equally Weighted Composite Parameter – Parameter consisting of two (or more) normalized constituents, added together, and treated as a single entity. Mathematically, *a*(Normalized Parameter 1) + b*(Normalized Parameter 2), where a = b = 1*

HMSPL – Hourly minimum sound power level(s); also, 'hourly minimum', also, 'minima' in dB re 1 μPa^2 / Hz. This term reflects the lowest one-minute averaged sound power level within a given hour, recorded at a hydrophone

Ice Cull – Process of culling undesired acoustical noise and effects related to the presence of ice from an acoustical recording

Low Frequency Flat 'S' – Sub 1 kHz PSD shape observed when modelling wind type parameters using hourly minimum sound power levels. The three speed regions occur at approximately 0 to 10 kts, 10 to 33 kts, and 33 to 50 kts

Two-term exponential function, also 2 Term Exp – Regression function yielding highest performing model fit (R^2) during modelling out of five tested in this study

Weighted Composite Parameter – Parameter consisting of two (or more) normalized constituents added together which have undergone regression modelling at incremental iterations in order to determine the influence afforded to each respective constituent at each explicit frequency. The weighted composite parameter when graphed or tabulated reflects the highest R^2 achieved during 121 iterated regressions and is associated with a specific value of weight or influence of the respective constituent parameters at a specific hydrophone station. The weight / influence is described as coefficients: α and (α-1). Values of R^2, α and (α-1) will vary at each explicit frequency and each explicit set of physical conditions (i.e., water column depth, bathymetry, SVP)

Abstract

Knowledge of the nature and impact of wind and sea surface conditions on the subsurface ambient noise field are essential for acoustic research and operations within the subsurface environment. The objective of this thesis is to determine the frequency and wind-wave forcing dependent effective sea surface noise source level per unit area extracted from the hourly minimum sound power levels of six month-long acoustic recordings, while accounting for bathymetric and oceanographic effects. The effect of the propagation environment is accounted for using Bellhop, a high fidelity transmission loss (*TL*) model produced by a computational beam tracing program to predict acoustic pressure fields in ocean environments. The simulated environment is configured using climatological sound velocity profiles (*SVP*) extracted from the World Ocean Database (*WOD*) to capture seasonal effects and bottom sound speed estimates made from Geological Survey of Canada seabed maps. Hourly meteorological data were extracted from the European Centre for Medium-Range Weather Forecasts Reanalysis, 5th generation (*ERA5*) providing relevant wind and wave parameters from which noise levels may be predicted. The model outputs were regressed against noise data as individual terms and in weighted composites using several different functional forms. A weighted composite model consisting of neutral wind and significant wave height leveraging the two-term exponential regression function proved to maximize model R^2. The cross-correlative characteristics of the employed meteorological parameters illustrate the time scales of genesis of wind-wave noise. Received level data originating from 16 hydrophone stations in the North Atlantic and Labrador Sea were combined with the Bellhop *TL* simulations in order to produce estimates of the effective noise source level per unit area (*NSL/A*) for changing surface environmental conditions and inter-compared. Comparisons between data analyzed at stations on the continental shelf and slope with varying depths demonstrate the algorithm's ability to account for bathymetric effects. Hourly minimum sound power level derived model-data comparisons using horizontal wind speed magnitude 10 m above sea level expressed a decrease in *NSL/A* estimates versus Kewley (1990) by 10 to 15 dB from 1 to 3 kHz.

Acknowledgements

1. Introduction

The characteristics of ambient noise vary, and this variation is characterized or described by the *PSD*. Sound energy takes the form of disturbances of the pressure and density of some medium. Therefore, the basic relationships between impressed forces and resulting changes in pressure and density are useful in an understanding of sound transmission (Urick, 1969). Ambient noise may be said to be the noise of the sea itself. It is that part of the total noise background observed with an omnidirectional hydrophone which is not due to the hydrophone and its manner of mounting called "self-noise," or to some identifiable localized source of noise (Urick, 1983). It is the residual background noise of the natural environment devoid of individual identifiable sources. The literature indicates that typical underwater ambient noise sources include tides and waves, seismic disturbances, oceanic turbulence in the form of irregular random water currents, ship traffic, thermal noise, and wind.
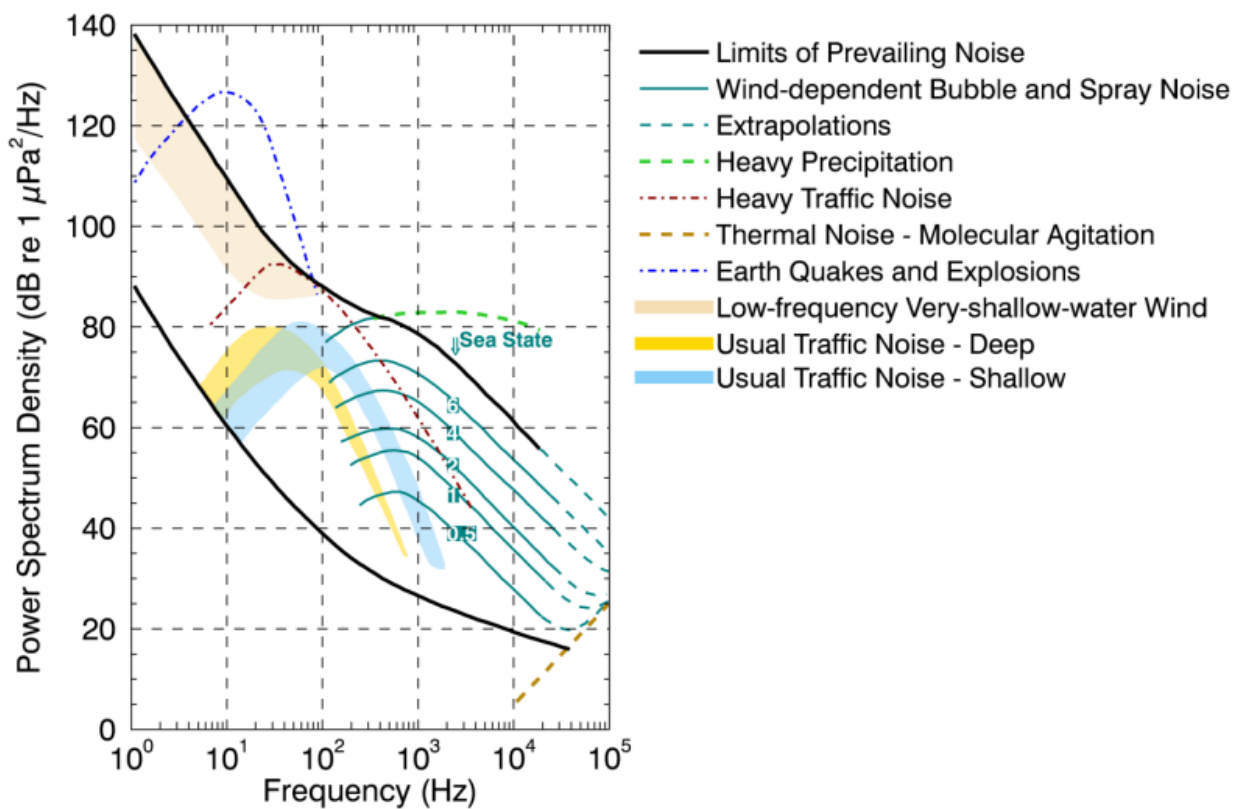
Figure 1: Wenz curves (National Research Council, 2003) describing power spectrum density levels of marine ambient noise from weather, wind, geologic activity, and commercial shipping; adapted from Wenz (1962).

Energy and intensity are related; intensity refers to the average rate of flow of energy per unit area. The ambient-noise level, as a sonar parameter, is the intensity, in decibels, of the ambient background measured with a nondirectional hydrophone and referred to the intensity of a plane wave having a root-mean-square (*RMS*) pressure of 1 μPa. Ambient noise power spectral density (*PSD*) indicates that the characteristics of ambient noise will vary at different frequencies as a function of varying conditions including wind and wave generated surface noise, seismic disturbances, oceanic turbulence, and shipping.

The propagation of sound could be completely determined if the nature of the medium through which the sound passes was known. However, the ocean is dynamic with spatial and temporal variability on many different scales. The constituent and ever-changing elements of transmission loss: reflection, refraction, and attenuation make it impossible to completely know the nature of the medium through which sound travels. From instant to instant, the physical characteristics of the water column and its boundaries shift.

1.1 Ambient Noise Measurement

The Environment Studies Research Fund (*ESRF*) contracted JASCO Applied Sciences to measure the existing Canadian east coast maritime soundscape and the presence of vocalizing marine life. Additionally, the acoustic footprint of seismic surveys in the study area was analyzed. The *ESRF* study harvested and processed data from 20 sites between August 2015 and July 2017.
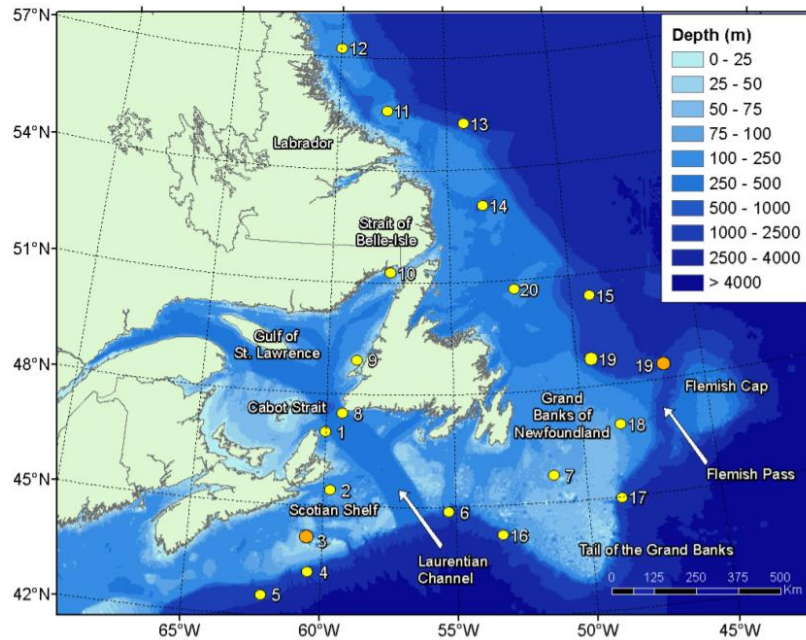
Station	Latitude	Longitude	Depth (m)	Deployment	Retrieval	Duration (days)
1	46.98697	−60.0209	175	8 Jul 2016	10 Jul 2017	367
2	45.43153	−59.7725	120	21 Jul 2016	9 Jul 2017	353
3	44.14955	−60.596	72	22 Jul 2016	8 Jul 2017	351
4	43.216	−60.5017	1558	22 Jul 2016	8 Jul 2017	351
5	42.54767	−62.1769	1831	23 Jul 2016	8 Jul 2017	350
6	44.8521	−55.2707	1790	20 Jul 2016	23 Jul 2017	368
8	47.49302	−59.4124	420	8 Jul 2016	10 Jul 2017	367
9	48.9274	−58.8774	43	9 Jul 2016	10 Jul 2017	366[1]
10	51.27692	−57.5349	110	10 Jul 2016	11 Jul 2017	366
11	55.60505	−57.7488	150	14 Jul 2016	14 Jul 2017	365
12	57.24852	−60.0079	142	13 Jul 2016	14 Jul 2017	366
13	55.22788	−54.1901	1700	12 Jul 2016	15 Jul 2017	368
14	53.02073	−53.4605	551	15 Jul 2016	16 Jul 2017	366
15	50.41112	−49.1959	1993	16 Jul 2016	18 Jul 2017	367
16	44.19273	−53.2748	1608	20 Jul 2016	22 Jul 2017	367
17	44.96777	−48.7336	1273	19 Jul 2016	21 Jul 2017	367
18	46.9118	−48.5012	214	18 Jul 2016	20 Jul 2017	367
19	48.3802	−46.5254	1547	17 Jul 2016	19 Jul 2017	367
20	50.75857	−52.3303	236	16 Jul 2016	18 Jul 2017	367

[1] Corrupt data, no analysis performed

Figure 2: Map and operational characteristics of JASCO acoustic recorders (yellow dots) off the Canadian East coast from August 2015 to July 2017. The two orange dots indicate a change in location between 2015–16 and 2016–17. The recorders at Stn 3 in 2015-16 and Stn 7 in 2016-17 were not recovered (reproduced from Delarue et al, 2018).

3

The study used automated algorithms to detect and classify non-ambient noise sources. This study harvested data from 16 sites from 1 January to 30 June 2016. The time-period was selected to encompass the Winter and Spring seasons. The hydrophone recordings taken from January to June of 2016 contain a wide range of anthropogenic, biological, and meteorological features which inform on acoustical information including shipping, fishing, marine mammal migrations, ice formation, and windstorms (Delarue et al, 2018). Underwater sound was recorded with Autonomous Multichannel Acoustic Recorders (*AMAR*s) by JASCO. In 2016–17, each *AMAR* was fitted with a GTI M36-V35-100 omnidirectional hydrophone (GeoSpectrum, Inc., −165 ± 3 dB re 1 V/μPa sensitivity). The low-frequency recording channel had 24-bit resolution with a nominal ceiling of 164 dB re 1 μPa. The high-frequency recording channel had 16-bit resolution with a nominal ceiling of 171 dB re 1 μPa. The *AMAR* hydrophones were protected by a hydrophone cage, which was covered with a cloth shroud to minimize non-acoustic noise caused by water flow past the hydrophone. The *AMAR*s operated on a continuous duty cycle. They recorded at 8,000 samples per second (for a recording bandwidth of 10 Hz to 4 kHz) during 11 min 18 s and at 250,000 samples per second (for a recording bandwidth of 10 Hz to 125 kHz) during 1 min 4 s, for a total cycle of 20 min. This thesis investigated *TL* at 4 kHz and below and thus used the 8,000 sample per second recordings.

It is predicted that the hourly minimum sound power levels in the 1 to 4 kHz band, derived from six months of recordings, will yield an ambient noise baseline from which statistically significant models can be created to forecast noise source levels. The 100 Hz band was also studied in order to investigate the relationship of wind driven low frequency noise. Hourly minimum sound power levels were used in this thesis as they were found to correlate best with wind driven ambient noise in previous studies (Robinson, 2020). Figure 3 expresses Robinson's (2020) model performance for wind speed and rain rate source terms as a predictor of hourly minimum sound power levels. The y-axis in Figure 3 is entitled R^2. R^2 is a statistical measure which provides information about the goodness of fit of a model by quantifying the correlation between a model fit line and the underlying data.
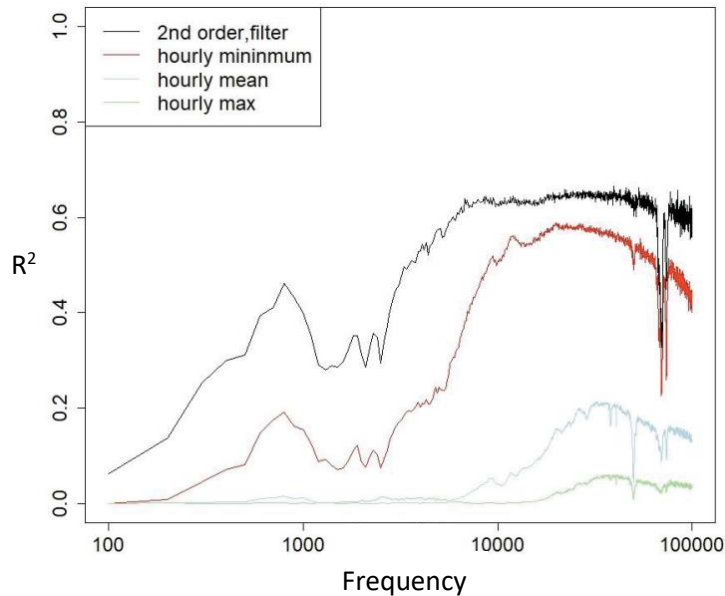
Figure 3: R^2 as a function of frequency for linear relationship between hourly minimum, mean, and maximum noise power level and wind speed (m/s), and model after spectral component filtering (reproduced from Robinson, 2020).

Hourly minimum sound power level derived *NSL/A* have application in the study of ocean noise and marine mammal responses including changes to seasonal migration patterns; marine seismology including seismic surveying for oil and gas deposits (National Research Council (US) Committee on Potential Impacts of Ambient Noise in the Ocean on Marine Mammals, 2003), and the development of naval tactical doctrine including the search for and prosecution of enemy submarine assets.

Of the 16 hydrophone stations studied, hydrophone depths varied between ~ 100m and ~ 2000m. All stations were in open water areas and were located on either the Scotian Shelf, Labrador Shelf, or Grand Banks of Newfoundland (the eastern Canadian continental shelf) and are shown in Figure 2. Eight stations are located on the continental shelf and eight stations are located on the continental slope.

In coastal waters, such as on the continental shelves, wind speed appears to determine the noise level over a wide frequency range (Urick and Kuperman, 1984). The literature indicates that wind speed and collective bubble oscillations are primary contributors to the ambient noise field in the low kHz range. Relevant ambient noise contributors are likely to be of hydrostatic origin (tides and waves) or seismic unrest in the 0 to 1 Hz band. The 1 to 10 Hz band has a wind-speed dependence, but the most probable source of noise is oceanic turbulence (Urick, 1983). At 100 Hz, ambient noise

measurements express high power and high variance. Piggott (1965) showed a dependence of noise level on wind speed at all frequencies between 10 and 3000 Hz. The increase of level with wind speed was found to be 7.2 dB per wind speed doubled, or an increase of intensity slightly greater than the square of the wind speed (Piggott, 1965). Notably, Piggott (1965) conducted this study on the Scotian Shelf. Additionally, Furduev (1966) proposed that the cavitation of air bubbles formed by turbulent wave action at the air-sea interface generates broadband signals in the ambient ocean noise spectrum from 200 Hz to 1 kHz (Furduev, 1966).

From 1 to 4 kHz a consistent, nearly linear on a logarithmic scale, and decreasing variance with increasing wind speed spectral signature manifests. A greater spread of spectral power at lower wind speeds indicates the influence of other noise sources. These spectra are lower power than at 100 Hz indicating that the high power, low frequency radiated-noise spectra of ships mask the low power, low frequency wind generated spectra. In the 500 to 50000 Hz band, the Knudsen spectra indicate that ambient noise generation occurs at the sea surface and that the noise generating mechanism in this band must be different from that in the 20 to 500 Hz band because the two frequency bands have different spectral slopes (Knudsen et al, 1948). This is consistent with the observation that lower frequency ambient noise recordings are those of ships and higher frequency ambient recordings are correlated to local wind speed over the measurement hydrophone (Urick, 1967). Processes occurring at the sea surface which may generate noise in the 500 Hz to 25 kHz band include noise produced from breaking waves, spray, and flow noise of wind passing over the rough sea surface.

1.2 Objective 1: Power Spectral Density Relationships

This thesis will produce precise underwater ambient noise prediction figures based on thirteen different meteorological and physical characteristics at 16 hydrophone stations. The first objective is to explore the *PSD* relationships of these environmental characteristics at all stations and determine the optimal ambient noise predictor. Hourly minimum sound power levels are used to this end as low power ambient noise generated by persistent natural effects manifest as the underlying acoustical susurrus. All acoustical recordings are taken from the Canadian east coast. The resulting empirical relationships cannot be applied globally due to variations in weather patterns, water column temperature characteristics, seismic activity, and shipping concentrations, and the propagation environment. For example, Kewley (1990) found that in the Northern Hemisphere, in the 300 - 400 Hz band, noise levels are about 3 dB re 1 µPa higher than those from the Southern Hemisphere and at frequencies less

than 100 Hz, the Northern Hemisphere levels are similar to the Southern Hemisphere levels. However, by leveraging hourly minimum sound power levels, high power transient and persistent noise generators should be, to a great extent, culled from the modelled power spectra from 1 to 4 kHz. Wind noise above 1 kHz originates locally, above a bottomed-mounted hydrophone and characteristically travels using direct path from high angles. In this thesis, it was not possible to accurately model power spectra at 100 Hz as at this frequency, noise arrives at a bottomed hydrophone principally from low angles and power spectra express distant shipping and seismic sources (Urick, 1967) which travel over refracted and reflected paths. At this frequency, low power wind noise is masked by high power shipping and seismic noise. At Figure 4, a JASCO *AMAR* mooring configuration can be seen. *AMAR*s were suspended 25 m above the seafloor.

Figure 4: Mooring setup prior to deployment (reproduced from Delarue et al, 2018). Closest to camera is the fibreglass mast including tracking and flashing beacon, the yellow ball is a syntactic float, the double barrel black cylinders are the hydrophone and battery packs followed by 20 m of yellow rope, acoustic release assembly, and at the starboard quarter, an anchor assembly consisting of 5 or 6 Olympic weightlifting plates depending on shallow or deep-water mooring configuration.

1.3 Objective 2: Noise Source Level per Unit Area Estimation

The secondary objective of this thesis is to compare measured and modelled noise data using a computational propagation model configured by climatological and historical environmental data to determine the best estimate of the effective noise source level per unit area *(NSL/A)* for ambient noise at each station.

$$SL_N = \frac{RL_N + TL_N}{A}$$
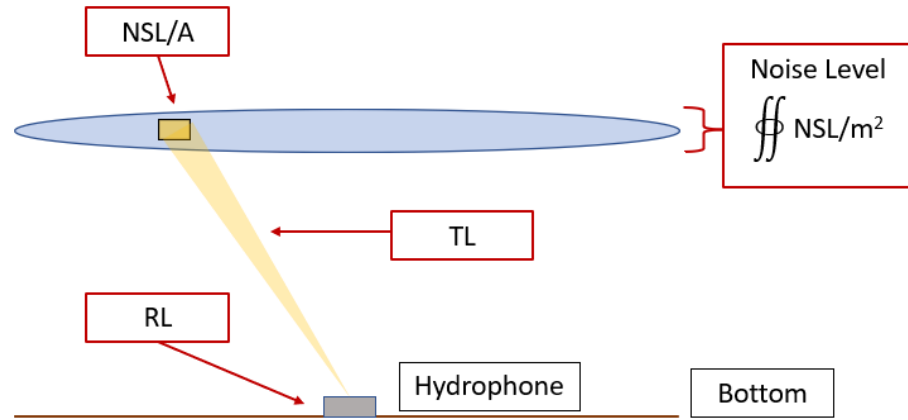
Figure 5: *NSL/A* concept.

In the example at Figure 5, a known *NSL/A* is used to represent the noise generated by breaking waves driving bubbles beneath the surface within a unit area. As the bubbles cavitate, sound propagates omnidirectionally. A bottom-mounted hydrophone makes a recording of the wind noise as *RL = SL - TL*, for the particular patch of ocean. The sum of contributions from all such patches over the relevant domain, the blue circle, gives the total received noise level, represented by the double surface integral. Alternatively, if the *TL* to each patch is modelled, and the received noise level measured, the value for the *NSL/A* may be determined.

Transmission loss was modelled using the principle of reciprocity such that the model source and receiver positions were reversed. Reciprocity alleviates the need to model a grid of real-world sources at the ocean surface. Considering a single fictitious radiating source at the location of a real-world receiver, the instances where rays cross a fictitious sub-surface plane represent the notional depth and acoustical power of a grid of real-world sources. In this thesis, the modelled depth of noise generation was assumed to be 0.5 m; however, other depths were studied as per Section 2.4.4. Integrating the closed surface integral, the *TL* per area per frequency was obtained as per Figure 5; *RL* was obtained using hourly minimum sound power levels; and the *SL_N* at a given frequency and for specific meteorological conditions, was calculated by

$$SL_N = \frac{RL_N + TL_N}{A} \tag{1}$$

Expounding, RL_N is the regression modelled received level, TL_N is the integrated noise transmission loss and A is the area of the computational domain.

The general goal of this thesis is to improve noise level predictions in order to enhance active and passive sonar performance predictions. Optimized noise prediction models leveraging hourly minimum sound power levels will be developed based on significant wave height (SWH), horizontal wind speed magnitude 10m above sea level, neutral wind speed magnitude 10m above sea level, and others. Ambient noise measurement, PSD generation, extraction of hourly minimum sound power levels, regression analysis, and noise source level development are used to this end. The noise prediction models have significant application in the study of the impact of acoustical noise on marine mammals, and masking of tonal and transient signatures relevant to defence applications.

1.4 Computational Sub-Studies

Several computational sub-studies are conducted in support of the two objectives. The optimal $ERA5$ derived wind and wave parameter combination is determined for predicting the ambient noise PSD, along with the best functional form of the empirical relationship (from a choice of linear, logarithmic, quadratic, exponential, and two-term exponential). The choice of computation domain size is determined systematically. Twenty-one combinations of parametric cross correlations were executed in order to establish the lag times and correlative strength of respective combinatory growth and decay. Nine parameters were cross correlated with 4 kHz hourly minimum sound power levels in order to establish the cause/effect relationship and acoustical growth dynamics of the former with the latter.

1.5 Sound Generation Mechanism and Depth

The effect of sound generation mechanism depth (0.25m, 0.5m, 0.75m, 1m, 1.25m, 1.5m) in the propagation model is investigated as it is possible that the optimal sound generation depth will differ according to the meteorological data as well as frequency of interest. Prosperetti (1988) identifies three primary mechanisms through which sound is likely to be created at the air/sea interface. (1) In low frequency range, a few Hz to 100 – 200 Hz, bubbly liquid resultant from a breaking wave may penetrate several metres under the surface due to turbulence. Bubbles act to amplify turbulence noise by responding with volume pulsations to turbulent pressure fluctuations. (2) From a few hundred Hz to 1 kHz, noise is due to collective oscillations of bubble clouds. That is, the cloud of bubbles acts as a system of coupled oscillators pulsating

according to collective modes. (3) From 1 to 10 kHz, noise is produced by freely oscillating individual bubbles which dissipate their energy after spilling down the face of a wave (Prosperetti, 1988). The source level spectrum in *FASINEX* (Frontal Air-Sea Interaction Experiment) (Pennington and Weller, 1986) shows a strong dependence on source depth. Acoustically active bubbles generated by spilling breakers under wind-free conditions in a laboratory tank are known to be located within a few millimetres of the surface while bubble sound sources in *FASINEX* were determined to be at 1.5 m depth by inversion (Buckingham, 1991). Failure to appreciate the extent to which bubbles may be driven below the surface as well as the depth over which those bubbles are behaving may impact *TL* modelling and therefore *NSL/A* estimates in a not insignificant way.

2. Background and Theory

2.1 Previous Work

      The most recent studies into ambient noise source levels were conducted by DJ Kewley (Kewley, 1990), S Vagle (Vagle et al, 1990), and C Robinson (Robinson, 2020). Kewley consolidated the data from Wilson (Wilson, 1983) in deep water; Kuperman and Ferla (Kuperman and Ferla, 1985) in deep and shallow water, and Schmidt and Kuperman (Schmidt and Kuperman, 1988) in shallow water. Kewley used a two mechanism least squares fit relationship when modelling noise spectrum level vs wind speed and vertical beam data was processed to obtain *TL* estimates. The *NSL/A* results shown in Figure 6, did not give any values for the actual effective depth of the wind generated noise source.
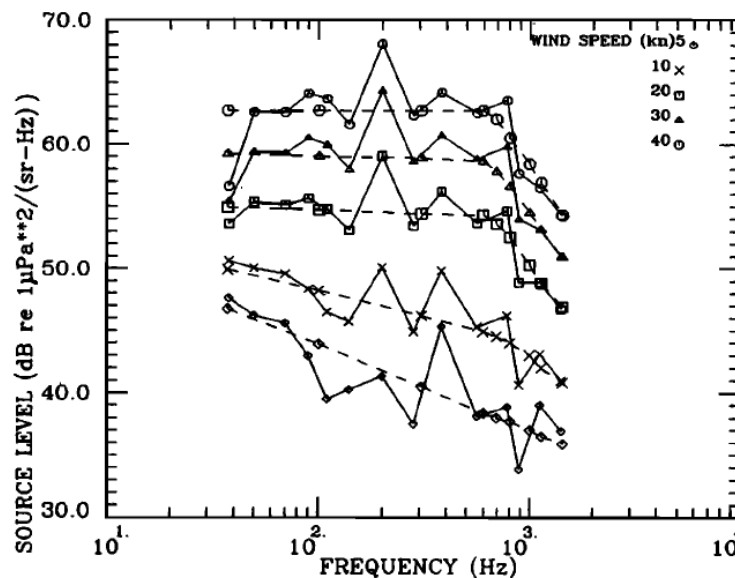
Figure 6: Summary of all source level data available to Kewley using two-mechanism fit, combined Northern and Southern Hemisphere (reproduced from Kewley, 1990).

      One aspect of Kewley's study that warrants further discussion is the way in which he compares the three sets of data. The source authors used different modelling software and parameters in their studies as well as differing source level conventions. Some data sets used monopole sound sources while others used dipole sound sources. Some authors employed noise models using ray tracing or simplified propagation models while other authors used more complex models requiring a directionality function and source depth. Kewley made all attempts to reparametrize and equalize the data however this was not wholly achievable as parametric assumptions had to be

11

made. His comparison showed good results between those in Figure 6 and Kuperman and Ferla's data. The data of Wilson diverge at higher wind speeds from Figure 6. At the lowest frequencies, the data of Schmidt and Kuperman were reasonably consistent with Kewley's results (Kewley, 1990).

Vagle's (Vagle et al, 1990) evaluation of the Wind Observations Through Ambient Noise (*WOTAN*) technique focussed specifically on measuring or predicting oceanic winds using the *PSD* at 11 frequencies in the 3 – 25 kHz range. *WOTAN* oceanographic instruments had been developed to be placed beneath the ocean surface to record the sounds produced by breaking waves. Because the sound produced by breaking waves depends on wind speed, it was proposed that they be used to measure winds over the ocean. The instrument consists of a hydrophone and some electronics that record the ambient noise. Vagle's goal was to establish both the frequency and wind speed dependence of the sound power. His method was more sophisticated than Kewley's in that his procedure included temperature dependent calibrations, accommodations for shipping and precipitation contamination, and standardization to measurements within 1 m depth. While Vagle found success in deep water, his algorithm did not hold in shallow water due to changes in the ambient sound field caused by environmental factors such as transient industrial noise and inconsistent and unpredictable bottom effects.

Vagle also cites inadequate performance of *FASINEX* anemometers and/or acoustic instrumentation as a possible contributor to dubious results. Additionally, the technique only works for wind speeds greater than about 6 kts (3 m/s). Waves do not break at lower wind speeds and therefore there is little or no acoustic signal with which to measure it (DOSITS, 2021). Vagle had a great deal of success in that he was able to predict wind speed sound power levels within +/- 0.5 m/s of anemometer wind values for wind speeds between 4 and 15 m/s. Further, he concluded that the errors due to problems such as a lack of understanding of the underlying physics of sound generation, undetected extraneous sound, data gaps, and low wind speeds did not appear to be serious (Vagle et al, 1990).

Vagle averaged wind estimates in 12-hour blocks which may reduce the fidelity of his results as the data is coarsely resolved. Wind speeds can fluctuate significantly within short time periods and for reasons of accurate data correlation, it is argued that wind speeds should be estimated with greater resolution. Vagle did not use a realistic propagation model which may explain the discrepancy of his results in shallow water environments. Additionally, the *WOTAN* instruments used to record ambient noise were in operation from 27 Jan to 12 May 1986 approximately 580 km North-Northeast of the Greater Antilles and sampled the sound field during 20.125 s intervals, 16 times per hour. Vagle's dataset consistency was a significant improvement on the work of

Kewley; however, data below 3 kHz was not available due to limitations on the Sea Data model 661 hydrophone. Also, in shallow water the effect of the propagation environment needs to be addressed.

This thesis is most closely related to the work of Robinson (Robinson, 2020) who modelled ambient noise levels in time, frequency, and space, in the coastal region of British Columbia, Canada. His model was based on local environmental forcing and propagation conditions. He developed an ambient noise model in the form of a linear combination of wind speed and rain rate source terms, modulated by a tidally driven amplitude term. Robinson's computational sound propagation model was used to compute the source level per unit of area of the natural noise generating mechanisms. His model-data comparisons of monthly sound power levels from April 2018 to February 2019 show less than 5 dB re 1 μPa error above 1 kHz, and less than 3 dB re 1 μPa error above 20 kHz.

The 100 Hz to 4 kHz band was selected to match other literature in the study of wind generated NSL/A. A large set of fit models was tried while minimizing the number of independent parameters. Literature conventionally models ambient NSL/A using a bi-mechanism linear fit. However, as will be seen, the two-term exponential regression model is able to trace the inherent curvature of the wind generated low frequency PSD. The linear fit, although easily interpretable, does not capture the PSD growth dynamics to the same extent as the two-term exponential regression which has the ability to approximate PSD curvature. The author suggests that a bi-mechanism linear fit is inferior to the two-term regression model as is seen in the results of this study.

2.2 Background

This thesis employed JASCO hydrophones and received noise levels processed to find their hourly minimum sound power levels. Highly resolved hourly minimum sound power levels were achieved by averaging acoustical spectra every 60 seconds using 1 second bins with 50% overlap. The $AMAR$ duty cycle was such that in any given hour, the 8 kHz sample rate would record 2034 seconds (33.9 minutes) and the hourly minimum sound power level was selected as the minute whose power averaged over sixty 1 - second time windows was lowest. The 1 second time domain resolution translated to 1 Hz frequency domain resolution. The Nyquist theorem states that in order to digitally reproduce a sinusoidal function in time or distance with no loss of information, the upper frequency limit of the sinusoidal function must be less than or equal to twice the sampling frequency. The employed $AMAR$ sampling rate is 8000 Hz and the corresponding Nyquist frequency is 4000 Hz. $AMAR$ anti-aliasing filter roll-off commences at approximately 3600 Hz and as a result, 4 kHz power levels are reduced.

This thesis takes hourly *ERA5* meteorological data and decimated hourly acoustical data in 5 frequency bands: 100 Hz, 1, 2, 3, 4 kHz, and runs the time-synchronized data through a series of regression models including linear, logarithmic, 2nd order polynomial, one-term exponential, and two-term exponential. The regression model with the highest R^2 per frequency band is assessed as the best model for predicting noise levels. Regression fits are made for each band separately.

Where Robinson used isovelocity sound velocity profiles, this thesis will use climatological sound velocity profiles. Where Robinson used one recording location, this thesis will use 16. Where Robinson focussed in a region of the world with high traffic density and coastal industry, this thesis will use a spread of high and low trafficked regions including some regions almost devoid of coastal industry and local anthropogenic noise pollution. Both Robinson and this work used the coherent ray tracing function within the Bellhop software, in order to model the characteristics of a pressure field. As an added advantage, this thesis will incorporate regionally varying, geophysically informed bottom loss characteristics. It is hoped that this thesis will generate the most accurate and field applicable noise source level per unit area estimates to date at the frequencies of 100 Hz, 1 kHz, 2 kHz, 3 kHz, and 4 kHz.

2.3 The SONAR Equations

The sonar equations are used to quantitatively relate the physical processes that occur when sound is emitted, transits through the water column, and is received. Processes such as transmission loss, scattering, spreading, and attenuation are taken into consideration. A signal of interest will be hidden within the background noise of the ocean. The higher the signal level generated by a source such as an active sonar, the higher the probability of detection at a hydrophone. In order for a sonar detection to occur, the signal (S) minus the noise (N) must be greater than or equal to the detection threshold, expressed as

$$S - N \geq DT, \tag{2}$$

where S is the signal received level in dB re 1 μPa , N is the noise in dB re 1 μPa, and DT is the detection threshold in dB re 1 μPa (Payne, 2010). The detection threshold is defined as the ratio, in decibel units, of the signal power (or mean-squared voltage) in the receiver frequency bandwidth to the noise power (or mean-squared voltage) in a 1 Hz frequency band, measured at the receiver input terminals, required for detection and is qualified by a desired probability of detection for a given probability of false alarm (Urick, 1983). Detection threshold is functionally described via detection index, bandwidth, and time (Dawe, 1997).

2.3.1 Passive SONAR Equation

A source signal can be generated by biological sources such as marine mammals or by anthropogenic contributors like coastal machinery, the propeller noise or acoustic equipment from a ship. Whatever the source, the fundamental signal-to-noise ratio requirement at Eqn (2) must be satisfied.

The passive sonar equation is constructed in terms of signal and noise and is described by Eqn (3)

$$SL - TL - NL + AG \geq DT, \tag{3}$$

where SL is signal level in dB re 1 µPa, TL is transmission loss in dB re 1 µPa, NL is noise level in dB re 1 µPa, AG is array gain in dB re 1 µPa, DT is detection threshold in dB re 1 µPa.

The passive sonar equation will now be derived. At the receiver, the passive equation begins as Eqn (2). If the sound source radiates an acoustic signal of SL, the sound intensity decreases while transiting to the receiver because of the environmental factors described in the *Losses* section.

The decrease in intensity level due to *loss* is described as transmission loss (TL). Therefore, the intensity level of the signal arriving at the hydrophone is

$$S = SL - TL. \tag{4}$$

S is commonly referred to as the received level.

The signal of interest may be masked by the noise (N) variable. In the case of a passive sonar array, the array is manufactured with multiple receiver units and the units are focussed to discriminate against noise coming from any direction other than the direction of the target of interest. The discrimination characteristic of the array is the directivity index (DI). The DI represents the reduction in noise level obtained by the directional properties of the transducer array. The directivity index is a special case of array gain (AG) for the condition when the signal is a plane wave and the noise field is isotropic. DI is usually employed to measure an array's utility but does not represent real world conditions, unlike AG (Herstein, 1984). Therefore, in the passive sonar equation, noise is reduced in magnitude and becomes

$$N = NL - AG. \tag{5}$$

15

In this project, arrays were not employed. Therefore, the *AG* term is 0 and the total noise term is equivalent to the noise level. The parameter *NL* represents the sum of self-noise level *(NL$_{self}$)* of the hydrophone or passive sonar array as well as the ambient noise level *(NL$_{ambient}$)*. In Eqn (5), *AG* is a positive quantity such that *NL – AG* is always less than or equal to *NL*.

The passive sonar equation is constructed in terms of signal and noise. When *S* and *N* are substituted from Eqns (4) and (5) into Eqn (2), the result is

$$SL - TL - NL + AG \geq DT. \qquad\qquad (6)$$

The passive sonar equation states that the source level of the target minus the loss due to propagation through the medium, minus the sum of all interfering noises, plus improvement by the spatial processing gain of the receiver, must be equal to or greater than the detection threshold in order for a detection to occur.

2.3.2 Active SONAR Equation

In an active sonar, a transducer radiates a pressure wave into the water column. The radiation strikes the target and the return signal, the echo, is received at the transducer a short time later. There are two different sonar equations which are needed to describe active sonar function. One equation is for the reverberation limited case and the other is for the noise limited case. As previous, sonar performance is governed by the requirement that signal minus noise must be equal to or greater than the detection threshold in order for a detection to occur.

The reverberation limited sonar equation applies when noise returns primarily from the direction in which the pressure wave was transmitted. The noise limited sonar equation applies when the ambient noise is isotropic (Payne, 2010).

2.3.3 Noise Limited Active SONAR Equation

The development of the active sonar equations is similar to that for the passive equation. The formal sonar parameters will be fitted to the signal and noise terms of Eqn (2). When a sonar transmits a pulse (*SL*), the pulse will travel to the target, reflect off of it, and return to the transducer. En route, the pulse will experience losses (*TL*) and the received signal will be of a lower magnitude than the one sent. The losses will be relatively equal during transit to the target and back to the receiver on account of the short transit time. The backscattered intensity is called target strength (*TS*) (Payne, 2010). Contingent on the transmitter and receiver being located together, the variables relate thus

$$S \ = \ SL - 2TL \ + \ TS. \tag{7}$$

Upon return of the echo, if the condition exists that the reverberation background has fallen below the ambient noise, the variables in the noise limited case will relate thus

$$SL - 2TL \ + \ TS - NL \ + \ DI \ \geq \ DT. \tag{8}$$

2.3.4 Reverberation Limited Active SONAR Equation

If the reverberation background has not decayed to a level below the ambient noise level, the background noise is given by RL. Where DI is a function of an isotropic background, reverberation is not isotropic and DI is not applicable in the reverberation limited case. That is to say, $NL - DI$ is replaced by RL (Payne, 2010). The variables in the reverberation limited case relate thus

$$SL - 2TL \ + \ TS - RL \ \geq \ DT. \tag{9}$$

RL is a function of inhomogeneities in the water column and varies with time. If an array were to have a DI, the reverberation level would be referenced to the beam.

The signal-to-noise parameters used in the passive and active sonar equations are functions of the environmental conditions, the target, and the sonar equipment.

Environmental parameters include transmission loss (TL); ambient noise level (NL$_{ambient}$); and in the active sonar case, reverberation level (RL).

Target parameters include target strength (TS) and target passive source level (SL).

The sonar equipment parameters include detection threshold (DT), receiving directivity index (DI), array gain (AG), self-noise level (NL_{self}), and own active sonar source level (SL).

Passive source levels are generated by the natural physical action of the sonar target. The wind passing across the ocean surface, precipitation, waves breaking, bubble clouds oscillating and/or cavitating, the passage of ships are all examples of noise sources which can mask a specific sonar target such as a whale or a submarine. However, as in the case of this thesis, wind or wave or other ambient noise generator is the sonar target in and of itself.

Active source levels are a function of a transducer generating a pulse of sound which propagates into the water column. The pulse strikes a target and the echo is returned to the transducer. The intensity of an active source will diminish due to spreading, absorption, and scattering. The sound pressure level (*SPL*) will therefore decrease with range from the source. Intensity (*I*) and pressure (*P*) are intrinsically related in this context such that

$$I \ \alpha \ P^2, \tag{10}$$

and the equation for acoustic intensity of a plane wave is

$$I = \frac{P^2}{\rho c} = \frac{Power}{Area}, \tag{11}$$

where *P* is defined as the *RMS* pressure measured by a pressure-sensitive hydrophone, ρ is fluid density, and c is the phase speed of the acoustical wave. Combined, ρc is acoustic impedance. The units of acoustic intensity are watts/m² (Power / Area). As a wave train propagates, a certain amount of energy per second (power), crosses a unit area (power density). Power density is equivalent to the intensity of the acoustical wave. Hydrophones and transducers leverage the property that if an *RMS* pressure can be measured, then sound intensity can be determined.

In making comparisons from system to system and situation to situation, sound source levels are defined in dB, with a reference pressure of 1 µPa at a range of 1 m from the sound source.

2.3.5 Losses

Spreading Loss

Consider an unbounded/infinite, homogeneous medium. Were a noise generating effect from a point source such as an explosion to occur within this medium, sound energy would radially propagate along straight paths in all directions and have a spherical wave front. Now consider a bounded environment, such as the ocean, with upper and lower limits – a surface and a bottom. Due to impedance, sound is contained within the limits and a previously spherically expanding wave front is shaped to diverge cylindrically. The examples serve to illustrate unbounded (spherical) and bounded (cylindrical) sound propagation and their qualities are described below.

Acoustic intensity spread over the surface of a sphere can be written as

$$I = P_t / 4\pi r^2, \tag{12}$$

where P_t is the acoustic power level immediately adjacent to the source and r is the radius from the point source in meters. If the intensity of the sound at 1m from the source is

$$I_1 = P_1 / 4\pi(1)^2, \tag{13}$$

and the acoustic intensity (I_r) at some distance r from the source is less than the acoustic intensity (I_1), then the reduction of the acoustic intensity as a function of a distance r is

$$1/r^2. \tag{14}$$

This indicates that energy twice as far from the source is spread over 4 times the area and is thus ¼th the intensity. This is known as spherical spreading and occurs when $r \leq$ *water depth* (Jensen et al, 2011). Because the ratio of I_r to I is small, the literature expresses these values on a logarithmic scale using the decibel where

$$10 \log (1/r^2) = -20 \log r. \tag{15}$$

For spherical spreading, which occurs when an omnidirectional acoustic wave propagates from a source without upper or lower boundaries, the transmission loss is

$$TL = 20 \log r, \tag{16}$$

where transmission loss is a definitionally positive for ranges beyond a 1 m reference range.

Once a spherical, omnidirectional wave becomes bounded or for sources that radiate energy in a horizontal direction, sound energy propagates in the form of an expanding cylinder. Cylindrical divergence is assumed when $r \gg$ *water depth* or when sound energy is trapped within a thermal layer or sound channel (Payne, 2010). The acoustic intensity of energy at the surface of a cylinder of radius r is

$$I_r = P_t / 2\pi r h, \tag{17}$$

where h is the vertical distance between upper and lower boundaries. In this instance, transmission loss is related to

$$10 \log (1/r) = -10 \log r, \tag{18}$$

and transmission loss is defined as a positive value

$$TL = 10 \log r. \tag{19}$$

Absorption Loss

Sound energy attenuation in sea water arises principally through absorption and scattering with additional losses from bottom loss.

Propagating sound waves generate compressions and rarefactions in the water column. These pressure fluctuations are the cause of all absorptive losses and involve a process of converting acoustic energy into heat. This conversion occurs through particle oscillation, particularly in the case of air bubbles, and internal friction due to water viscosity. A second absorption mechanism which is significant in seawater above 1 kHz relies on an ionic relation where certain chemicals dissociate under the pressure of a sound wave. The dissociation and reassociation of magnesium sulfate and boric acid are important factors affecting the absorption coefficient value (Urick, 1983).

The literature indicates that absorption increases roughly as the square of the frequency. The implication is that if higher frequencies are chosen for sonar operation in order to achieve greater target definition, there will be a correspondingly high attenuation which will decrease detection ranges (Payne, 2010).

Scattering loss

Attenuation of an acoustic signal also occurs when the signal strikes foreign bodies in the water and is reflected; this is called scattering. Ocean reflectors include surface and bottom boundaries, shorelines, bubbles, marine life, suspended particles, and shipping. The quantity of energy scattered is directly related to the frequency of the sound wave and how the wave interacts with the size, density, and concentration of the foreign bodies in its way. An object will be a more effective scatterer of sound if the area of the reflector is large compared to the wavelength of sound. Any acoustic energy returned to the transducer will appear as noise and is known as diffuse reverberation. The acoustic energy that scatters in directions other than the source is effectively lost.

An exception to the prior relation exists with the bubbles. When air is suspended as tiny bubbles, its scattering effect is profound. A minute amount of air substantially reduces the velocity of sound in a bubbly fluid. Bubbles of a resonant or near-resonant size will make a large contribution to scattering. A bubble of a given size will enter

resonance at a certain resonance frequency. At a given depth of water, the expression for resonance frequency is as Eqn (20)

$$f_r = \frac{1}{2\pi a} \sqrt{\frac{3\gamma P_0}{\rho}},$$ (20)

where f_r is the resonant frequency in Hz and a is the radius of the bubble in cm, γ is the ratio of specific heat of the gas in the bubble(s) and the density of the fluid around it, P_0 is the hydrostatic pressure and ρ is the density of water (Urick, 1983).

The attenuation coefficient of a bubble is related to the frequency of the sound wave(s) and the size of the bubble(s) being impacted by the wave. As a pressure wave propagates through a bubble cloud, bubble radii will change as a function of wave compression/rarefaction and restoring forces. This results in radial oscillation. At the same frequency, the larger the bubble size, the larger the attenuation coefficient will be (Han et al, 2019). Bubble extinction cross section consists of both an absorptive and scattering component such that

$$\sigma_e = \sigma_a + \sigma_s,$$ (21)

where σ_e is the extinction cross section of the bubble, σ_a is the absorption cross section of the bubble, and σ_s is the scattering cross section of the bubble (Urick, 1983). According to experimentation conducted by Han et al (2019), a cloud of 'small' bubbles of radius 300 μm and number density 3 x 10⁶ can attenuate sound power level by 3.9 dB/m at 20 kHz and 4.3 dB/m at 30 kHz. A 20 kHz pulse with a wavelength of approximately 0.075 m is substantially larger than a 300 μm radius bubble and yet attenuates sound to great effect.

Bottom Loss

Bottom losses occur when an acoustic wave strikes the ocean floor. The incident wave will penetrate and reradiate in different ways. In one instance, upon penetration of the floor, an acoustic wave will refract as a function of the bottom material density and will penetrate up to a point of total decay. In another instance, an acoustic wave will reflect off the surface of the floor. The remainder of the incident acoustic wave will scatter into various directions. The bottom composition, strike angle, and sound frequency will determine the amount of energy lost to the bottom (Payne, 2010). In general, bottom loss will tend to increase with frequency and with the angle of incidence. Soft bottoms such as mud or clay are acoustically absorptive and are

associated with high bottom losses while hard bottoms such as rock and sand are more acoustically reflective and will produce lower losses.

Surface Reflection Loss

Were the surface of the sea to be perfectly smooth, incident sound upon it would reflect perfectly and therefore without loss however this is not a physical reality. The magnitude of losses of this type are a function of frequency, grazing angle, and wave height. The Rayleigh Parameter is used to determine if the sea surface is rough or smooth, and therefore a scatterer or reflector of sound. The Rayleigh Parameter (R) is defined as follows

$$R = kH \sin \theta, \tag{22}$$

where k is the wave number $2\pi/\lambda$, λ the wavelength in metres, H is the *RMS* wave height from crest to trough in m, and θ is the grazing angle in degrees. When $R \ll 1$, the surface is primarily a reflector and produces a coherent reflection at the specular angle equal to the angle of incidence. When $R \gg 1$, the surface acts as a scatterer and sends incoherent energy in all directions. Relevant physical phenomena of surface reflections include the moving surface of the ocean producing a frequency-smearing effect on a constant-frequency signal, and sea surface-reflected acoustic pressure waves experience a phase reversal (Urick, 1983).

At 25 kHz, Urick and Saxton (1947) measured an average sea-surface reflection loss of about 3 dB under conditions of 0.3 m waves with grazing angles between 3 and 18 degrees. At lower frequencies, smaller losses can be expected because the sea becomes smoother relative to wavelength. Addlington (1963) found that between 400 Hz and 6400 Hz, at wind speeds from 5 to 20 kts and grazing angles 10 to 55 degrees, the median reflection loss was 0 dB.

Transmission Loss

Transmission loss (*TL*) is a generalized term which encompasses all of the forms of loss previously described. It is primarily a function of range between source and receiver (spreading); however, it also expresses the degree to which sound is attenuated by absorption, surface reflection loss, bottom loss, and scattering. Consequentially, it depends on the characteristics of the physical environment. Acoustical waves in the water column will decrease in acoustical power with distance from the source, reflect off boundaries and barriers; refract according to changes in temperature, salinity, and pressure in the water column, and diffract as the acoustical wave passes through

openings or around seamounts. The transmission loss term in the sonar equation expresses the magnitude of these effects and is measured in dB re 1 μPa. The definition of transmission loss is a ratio comparison of the intensity of the acoustical wave 1 m from the source (I_0) divided by the intensity of the acoustical wave at the location of the receiver (I). The equation is

$$TL = 10 \log n, \tag{23}$$

where n is the ratio (I_0 / I). If n is greater than 1, the acoustical intensity at the source is greater than at the receiver. There are instances where an intensity gain can occur due to focussing at caustics and n is less than 1. An example of this is a convergence zone (Urick, 1983).

Transmission loss can be computed in complex environments using a variety of models such as Normal Mode, Parabolic Equation, and Ray/Beam Trace propagation models. This work employs ray/beam tracing in order to determine TL values using Bellhop beam tracing software. The Bellhop algorithm solves the Wave Equation by employing high frequency approximations, reducing to an equation called the Eikonal Equation. Wave fronts are mapped as a function of index of refraction (sound speed) time, and phase. Velocity profiles are automatically divided into layers of constant linear gradient and the arcs of the rays leaving the source at different angles are followed using Snell's law. The sound field intensity is computed by beam tracing, then summing the pressure contribution of each beam with regard to phase via the Transport Equation. Beam density estimates are made at each defined step out to a maximum defined range. Resultant transmission loss is the ratio of received to source level at each step (Jensen et al, 2011).

2.3.6 Target Strength

The active sonar equation incorporates the target strength (TS) variable. Target strength is the magnitude of the return echo from a sonar target. Each sonar target has a specific shape, size, and density. The logarithmic value of the ratio of the intensity of sound returned by the target at a distance of 1 metre in some direction to the incident intensity from a distant source is called TS.

$$TS = 10 \log I_r / I_i, \tag{24}$$

where I_r is intensity of return at 1 metre from the target and I_i is the transmitted intensity at 1 metre from the source transducer. The variability of TS is a function of the target aspect presented of the incoming signal. In the case of a submarine or a whale, a

beam/side aspect target presents a greater reflective area than one with a bow aspect/head on aspect; hence more energy is reflected from a beam aspect target (Payne, 2010).

2.3.7 Noise Level

Where the desired portion of detected sound is called the signal, the undesired portion is called the background noise. The absolute measure of the background noise is called the noise level. Background noise can be divided into three different types: (1) non-target radiated noise, (2) self-noise, and (3) ambient noise. Non-target radiated noise includes machinery noise, propeller noise, and hydrodynamic noise generated from flow driven resonant excitation of hull-borne cavities, plates, and appendages; or the clicking and calling of non-target biota. Self-noise refers to hydrophone structure-borne noise generators such as clanking chains, the hum of electrical currents, and the rumble of mechanical parts. Ambient noise refers to the noise of the sea itself, that is, the remaining background noise after all other noise sources have been accounted for (Urick, 1983). Diffuse reverberation is described in the paragraph to follow. In this project, noise level was measured by hydrophones and was processed to determine the combined level of ambient ($NL_{ambient}$) and equipment (NL_{self}) noise. These levels were determined for each frequency from 1 Hz to 4000 Hz. A key feature of this project is its focus on quantifying the $NL_{ambient}$ values for various wind and wave characteristics.

2.3.8 Reverberation Level

Diffuse reverberation describes acoustic reflections by any object other than the desired sonar target and the acoustic reflections must return from the direction in which the sound signal was projected by an active sonar. Examples include schools of fish, air bubbles, particulate matter, physical objects on the sea floor, and returns from the ocean surface. The maximum source level is limited by reverberation because the diffuse reverberation level (RL) increases with an increase in the active source level. Sonar clutter, meaning non-target echoes from processed data that generate false alarms is not diffuse reverberation and is not part of this definition (Payne, 2010).

2.4 Software Parameterization

The author's noise transmission loss software integrates noise arriving over all vertical and horizontal angles and allows for bathymetric range dependence, using the ray tracing software Bellhop model as the model's core. The software models transmission loss using climatological sound speed profiles, realistic bottom

compositions, and high-resolution bathymetric data. The step-by-step procedure is as follows

Table 1: Table summarizing algorithm used to generate transmission loss values.

Step	Description
1	Assign bathymetry, bottom sediment type, *SVP*, based on station location
2	Define frequencies at which to run simulation
3	Define Bellhop configuration parameters to include beam number, coherent processing characteristics, and range resolution. Vertical take-off angles were defined as -90° to +90°.
4	Compute the complex pressure field between the receiver and each source at the desired depth for each horizontal angle spacing based on desired angular resolution.
5	Integrate the pressure field over range and radial angle out to maximum range and compute a single value of *TL* per frequency by normalizing the pressure field to its maximum value, then convert to decibels to give units of dB re 1 Pa / Hz*m^2
6	Interpolate pressure field in 6° azimuthal steps to facilitate colour plotting of entire area's acoustic transmission behaviour
7	Plot results and save data

2.4.1 Transmission Loss Integration Range

To experimentally determine a practical maximum range for the model area, integrated sound energy ratios were taken of integrated acoustical pressure at 10 km vs 20 km ranges and then again at 20 km vs 25 km ranges using Station 2 bathymetry and associated *SVP*. It can be seen Figure 7 that most (82%) high frequency (5 kHz) energy is expressed within 10 km from the sound source however at low frequency (1 kHz), only 56% of the energy is expressed when comparing a 10 km integration range vs a 20 km integration range.
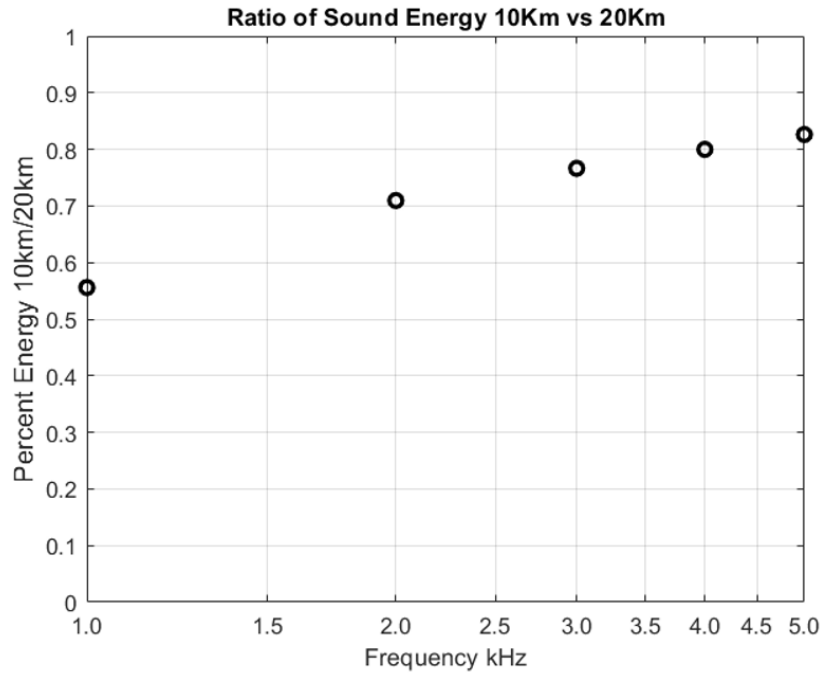
Figure 7: Ratio of sound energy 10 km versus 20 km.

In Figure 8, it can be seen that at 5 kHz, 97% of the energy at 20 km is present at 25 km and that at 1 kHz, 89% of the energy is present at 20 km vs 25 km.
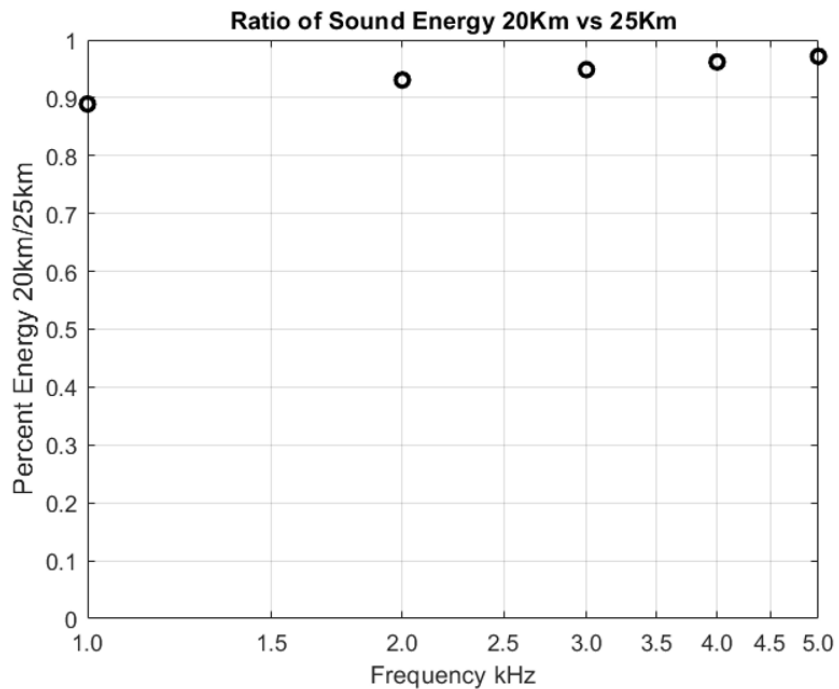
Figure 8: Ratio of sound energy 20 km versus 25 km.

It was concluded that a 20 km maximum range was the preferred range to study considering that almost all generated acoustical data would be present and accounted for in the software integrations. While examining out to longer ranges would yield more accurate results, for practical reasons, 20 km facilitated a reasonable balance of accuracy (89% of energy captured within the studied band) versus computational time. Bellhop was setup to execute computations with 6 degrees of angular resolution in azimuth, 180 degrees of vertical resolution, 10 m of range resolution, 20 km maximum range, and 2000 beams (1 beam per 0.09 degrees in altitude) for each of the frequencies of 100 Hz, 1, 2, 3, 4 kHz. The minimal added value of integrating at 25 km would add an extra day to the computations and was deemed neither practical nor necessary.

2.4.2 Reciprocity

To simplify the computation, the principle of reciprocity was invoked and programmatically, the source was placed at the receiver location to avoid the requirement for a distributed grid of sources on the surface. The surface noise model assumes that sources are placed uniformly. Reciprocity exploits the fact that the reflections off the ocean surface and floor are symmetric in angle and therefore all paths between the source and receiver are reversible. Because of this, the eigenrays from the source position to the receiver position are the same even when their positions are exchanged. Regardless of direction, the same amplitude loss and phase change is experienced by the signal along the path. In Figure 9, the JASCO Station 4 hydrophone is located at the location of the star, 25 m above the sea floor while the source's assigned location is at the circle, 0.5 m below the surface. In Bellhop, the location of the star is used for the source, while the field is computed at the circle, and all possible source positions simultaneously. The first set of integrations was executed at 0.5 m below the surface which is a reasonable expected penetration depth of the bubble cloud (Deane and Stokes, 2002).
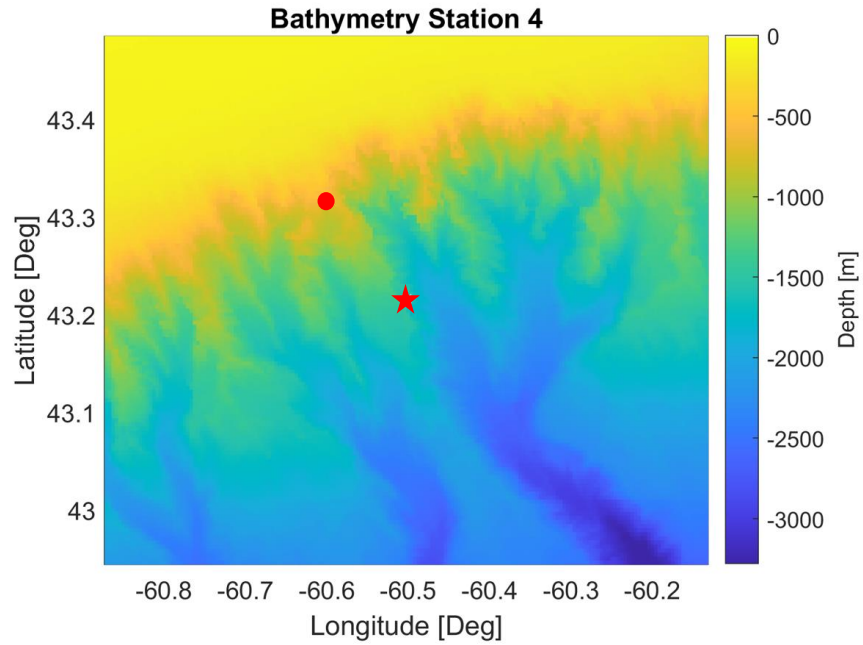
Figure 9: Bathymetry at JASCO Station 4, southeast Nova Scotia continental shelf. The star is the location of the hydrophone, and the circle is the position of an arbitrarily assigned receiver.

An example transmission loss radial is below in which beams originating 25 m above the sea floor shoot 330 degrees true to the North-Northwest.
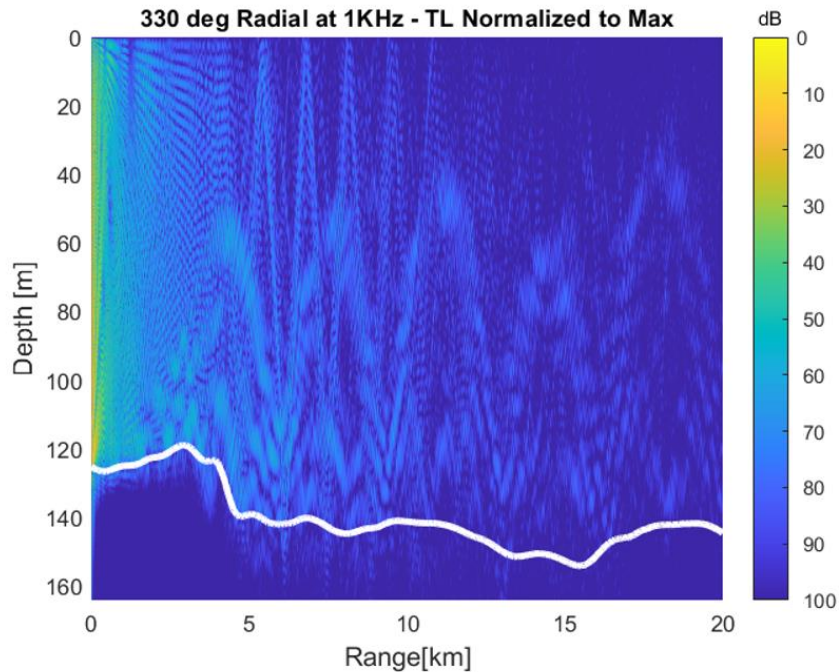
Figure 10: Bellhop transmission loss along a radial with bathymetry shown by the solid white line at JASCO Station 2.

2.4.3 Surface Receive Sensitivity

Surface receive sensitivity is defined as the level received at the surface, normalized to the power level from the bottomed source. An example surface receive sensitivity output at 0.5 m depth, for the receiver placed at the origin is at Figure 11. Regions of low transmission power loss are depicted by yellow colouration (0 to 20 dB of loss) and occur primarily at the centre of each figure because this is the origin of the relatively unabated source power. The green/turquoise regions indicate a loss of 35 to 45 dB compared to the source. Yellow ripples of low transmission loss, distant from the centre of each figure (the source) indicate constructive interference. At Figure 11 A), there is a 2 km wide annulus at approximately 10 km from the source representative of concentrated coherent (in phase) rays. This is an example of a ray acoustic caustic.
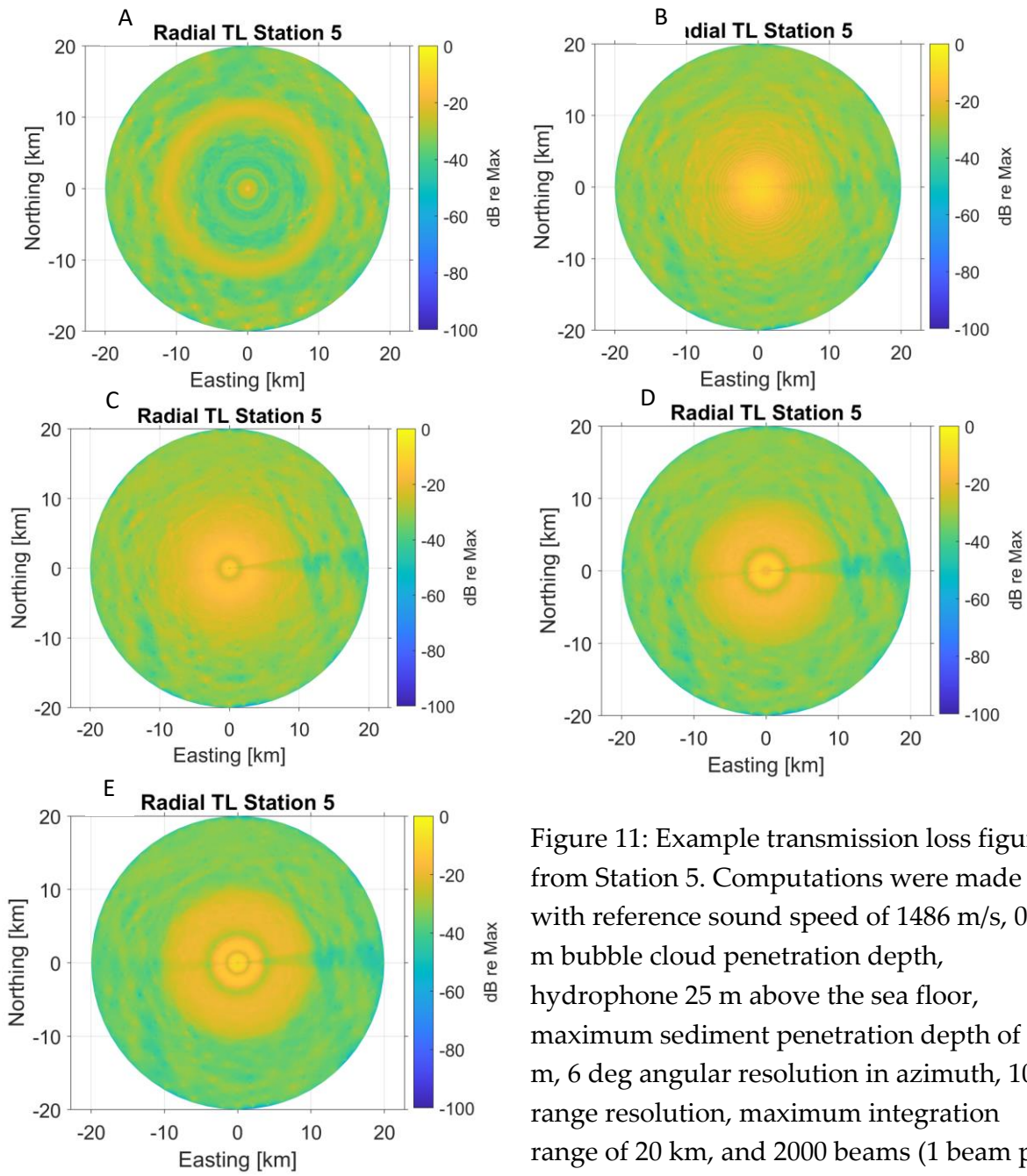
Figure 11: Example transmission loss figures from Station 5. Computations were made with reference sound speed of 1486 m/s, 0.5 m bubble cloud penetration depth, hydrophone 25 m above the sea floor, maximum sediment penetration depth of 30 m, 6 deg angular resolution in azimuth, 10 m range resolution, maximum integration range of 20 km, and 2000 beams (1 beam per 0.09 degree in altitude). Additionally, computations were made using climatological *SVP* and representative sediment sound speed values. Fig A) represents 100 Hz frequency bin, B) 1 kHz, C) 2 kHz, D) 3 kHz, E) 4 kHz.

2.4.4 Bubble Cloud Penetration Depth

A point of interest is in determining which bubble cloud penetration depth is most accurate in terms of predicting *TL* and therefore the more realistic source level term. Concurrently, a point of interest is in understanding the nature of how Bellhop computes *TL* as a function of source depth. Figures 12 through 17 present the modelled *RL*, area integrated *TL*, and resultant *NSL/A* estimates from 100 Hz to 4 kHz at source level depths 25 cm, 50 cm, 75 cm, 100 cm, 125 cm, and 150 cm at two different locations. Station 15 is located East-North-East of Newfoundland in 1993 m of water on the continental slope. Station 1 is located North-East of the Cape Breton Highlands on the edge of the Laurentian Channel in 175 m of water. Station 15 was covered by sea ice 1.4% of the period of study and Station 1 was covered by sea ice for a 0.11% of the period of study. At both stations, sea ice was assessed to be insignificant in terms of *NSL/A* estimation. Both stations expressed high R^2 from 1 to 4 kHz.

Station 15 bubble cloud penetration depth analysis is as follows. Per Figure 12, the analysis begins by generating models of the wind speed vs *PSD* relationship at the Station 15 hydrophone. The two-term exponential model (pink regression line) which yields the highest R^2 and *RL* based on 5 kts, 20 kts, and 40 kts wind speed are extracted.
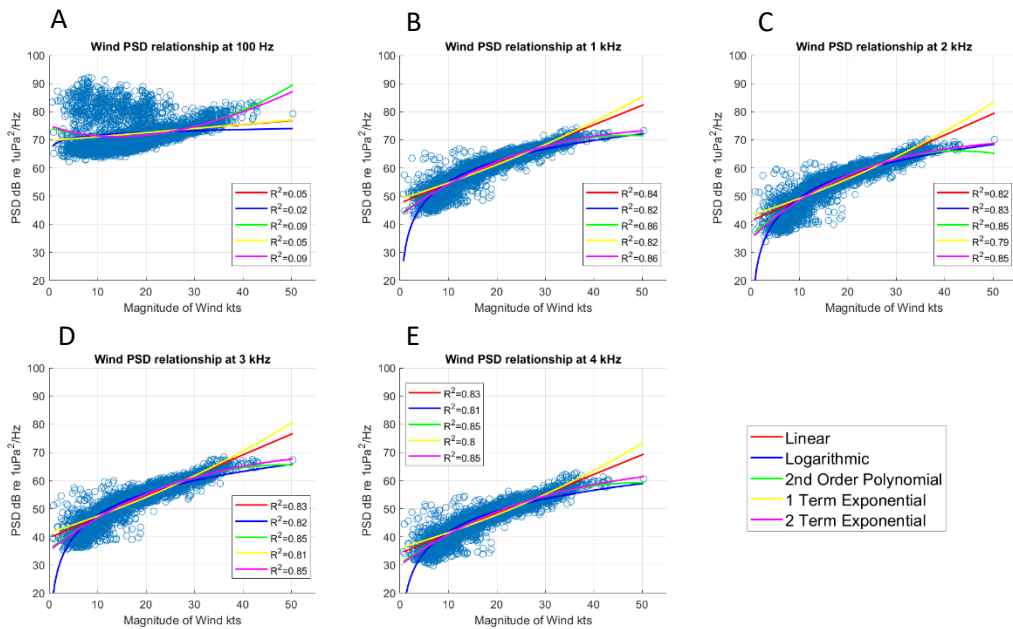
Figure 12: Wind *PSD* models linking horizontal wind speed magnitude 10 m above sea level and hourly minimum sound power levels taken between Jan and June 2016 at Station 15. Figure A) wind *PSD* at 100 Hz frequency bin, B) 1 kHz, C) 2 kHz, D) 3 kHz, E) 4 kHz.

Bellhop software was used to model transmission loss at 25 cm, 50 cm, 75 cm, 100 cm, 125 cm, and 150 cm bubble cloud penetration depths (modelled as the source depth in Bellhop). Realistic bottom type and climatological *SVP* were used for maximum realism.
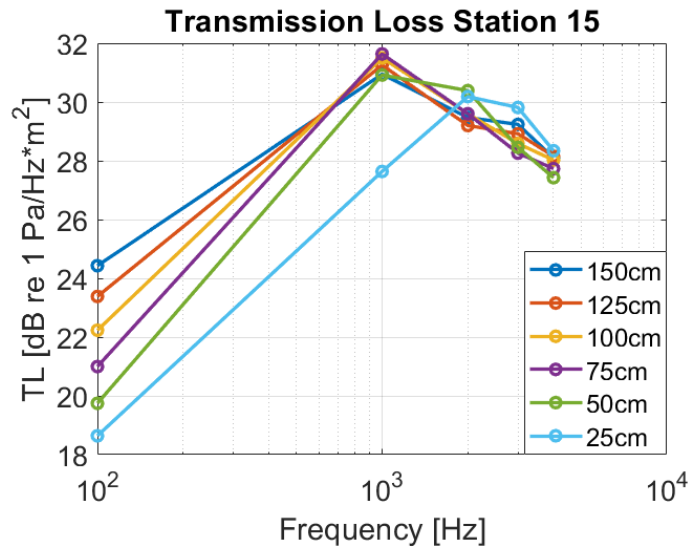
Figure 13: Station 15 integrated Transmission Loss vs Frequency at various source level depths.

Noise source levels as a function of bubble cloud penetration depth were plotted at Figure 14. Modelled received levels from Figure 12 were added to the integrated transmission loss values at Figure 13 in order to produce *NSL/A* values at Figure 14.
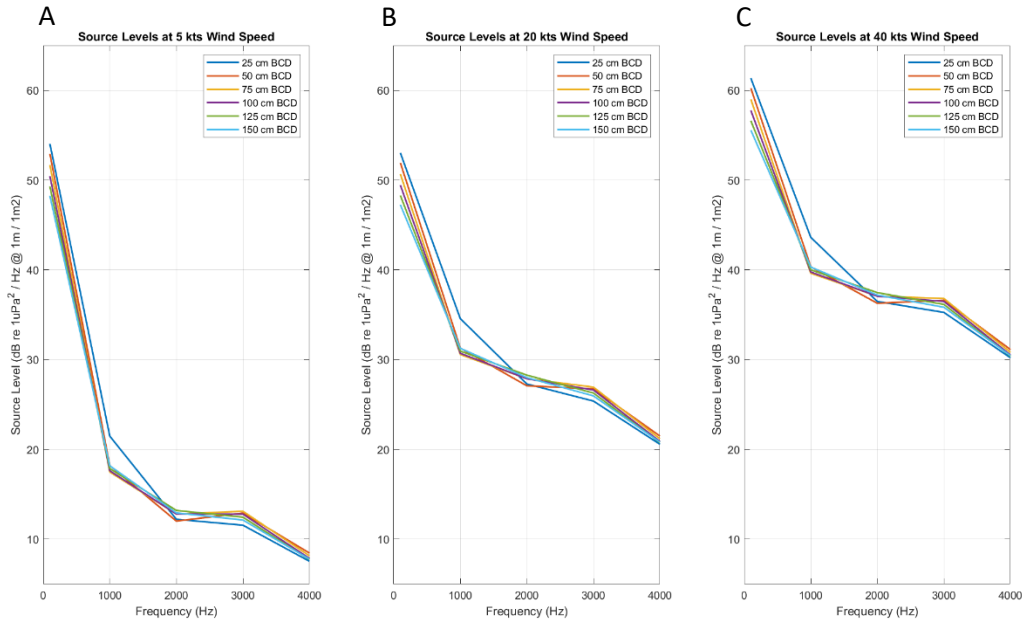
Figure 14: Plot of Station 15 source level estimates (*NSL/A*) as a function of frequency at low, medium, and high values of horizontal wind speed magnitude 10 m above sea level for varying source level depths; Figure A) 5 kts, B) 20 kts, and C) 40 kts respectively.

In the deep (1993 m), ice free water of Station 15, with horizontal wind R^2 modelling from 0.85 to 0.86 in the 1 to 4 kHz band using the two-term exponential regression, *NSL/A* estimates are relatively consistent. The 25 cm bubble cloud penetration depth is the singular outlier with an approximate 3 dB increase across the three measured wind speeds at 1 kHz. This feature can also be seen in Figure 13 where at 1 kHz, the *TL* for 25 cm bubble cloud penetration depth sits at approximately 3 dB below the cluster. The fact that this penetration depth is an outlier does not necessarily indicate it is wrong.

At 1 kHz and with a notional 1500 m/s sound speed, the acoustic wavelength is 1.5 m, thus the 25 cm bubble cloud penetration depth is 1/6 of a wavelength, whereas all other depths are 1/3 of a wavelength or greater. The other penetration depths produce results which behave similarly in shape and power with a variance of 1 to 2 dB in *NSL/A* and *TL* within the general cluster. *NSL/A* estimates at 100 Hz are not reliable as per the poor R^2 expressed at Figure 12. However, it is interesting to note that at 100 Hz the *TL* increases by 1 dB for each 25 cm increase in bubble cloud penetration depth per Figure 13.

33

The Station 1 bubble cloud penetration depth analysis is as follows, with the regression relationships shown in Figure 15, the integrated *TL* in Figure 16, and the *NSL/A* in Figure 17.
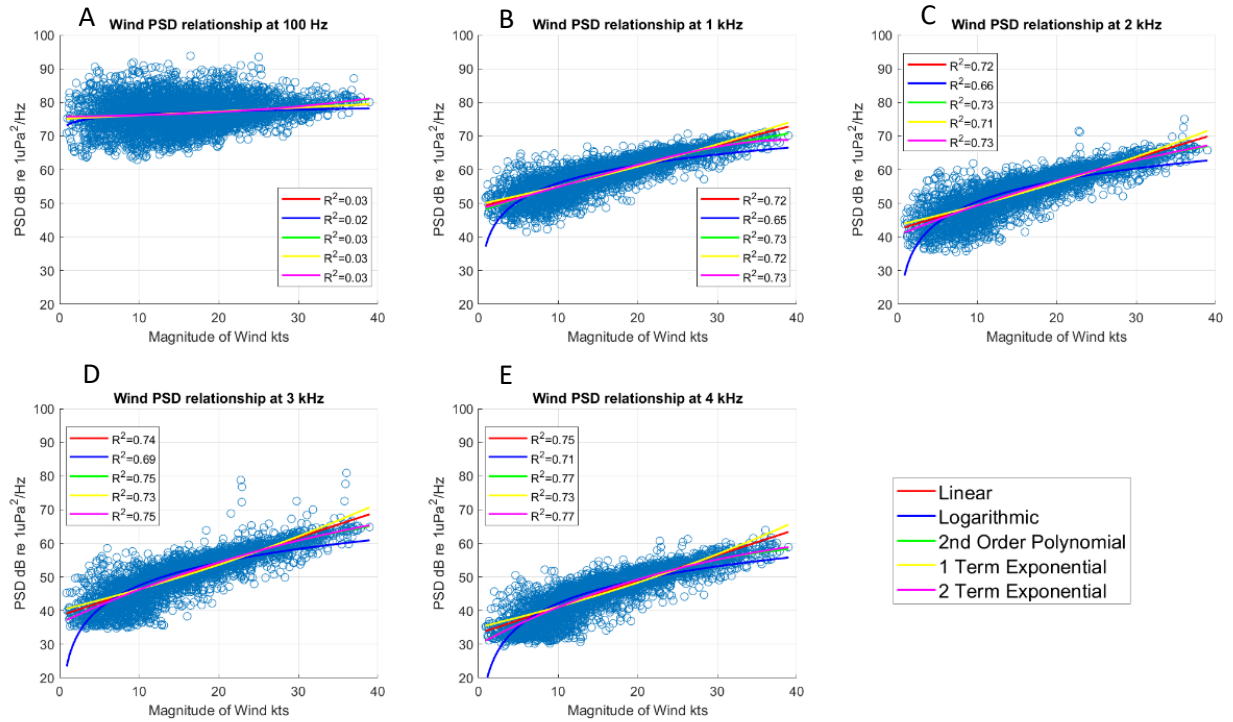
Figure 15: Wind *PSD* models linking horizontal wind speed magnitude 10 m above sea level and hourly minimum sound power levels taken between Jan and June 2016 at Station 1. Figure A) wind *PSD* at 100 Hz frequency bin, B) 1 kHz, C) 2 kHz, D) 3 kHz, E) 4 kHz.
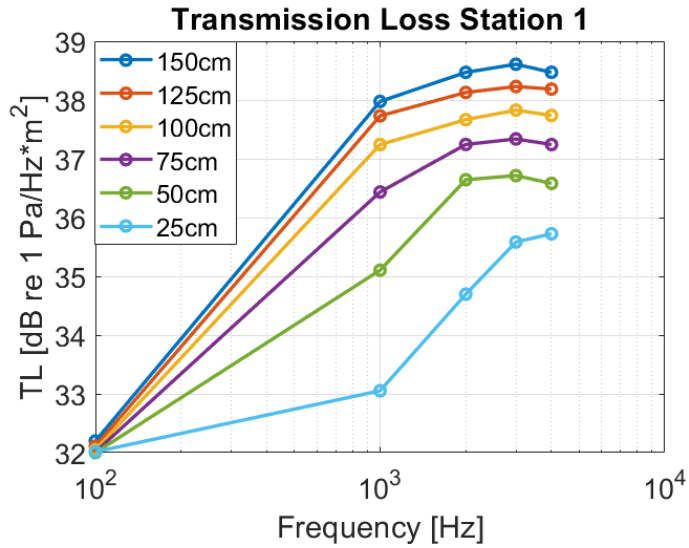
Figure 16: Station 1 transmission loss vs source level depth.
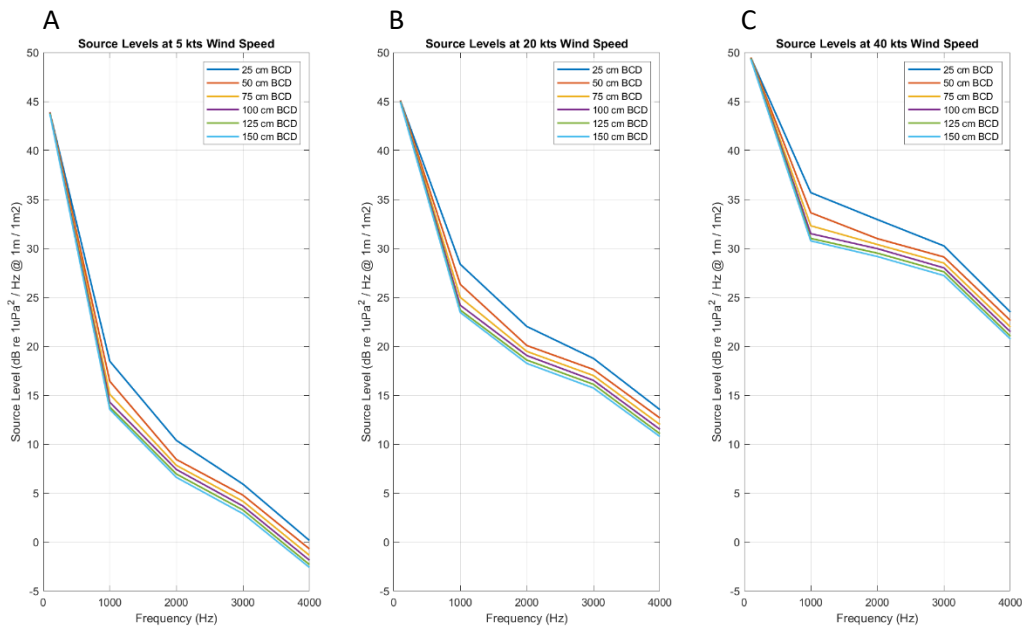
Figure 17: Plot Station 1 of source level estimates as a function of horizontal wind speed magnitude 10 m above sea level as a function of source level depth at A) 5 kts, B) 20 kts, and C) 40 kts respectively.

In the shallow (175 m), ice free water of Station 1, with horizontal wind R^2 modelling from 0.73 to 0.77 in the 1 to 4 kHz band using the two-term exponential regression, *NSL/A* estimates express a consistent shape. The 25 cm bubble cloud

penetration depth and to a small extent, the 50 cm bubble cloud penetration depth behave somewhat differently from the others in that the shape of the *TL* is concave from 100 Hz to 3 kHz and then plateaus out to 4 kHz; similar to an 'S' shape, whereas the curves at other depths have a convex logarithmic shape. This feature can also be seen in Figure 17 where the *NSL/A* of the 25 cm and 50 cm bubble cloud penetration depth are slightly higher than the cluster at all wind speeds. *NSL/A* estimates at 100 Hz are not reliable as per the poor R^2 exhibited at Figure 15. Contrary to the deep slope station which exhibited a 1 dB increase in *TL* spacing per 25 cm bubble cloud penetration depth at Figure 13, the shallow shelf station at Figure 16 indicates that in shallow water, 100 Hz *TL* tends to commence at 32 dB regardless of bubble cloud penetration depth.

Prosperetti (1988) states that from 1 to 10 kHz, noise is produced by freely oscillating individual bubbles which dissipate their energy after spilling down the face of a wave. Buckingham (1991) references a similar effect in a laboratory where spilling breakers generate acoustically active bubbles under wind-free conditions in a laboratory tank which are known to be within a few millimetres of the surface. If it is true that extremely shallow acoustically active bubbles generate noise in the 1 to 10 kHz band, the 25 cm bubble cloud penetration depth at Figures 14 and 17 would be the most accurate representation of *NSL/A* based on horizontal wind speed magnitude.

Buckingham (1991) states that bubble sound sources in *FASINEX* were determined to be at 1.5 m depth by inversion which would correspond to the base of the bubbly layer. He also states that this was an unexpected conclusion. Prosperetti (1988) would indicate that at this depth, the noise generating mechanism is turbulent noise amplified by bubble pulsations from a few Hz to 100 – 200 Hz. This thesis cannot draw conclusions at 100 Hz as all modelled R^2 were poor however, *NSL/A* clustering is extremely strong from 75 cm to 150 cm using horizontal wind over both the shelf and the slope. The fact that the models are generating similar *NSL/A* from 75 cm to 150 cm would indicate that something acoustically consistent is occurring in the deeper bubble penetration region, perhaps greater than 75 cm.

There are two salient points to note. First, based on the results of Prosperetti (1988) and Buckingham (1991), lower frequencies ~100 Hz would be generated at deeper bubble cloud penetration depths, higher frequencies ~ 1 to 4 kHz would be generated at shallower bubble cloud penetration depths. Second, based on the above analysis, *NSL/A* values are directly related to the depth of the water column. In a deep-water environment, the depth of the bubble cloud penetration is insignificant compared to the depth of the water column and there is extremely little effect on the resultant transmission loss. This is the reason for the clustering of the transmission loss and

NSL/A at Station 15 for most of the bubble cloud penetration depths; the difference in the noise generation depth relative to the depth of the water column is insignificant, and therefore the resultant transmission loss is effectively the same. However, in a shallow water column such as that at Station 1, the bubble cloud penetration depth has more significance when compared to the depth of the water column and this manifests as increasing transmission loss with increasing depth.

The goal of the bubble cloud penetration depth modelling over shelf and slope was to determine how transmission loss and therefore *NSL/A* changes as a function of noise source level depth. Deane and Stokes (2002) state that bubble plumes generated by breaking waves in the open ocean can extend 0.5 m below the surface and have void fractions of air exceeding 10%. In this thesis, transmission loss modelling and therefore *NSL/A* estimates were generated using a 50 cm bubble cloud penetration depth. Based on bubble cloud penetration depth analysis, a 75 cm bubble penetration depth on a shelf or slope may generate answers more representative of the mean of the group at those types of stations. It should be re-emphasized that participation in a group or cluster does not necessarily indicate that an *NSL/A* or *TL* is correct. There is no one correct answer to this problem as individual bubbles, collective bubble plumes, bubble density, individual bubble diameters, and air void fractions in plumes are so variant from environment to environment and time to time that the noise generating response to individual/collective oscillations and turbulent amplification is difficult to model with precision. However, a reasonable assumption of a correct answer in the deep-water case is any depth from 50 cm to 150 cm; the resultant transmission loss will be effectively the same. The problem becomes more complex in the shallow water environment because depth takes on physical import. Given the difficulty in knowing and therefore modelling the physical dynamics within the surface layer of the ocean; a 75 cm bubble cloud penetration depth, in effect the median depth, is the most generalized answer to the problem. Therefore, for ease of use a 75 cm bubble cloud penetration depth is recommended under both deep and shallow water conditions.

3. Data Selection and Methods

3.1 PAMGuide Software
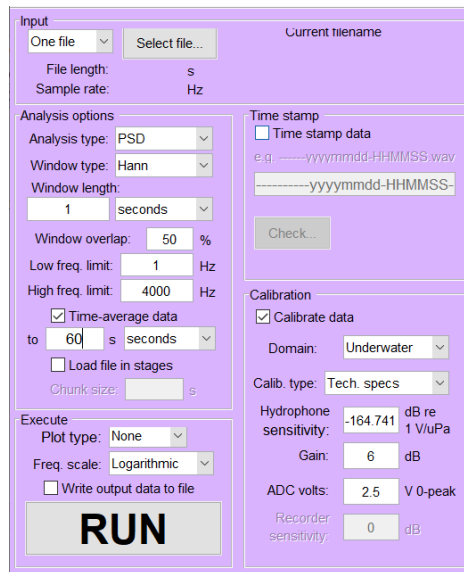
Figure 18: PAMGuide GUI with calibration specifications.

PAMGuide (Merchant et al, 2014) is acoustic analysis software used for the characterisation of the acoustic environment from sound recordings. The software was used to produce calibrated spectrograms and *PSD* files of each hydrophone on a month-by-month basis. The parameters and calibration used are shown in Figure 18. Batches of monthly JASCO *AMAR* data were selected for input which resulted in a monthly *PSD* output. In this project, *AMAR* data were analyzed from 1 Jan to 30 Jun 2016 (6 complete months). The nature of the *AMAR* duty cycle was such that in any given hour, three duty cycles would elapse, and the 8 kHz sample rate would record 2034 seconds (33.9 minutes). Acoustical spectra were averaged every 60 seconds using 1 second bins with 50% overlap. The 1 second time domain resolution translated to 1 Hz frequency domain resolution. A Hann window was applied to each *FFT* (Fast Fourier Transform) window. The author selected the Hann window as it is a simple window with favourable spectral characteristics in that it reduces spectral leakage. The employed *AMAR* sampling rate is 8000 Hz and the corresponding Nyquist frequency is 4000 Hz. *AMAR* anti-aliasing filter roll-off commences at approximately 3600 Hz and as a result, 4 kHz power levels are reduced. Fortunately, the nature of the roll off has no effect on the ability to model the hourly minimum sound power levels and consistently strong R^2 at 4 kHz is exhibited during regressions. Conclusions can still be made about 4 kHz data in terms of *PSD*. The effects of the roll off negatively manifest in the *NSL/A* figures at Figures 88 and 89. There is a characteristic steep drop from 3 to 4 kHz.

On occasion, some of the wav files were corrupted in that a particular file would contain 0 bytes of data. This was not common. In any given month, there would be between approximately 2100 and 2200 recorded wav files, depending on the number of days in the month. At any given hydrophone station, the maximum number of corrupted 20 min wav files was 7, the minimum was 0, and the average was 2.

Upon encountering a corrupted wav file, PAMGuide would cease operation and issue an error message. Deleting the corrupted wav file was not a valid means of addressing the problem as in the case of the month with 7 such files, each corrupted wave file would skew the timing of the *PSD* by 20 min. After 7 such issues, the chronology of the *PSD* would be advanced by 140 min (2 hr 20 min). This was addressed by creating a replacement wav file, 20 min in size with 0 sound data thus the timing of the chronology was sustained without modification to the noise field. Although the effect of this process would be to introduce zeros into the acoustical averaging process, the overall effect was insignificant in terms of regression function modelling. In the worst-case scenario in which one month contained 7 such corrupted files, the impacted data was 0.3% of the month. Most stations were significantly less affected than this.

Each PAMGuide *PSD* output which corresponds to one of six months of wav files which in turn corresponds to one of 16 hydrophones contains 4000 individual frequencies (1 to 4000 Hz) with audio power information averaged every 60 seconds per frequency.

3.2 Extraction of Hourly Minimum Sound Power Levels

Code was developed to extract the hourly minimum sound power levels from the PAMGuide *PSD* output. The hourly minimum sound power levels represent the ambient noise at the hydrophone location; ambient noise being the background noise largely devoid of transient contributions from anthropogenic and biological phenomena. Since each wav file was 11 min 18 sec in length, the wav file was rounded to 12 min in duration, assuming that the 18 seconds were representative of the final minute. Hence, each hour contained approximately 33 min of audio data (33.9 minutes exactly). The hourly minimum sound power level was selected as the minute out of 36 possible minutes whose power averaged over 60 seconds was lowest.

3.3 Meteorological Data

Meteorological data were extracted from *ERA5*. The database is produced by the Copernicus Climate Change Service (*C3S*) at *ECMWF*. The database provides hourly estimates of a large number of atmospheric, land and oceanic climate variables (*ERA5*,

2022). Data were extracted from *ERA5* for use in this thesis; specifically, the 10 m $\vec{U}$ and $\vec{V}$ component of wind, the 10 m neutral $\vec{U}$ and $\vec{V}$ component of wind, and the significant height of combined wind waves and swell. The data were localized to within a 25 km radius of each of the 16 hydrophones studied. The data extracted and analysed from *ERA5* were from Jan to July 2016.

3.4 Bathymetric Data

Bathymetric data were extracted from the General Bathymetric Chart of the Oceans (*GEBCO*) global terrain model for ocean and land. *GEBCO*'s aim is to provide the most authoritative publicly available bathymetry of the world's oceans. It operates under the joint auspices of the International Hydrographic Organization (*IHO*) and the Intergovernmental Oceanographic Commission (*IOC*) of UNESCO (*GEBCO*, 2021). As Bellhop was making calculations to a maximum range of 20 km, it was necessary to have the corresponding length and breadth of bathymetric data. *GEBCO* spatial resolution is 15 seconds of arc. Data were grided in terms of depth per latitudinal and longitudinal position and the geospatial resolution was thus developed.

3.5 Surficial Sediment Descriptor

Geological Survey of Canada seabed maps were used to determine the surficial sediment descriptor in the vicinity of the *AMAR* hydrophones. Sediment compressional properties were determined from Buckingham (2005). Compressional sound speed values were thus determined and programmed into Bellhop propagation software.

3.6 Sound Velocity Profiles

Climatological sound velocity profiles were extracted from the World Ocean Database (*WOD*). The World Ocean Database (Boyer et al., 2018) is the world's largest collection of uniformly formatted, quality controlled, publicly available ocean profile data. The author was occasionally conflicted with a lack of options in some regions. Sound velocity profiles (*SVP*s) were selected primarily based on a depth that best matched the depth of the hydrophone of interest. Depth was given priority over precision of location because while a seamount or canyon may have been the location of the closest available *CTD* cast to the hydrophone, the associated bathymetry would have skewed the acoustical propagation. All *CTD*s used were located within 30 km of the hydrophone being studied. After depth and location, if available, a cast taken between the months of January and June was prioritized. Sound propagation would certainly be affected by seasonal variation and resultant changes in the characteristics of the upper mixed layer. Greater accuracy in *NSL/A* estimates could be cultivated through modelling using seasonal, or monthly, or in the best case, daily *SVP*s. The most

perfect case is the real-time input of the *SVP* for immediate use. An example *SVP* is Figure 19.
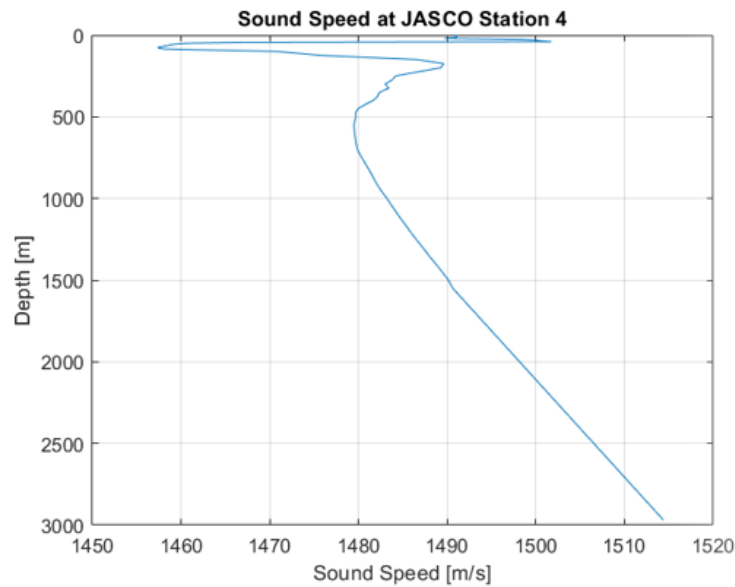
Figure 19: Scotian Shelf sound velocity profile extracted from the *WOD*.

Seasonal and sub-seasonal variability could significantly impact model results. This thesis modelled data from Jan – June 2016 (inclusive); encompassing the entirety of the Winter and Spring seasons. In the North Atlantic, Winter and Spring are associated with elevated winds, storms, and significant surface layer mixing while Summer and Fall are calmer and associated with a shallow and stable upper mixed layer. Conclusions in this study are subject to the dynamic wind and storm forces associated with Winter and Spring and it is recommended that further study be conducted with quieter and less potent Summer and Fall wind data to enhance the results and conclusion of this study. It is surmised that the inclusion of Summer and Fall hourly minimum sound power levels will result in even lower *NSL/A* values than those seen at Figures 88 and 89. The sound velocity profile, which varies on a seasonal basis will impact sound propagation.

3.7 Regression Functions

MATLAB functions were used to produce each *PSD* vs environmental characteristic best fit model. Linear, logarithmic, second order polynomial, single term exponential, and two-term exponential functions were explored as potential optimal candidates. The second order polynomial and two-term exponential functions generally yielded the highest R^2 values and were used to best advantage in estimating the noise

source per unit area levels. However, all regression models and their performance will be described in this section.

Scatterplots were useful in determining the strength of the relationship between the environmental phenomena and *PSD* on a per frequency basis. The visual aspect of the plots aided in determining the best functional choice for regression.

The linear regression attempts served to model the relationship between two variables by fitting a linear equation to observed data. A linear regression line has an equation of the form

$$y = a + bx, \tag{25}$$

where x is the independent environmental input variable and y is the dependent noise level variable. The slope of the line is b, and a is the intercept (the value of y when $x = 0$).

The logarithmic regression served to model the relationship between two variables where growth or decay accelerated rapidly at first and then slowed over time. The equation of a logarithmic regression model has the form

$$y = a + b * ln(x), \tag{26}$$

where y is the dependent variable, x is the independent variable and a and b were the regression coefficients that described the relationship between x and y.

The second order polynomial models were generated by calculating the coefficients for a polynomial *p(x)* of degree n that is a best fit (in a least-squares sense) for the data in y. The coefficients in p are in descending powers, and the length of p is *3*:

$$y = p(x) = p_2 x^2 + p_1 x + p_0. \tag{27}$$

A one term exponential model was calculated and has the form

$$y = a * e^{bx}, \tag{28}$$

where e is Euler's number, a is a constant, b is the growth rate, x is the wind magnitude, and y is the acoustical power level. Through trial and error, it was determined that a two-term exponential function would yield significantly higher R^2 then a single term exponential. This is indicative of two growth or decay mechanisms within the physical processes of study.

The two-term exponential function was calculated using

$$y = a * e^{bx} + c * e^{dx}, \tag{29}$$

where the coefficients are as described as above.

An important observation is that the best fitting functions had the most fitting parameters. While two fitting parameters are necessary to adequately describe the radii of curvature seen in the 1 to 4 kHz *PSD* figures, a third fitting function would be more appropriate to describe the low frequency flat 'S' seen in the 100 Hz *PSD* figures and described in Section 8.2. It could be argued that supplemental fitting parameters may result in an over-fit model and further, a measure of artificially high performing R^2. Considering that Kewley (1990) and others established the use of a bi-mechanistic linear fit, a bi-mechanism exponential fit would not be an unreasonable advancement in model progression. It is argued that a tri-mechanism fit is unnecessary from 1 to 4 kHz but may have validity in modelling sub 1 kHz wind based ambient noise.

3.8 Noise Source Level per Unit Area Estimation

Noise source level per unit area (*NSL/A*) figures were produced by soliciting the modelled received level corresponding to the frequency of interest and adding it to the Bellhop derived *TL*. The advantage of the Bellhop software is that it has the ability to resolve the vertical angular dependence of propagating sound as well as incorporate bottom loss characteristics, reflections, bathymetric blockages, and climatological Sound Velocity Profiles (*SVP*).

Example *PSD* model outputs are found at Figure 20. Note the value of the R^2 in each model type. Higher R^2 values indicate better model fit and a more realistic indication of the acousto-environmental dynamics in effect. Datasets were selected to determine *NSL/A* relationships not just on physical parameters but temporal variability as well.

4. Parametric Scrutinization

In this section conclusions are developed regarding which meteorological parameter is generating the hourly minimum sound power levels recorded at the hydrophones. Six months of hourly minimum sound power levels are plotted vs 6 months of hourly meteorological phenomena. This was achieved by aligning the date-time group of the specific instant of hourly minimum sound power level with the same date-time group of the specific instant of the meteorological parameter. Five different regression functions were fit to the data as per Section 3.5; this is seen as different coloured lines passing through the scatter plots and the legend is in the bottom right of each regression figure. The performance of each regression line in terms of data fit is expressed by R^2. Higher R^2 indicates that the regression function/line fits the data better than functions/lines of lower R^2. As will be seen, the two-term exponential function and 2nd order polynomial functions fit the data better than the linear, logarithmic and one-term exponential functions. While the two-term exponential function and 2nd order polynomial function occasionally produce the same R^2, when they are different the two-term exponential function is superior and never inferior to the 2nd order polynomial function. Therefore, the best performing regression function is determined to be the two-term exponential function. The parametric regressions shown were made with Station 4 data. Station 4 is a deep-water non-ice station with typical R^2 of a station of this type.

Holistic performance characterisation of each parameter required discussion of data variance, an *NSL/A* figure at Station 4, and an *NSL/A* figure for all stations for comparative reasons.

4.1 Unique Parametric Regressions

4.1.1 Horizontal Wind Speed Magnitude 10 m Above Sea Level

The first dataset to be examined is the horizontal wind speed magnitude at 10 m above sea level.
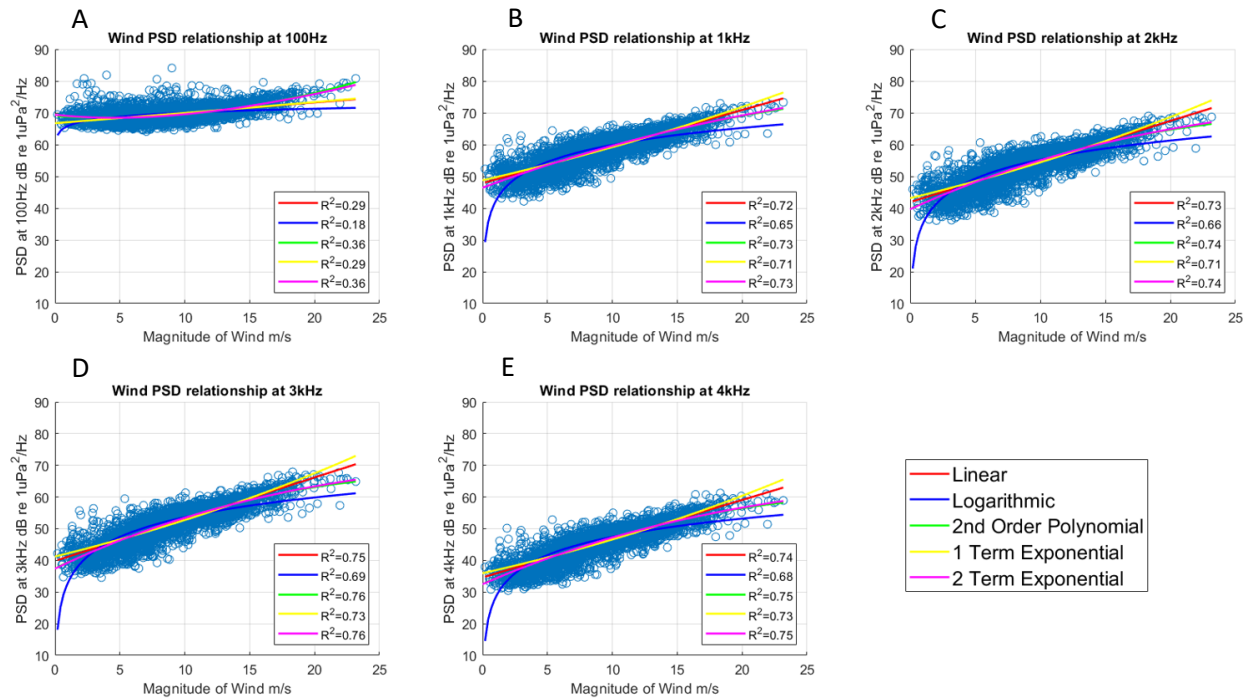
Figure 20: Wind *PSD* models linking horizontal wind speed magnitude 10 m above sea level and hourly minimum sound power levels taken between Jan and June 2016 at Station 4. Figure A) wind *PSD* at 100 Hz frequency bin, B) 1 kHz, C) 2 kHz, D) 3 kHz, E) 4 kHz.

The graphs in Figure 21 depicts the exceedance percentiles at Station 4. An exceedance percentile is a value on a scale of one hundred that indicates the percent of a distribution that is equal to or above it. Otherwise said, it is the sound power level exceeded n% of the time during a measurement.
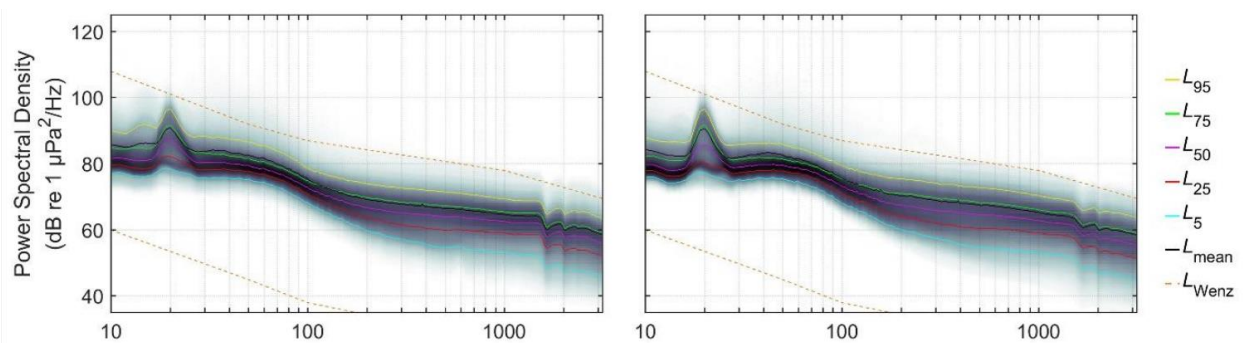
Figure 21: Station 4 exceedance percentiles; 2015-2016 (left), 2016-2017 (right), where the 5th, 25th, 50th (median), 75th, and 95th percentiles are plotted as lines, along with the mean and Wenz limits (Wenz, 1962) of noise (reproduced from Delarue et al., 2018).

45

From Figure 20, it is evident that at 100 Hz, the R^2 values for all models are poor. This is due to the fact that 100 Hz sound is not dominated by wind generated noise, but rather distant shipping and seismic anomalies (Urick, 1983). While nearby shipping generates noise over a broad range of frequencies, at longer range, higher frequencies become attenuated and only the lower frequencies remain in the spectrum. Thus, at 100 Hz, there is no way to link wind speed and acoustical *PSD* in a statistically significant way. Further, there are no data points below 64 dB at 100 Hz in Figure 20 A). This characteristic is approximately replicated in the L_5 exceedance percentile in Figure 21 (right). This is not the noise floor. This is due to the lack of sensitivity of the noise field to wind and wave noise at 100 Hz. At 1 kHz and above, the 2nd order polynomial and two-term exponential models rise above the others in their ability to model received levels from wind speed; in fact, to two decimal places, their R^2 values are equal at each frequency iteration. It is encouraging to see an increase in wind sound power level predictability with increasing frequency.

Upon close examination of any of the frequency bins except 100 Hz, at higher wind speeds, a flattening of the spectral slope manifests. The change in spectral shape of the data is not caused by a change in the noise generating mechanism, but rather by the thin layer of entrained bubbles that is known to occur at the surface of the ocean and serves both to absorb and scatter the sound originating at the air-sea interface (Farmer and Lemon, 1984). The anti-aliasing roll off in the *AMAR* may be evident in Figure 20E, where power levels are lower than in Figure 20 B), C), and D), though lower noise levels with increasing frequency are expected for wind driven sound. Fortunately, the nature of the roll off has no effect on the precision of the modelling of the hourly minimum sound power levels and an R^2 of 0.75 is exhibited for the two-term exponential regression.
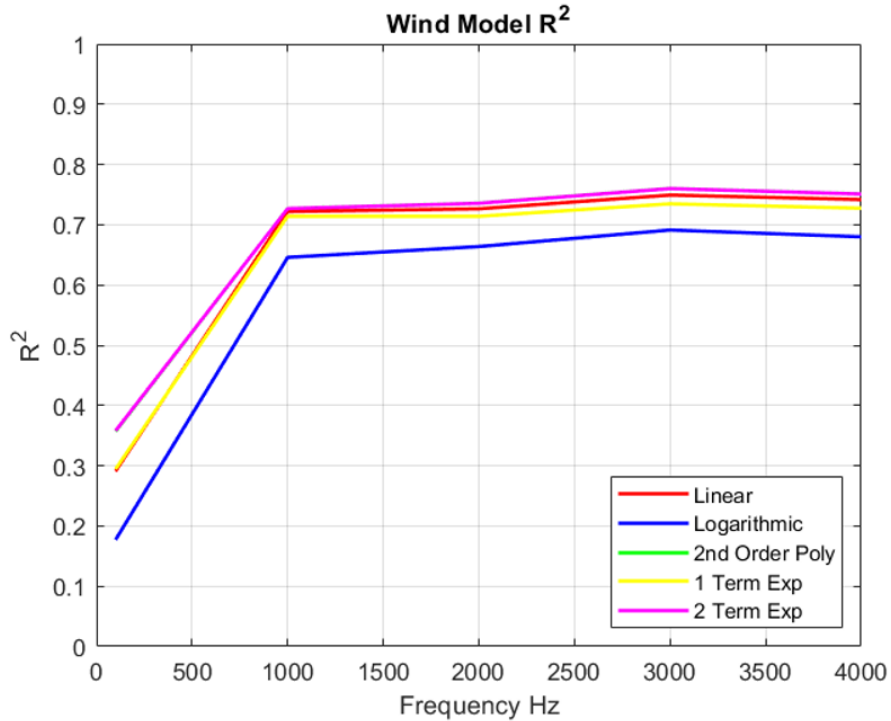
Figure 22: Summary of Station 4 wind model R^2 computed over all wind speeds.

In Figure 22, the R^2 values for the 5 regression models are shown over the frequency bandwidth considered. The two-term exponential R^2 values (pink) lay completely on top of the 2nd order polynomial values (green), illustrating their similar ability to model the received levels as generated by horizontal wind 10m above sea level. Both models outperform the others under consideration.
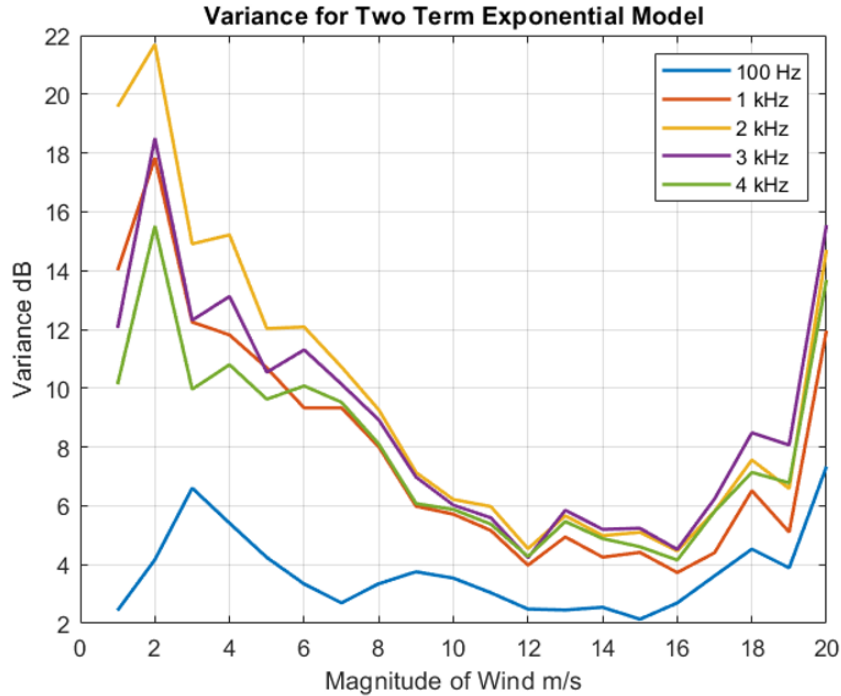
Figure 23: Variance of wind model data from Station 4, two-term exponential regression.

The variance represents the proportional variability in data when compared to the model prediction. Variance, σ^2, is given by

$$\sigma^2 = \frac{1}{n} \sum_{i=1}^{n} (x_i - \mu)^2 , \tag{30}$$

where n is the number of data points, x is the data, and μ is the best fit model.

Figure 23 shows the variance at 5 frequencies as a function of wind speed, and was constructed using the two-term exponential model as it consistently generates the highest R^2 values across frequency and recording site. In this instance, the two-term exponential R^2 was equivalent to the second order polynomial in correlative ability. At 100 Hz, model variance is low; this is because the 100 Hz data cloud does not vary greatly in *PSD* compared to the other frequency bins. At the other frequency bins, the *PSD* varies mostly at the model extremities but the models consolidate within 1 dB between 8 and 16 m/s wind speed. This visibly manifests as the data cloud becoming narrower about the model line in Figure 20. Lower data variance indicates stronger model predictability; however, this must be taken with the caveat that if the R^2 of the model is already poor, low variance, although desirable, is irrelevant.
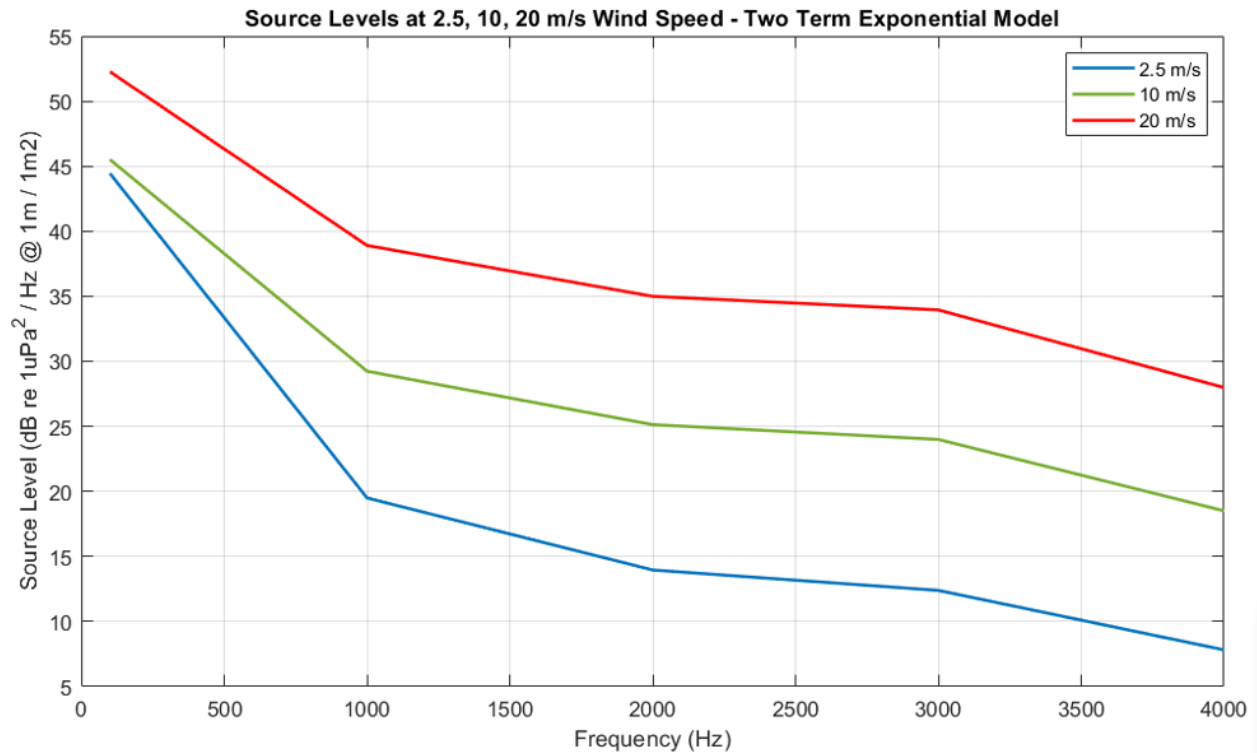
Figure 24: Plot of Station 4 wind speed estimated source levels at A) 2.5 m/s, B) 10 m/s, and C) 20 m/s wind speed respectively.

In Figure 24 the 2.5 m/s, 10 m/s, and 20 m/s wind speed values were arbitrarily chosen to reflect the low, medium, and high values of the wind speed metric. *NSL/A* values increase in sound power with increasing wind speed. The 100 Hz levels are suspect as per Figure 20 explanation and the 3 to 4 kHz decrease is due to anti-aliasing roll-off. At 1 kHz and above, horizontal wind speed magnitude at 10 m above sea level is a good predictor of ambient noise.
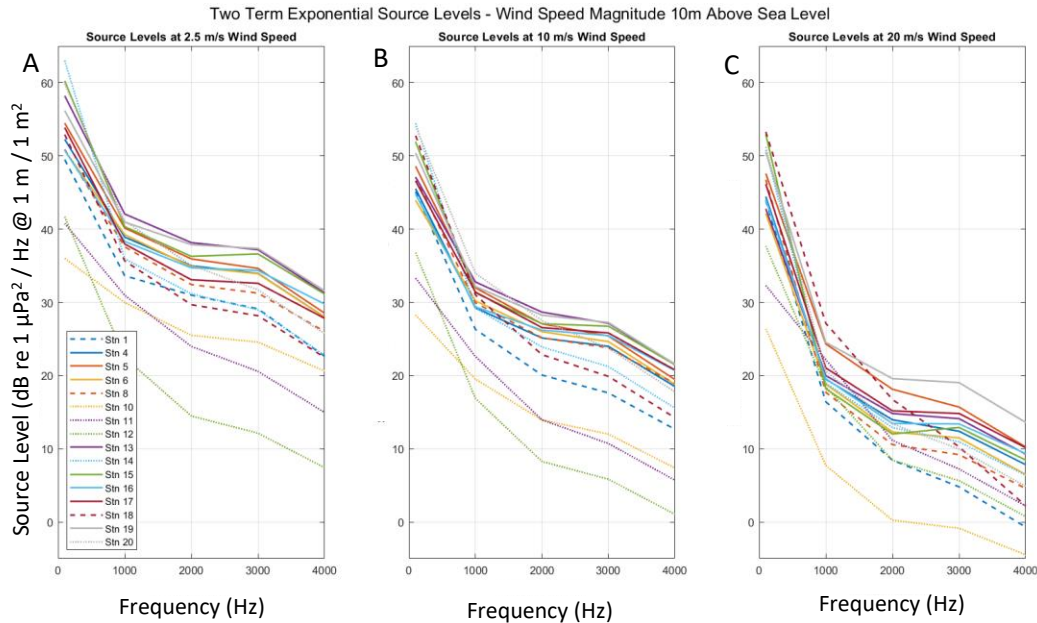
Figure 25: *NSL/A* based on horizontal wind speed magnitude 10 m above sea level, two-term exponential regression for all stations A) 2.5 m/s, B) 10 m/s, C) 20 m/s wind speed respectively. Solid lines are slope stations, dashed lines are shelf stations with less than 10% surface ice coverage, dotted lines are shelf stations with greater than 10% surface ice coverage.

At Figure 25, a plot of *NSL/A* for wind speed magnitude 10 m above sea level is presented. The three panels, from left to right, are *NSL/A* calculations based on low, medium, and high values of the horizontal wind speed metric. The slope stations, depicted by solid lines cluster together, as do the shelf stations depicted by dashed lines. This indicates that there is some consistent physical behaviour and predictability within each respective group. Further, the clustering characteristic occurs at each instance of the wind speed metric. This illustrates the functionality of the developed algorithm. The fact that the shelf and slope groups do not cluster together is also interesting because it speaks to the fact that the acoustical propagation dynamics within each group are different. The inconsistent and unpredictable *NSL/A* values of the dotted lines, the ice stations; indicates that ice severs the relationship between the noise generation mechanism, the wind; and the propagation environment, the ocean. This suggests that under the condition of significant ice presence, greater than 10% by the definition employed in this thesis, *NSL/A* values are not predictable. If a transmission loss model were developed which could account for all types of acoustical power losses and physical interference, and if all noise sources could be accounted for, all source levels at all stations would be the same value at each explicit wind speed.

4.1.2 Significant Height of Combined Wind Waves and Swell

The next parameter to be examined is significant height of combined wind waves and swell at Station 4 which is the average height of the highest third of surface ocean/sea waves generated by wind and swell.
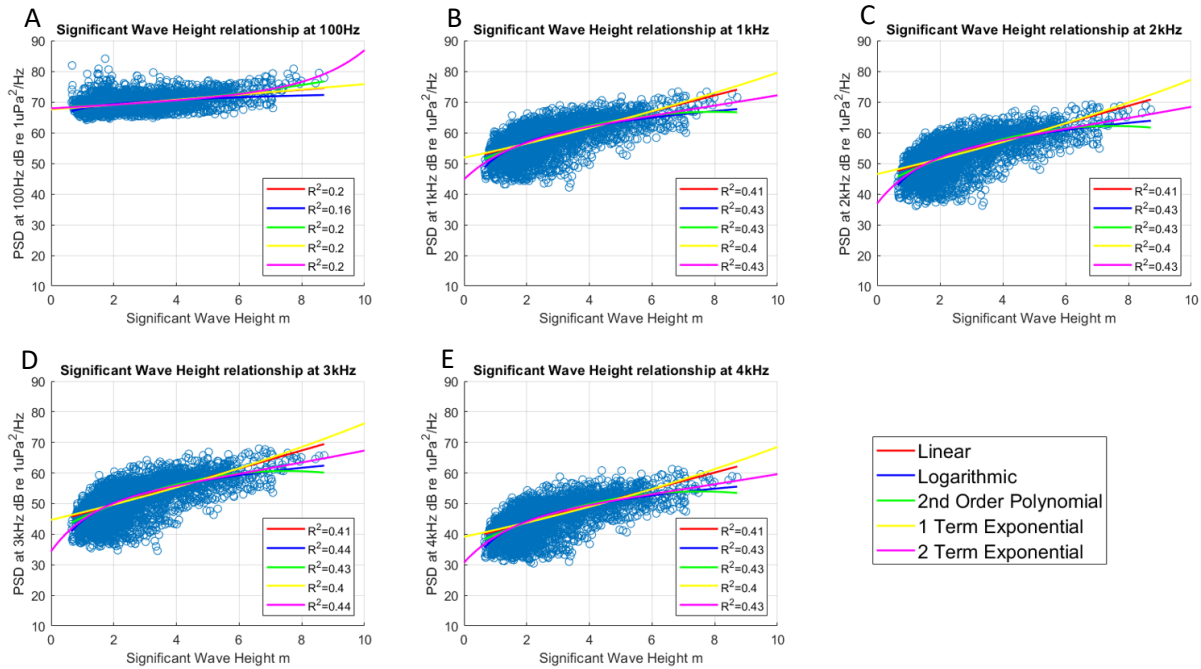
Figure 26: Significant wave height (*SWH*) models of combined wind waves and swell for predicting hourly minimum sound power levels at Station 4 taken between Jan and June 2016 at A) 100 Hz, B) 1 kHz, C) 2 kHz, D) 3 kHz, and E) 4 kHz.

As per the generally low R^2 values at Figures 26 and 27, there is not a strong correlation between *PSD* and *SWH* in the 1 to 4 kHz band. Within this frequency range, all models performed similarly however the two-term exponential model and the logarithmic model were most highly correlated with the data. The two-term exponential model ranged between 0.43 and 0.44 R^2 from 1 to 4 kHz. Wave development is a function of wind speed, direction, and fetch and the correlation between *PSD* and *SWH* is related to horizontal wind speed magnitude. Swell is differentiated from wind wave in that swell is formed by distant storms at sea and wind wave is generated by local winds. Because of the requirement for long fetch in order to attain higher wave heights and the fact that this parameter represents the highest third of wave heights recorded at the station, it is probable that this parameter is more reflective of swell and therefore more reflective of winds far away from the station. At all frequencies, horizontal wind

speed magnitude can be more accurately modelled than significant wave height and will therefore yield a more accurate measure of received level.
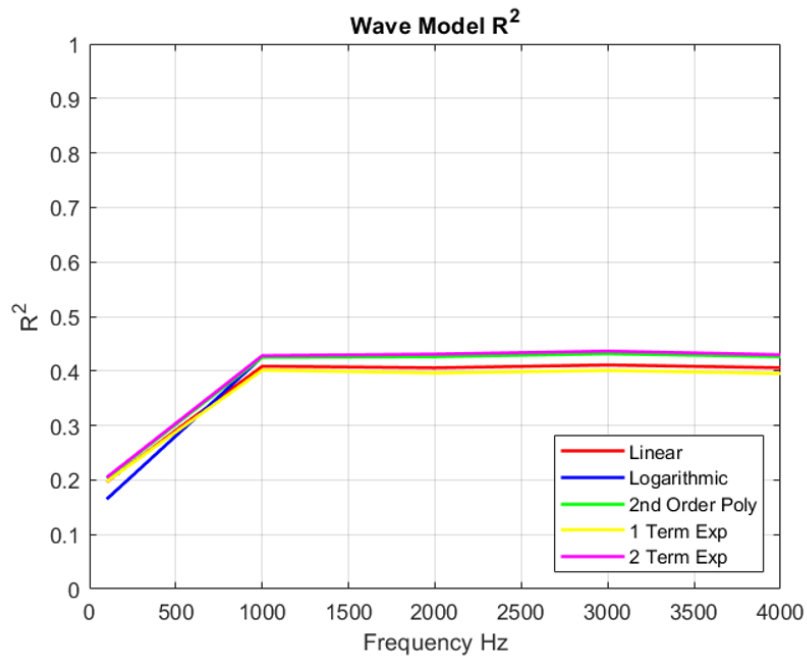
Figure 27: Summary of Station 4 *SWH* model R².
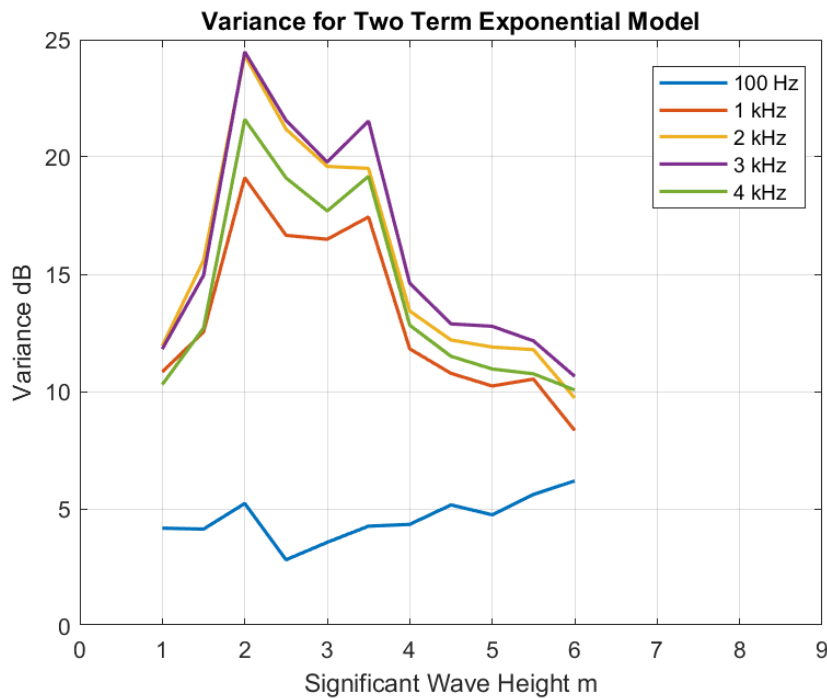
Figure 28: Variance of significant wave height model data from Station 4, two-term exponential regression.
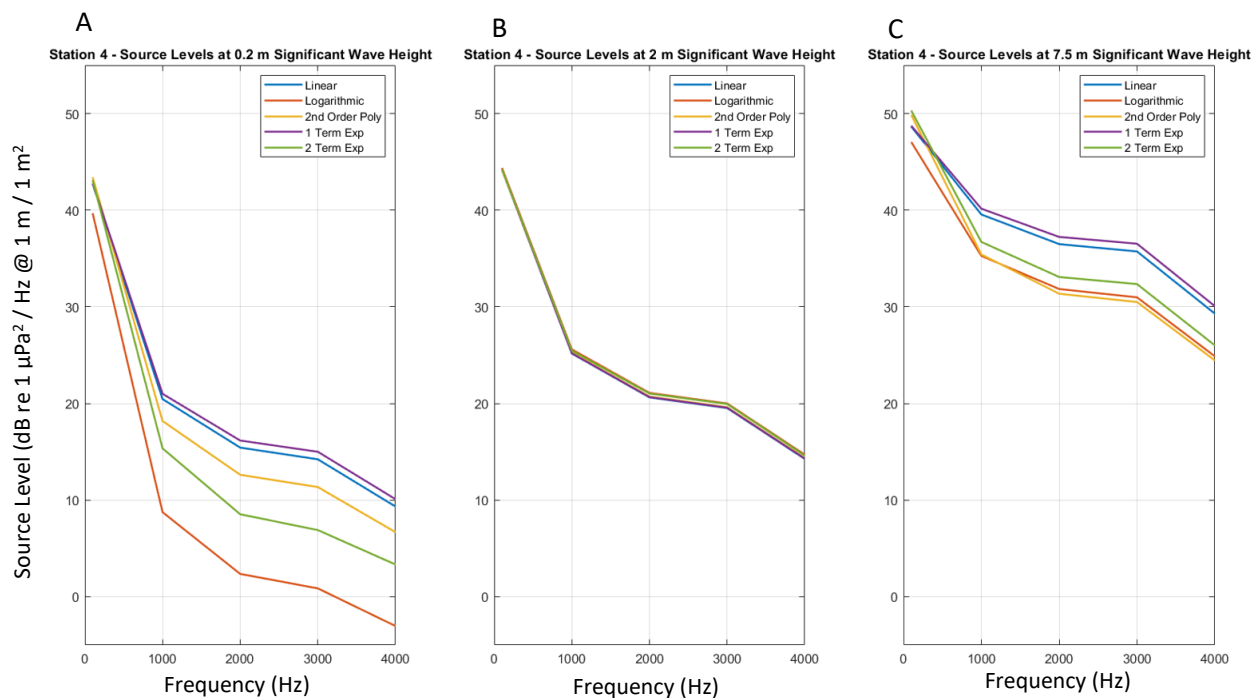
Figure 29: Plot of *SWH* estimated source levels from Station 4 at A) 0.2 m, B) 2 m, and C) 7.5 m *SWH* respectively.

The received levels at 100 Hz cannot be reliably modelled using *SWH*. Referencing Figure 29 and the Beaufort wind table, 0.2 m sea which is generated by 1.6 to 3.3 m/s winds (Payne, 2010), the surface conditions would appear as small, glassy, unbreaking wavelets. A 2 m sea is generated by a moderate to fresh breeze of 8 to 10.7 m/s. Under these conditions, white caps will begin to form, and some spray will tear off the wave crests. A 7.5 m sea is generated by wind speeds of 20.8 to 24.4 m/s and the surface would appear as rolling seas with sea foam blown in streaks and spray affecting visibility. Upon visual inspection, the divergence of the models at small and large wave heights indicates that the model functions best at moderate wave heights.
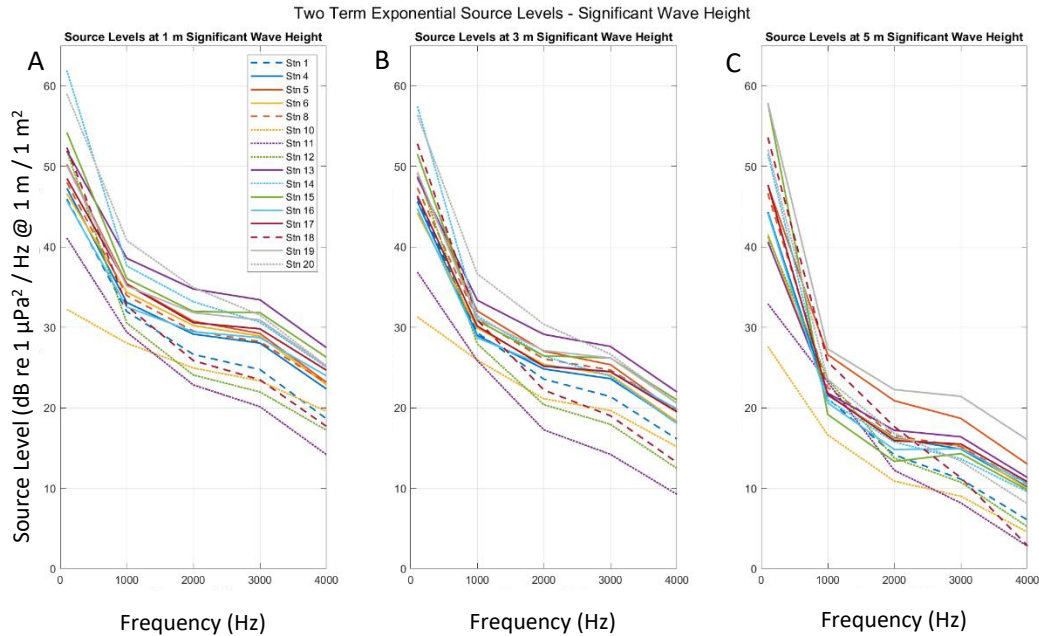
Figure 30: *NSL/A* based on significant wave height, two-term exponential regression for all stations A) 1 m, B) 3 m, C) 5 m significant wave height respectively. Solid lines are slope stations, dashed lines are shelf stations with less than 10% surface ice coverage, dotted lines are shelf stations with greater than 10% surface ice coverage.

At Figure 30, the *SWH NSL/A* values over the slope and shelf respectively group in a less distinctive fashion compared to horizontal wind speed. That is to say that the two groups overlap one another. Considering that the ability to accurately model *RL* using *SHW* is significantly lower than that of horizontal wind, the *NSL/A* values are less accurate.

4.1.3 Significant Height of Wind Waves

The next parameter to be examined is significant height of wind waves at Station 4 which is the average height of the highest third of surface ocean/sea waves generated by the local wind. This is distinct from the *SWH* parameter in that *SWH* represents the highest third of surface ocean/sea waves generated by the wind and the swell (*ERA5*, 2022). Swell tends to be long, rolling waves generated by distant storms and is therefore not a locally generated phenomenon. When comparing the two, conclusions can be made on whether swell is or is not significant on the local ambient noise field.
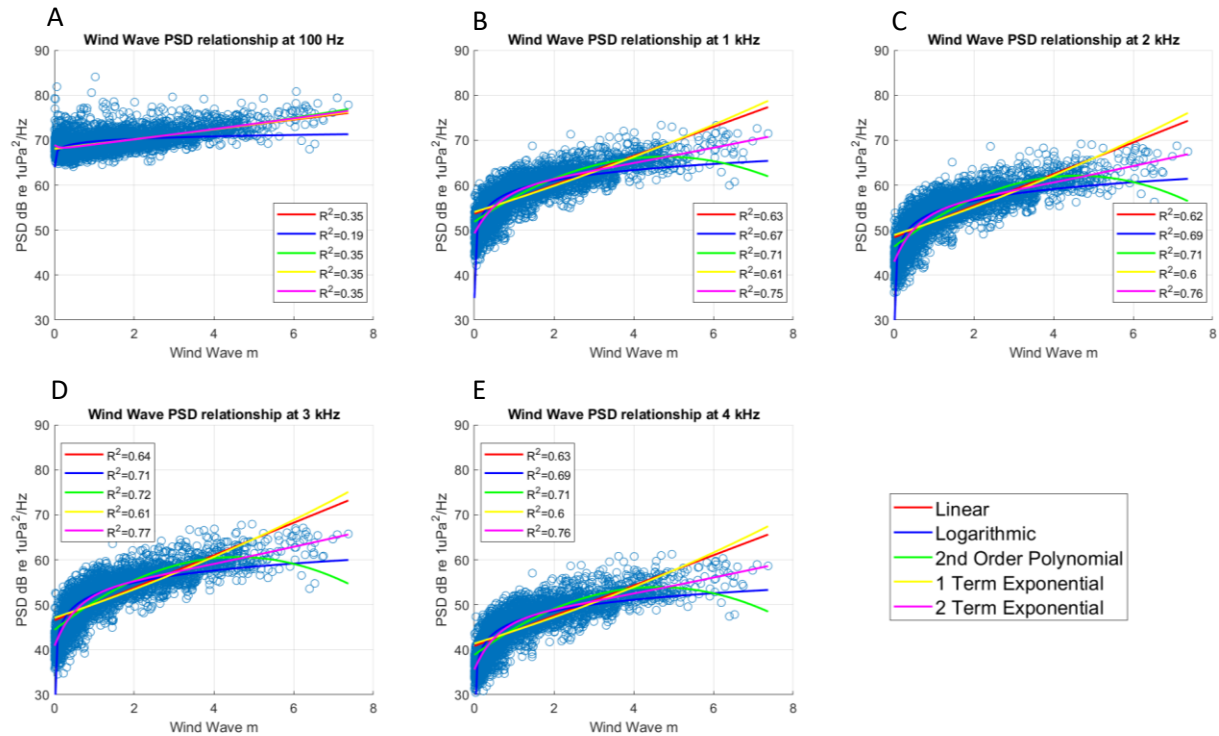
Figure 31: Wind wave models linking the average height of the highest third of surface ocean/sea waves generated by the local wind with hourly minimum sound power levels at Station 4 taken between Jan and June 2016. Figure A) wind wave *PSD* at 100 Hz frequency bin, B) 1 kHz, C) 2 kHz, D) 3 kHz, E) 4 kHz.

At Figure 31 and 32, there is a strong correlation between wind wave and *PSD* in the 1 to 4 kHz band. Within this frequency range, the two-term exponential model was more highly correlated with the data than the logarithmic and 2nd order polynomial. The two-term exponential model ranged between 0.75 and 0.77 R^2 from 1 to 4 kHz. Wind waves are the direct result of the action of the horizontal wind over the local area. Wind waves are colloquially known as "chop" and the average height is shorter than the long, tall, rolling swell. Because wind waves are the child of wind, it would make sense that they model similarly well, and they do. Tabulated data at Table 2 will later show that in the 1 to 4 kHz band, wind wave R^2 is inferior to horizonal wind (U_{10}) R^2 by 0.00 to 0.02 at each respective frequency whether over the shelf or slope.
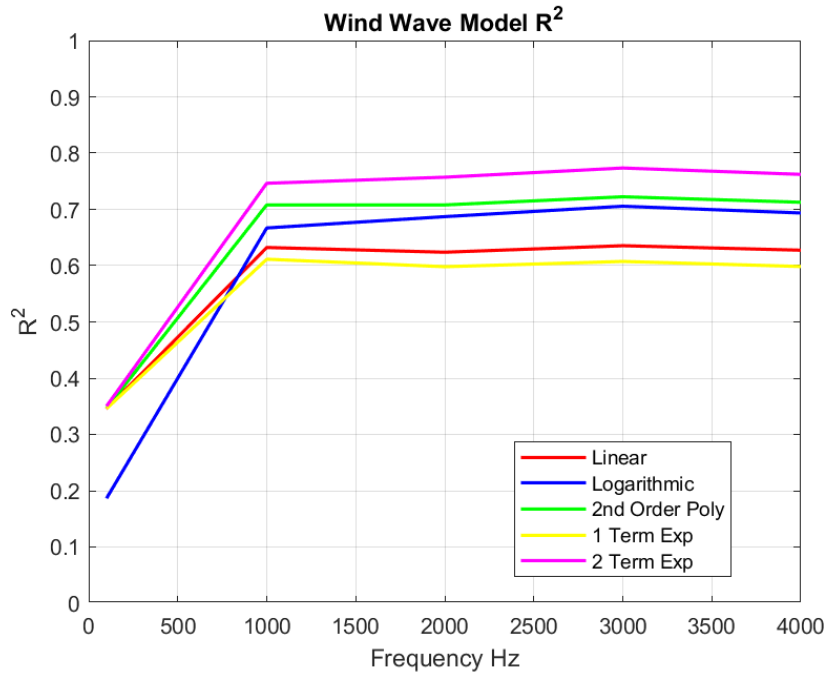
Figure 32: Summary of Station 4 wind wave model R^2.
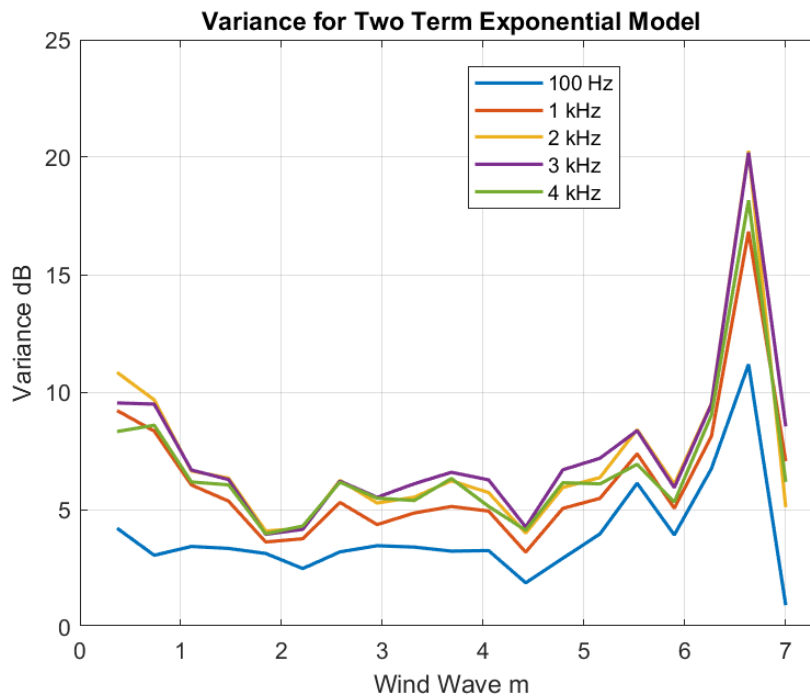
Figure 33: Variance of wind wave model data from Station 4, two-term exponential regression.

At Figure 33, the spike in variance between 6 and 7 m wind wave is due to the relatively few data points within that wave height bin. The variance level within that

bin is not reduced by the voluminous data that would reduce spectral variance as occurred in lower bins and this give the illusion of broad spectral power but in reality, this is a fallacy.
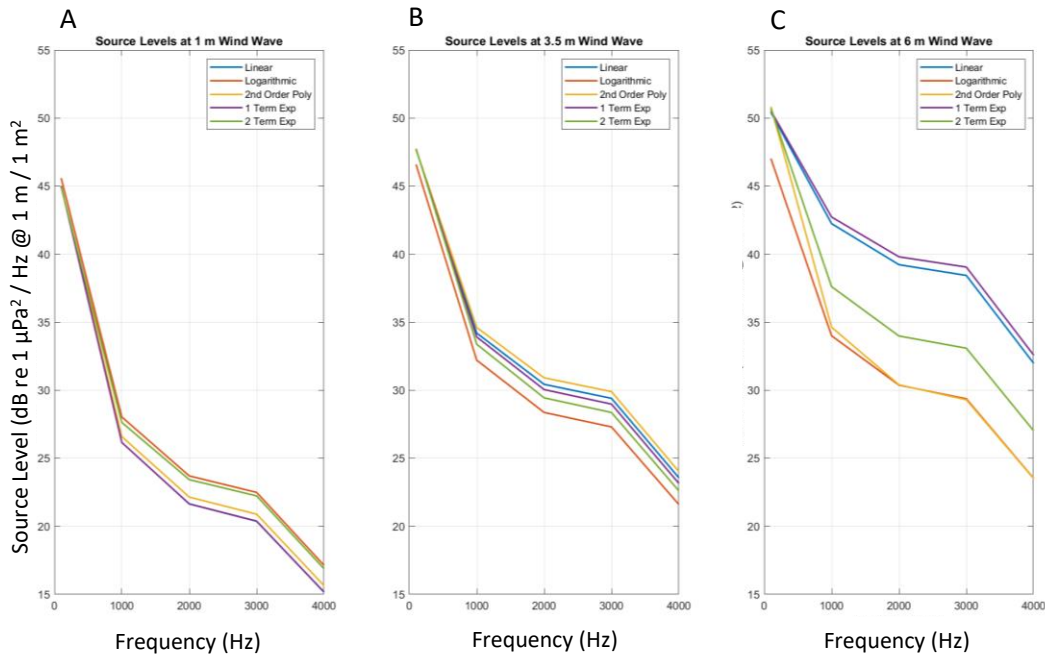
Figure 34: Plot of wind wave estimated source levels from Station 4 at A) 1 m, B) 3.5 m, and C) 6 m wind wave respectively.

Referencing Figure 34 and the Beaufort wind table, 1 m sea which is generated by 5.5 m/s winds (Payne, 2010), the surface conditions would appear as small waves with the possibility of spray. A 3.5 m sea is generated by near gale winds in the vicinity of 13.8 m/s with surface conditions appearing as heaping seas, breaking crests everywhere and some spray. A 6 m sea is generated by gale force winds between 17.2 and 20.7 m/s and violent surface conditions including long, moderately high waves, foam blown in well-marked streaks, and spindrift flying off wave crests. Upon visual inspection, the divergence of the models at large wave heights indicate that the models function dissimilarly, and at small and moderate wave heights, they generate similar answers and function reasonably well.

4.1.4 Edson Wave Age

The next model is Edson wave age. Lin and Sheng (Lin and Sheng, 2020) parametrized the dependences of sea surface roughness on wind speed and sea state. Their analysis indicated that the sea surface roughness is more highly correlated with wave age than wave steepness. This indicates that wave age is more closely related to local wind conditions than swell; swell is a state in which peak wave phase speed

exceeds the local wind speed. Edson wave age uses neutral wind speed 10 m above sea level, U_{10N}. The neutral wind is calculated from the surface stress and the corresponding roughness length by assuming that the air is neutrally stratified; meaning that within the atmospheric boundary layer, the air is a constant temperature and pressure. The neutral wind is slower than the actual wind in stable conditions, and faster in unstable conditions. Lin and Sheng (2020) approximated the relationship between Edson wave age and neutral wind speed by a linear function of neutral wind speed given below in Eqn (31)

$$C_p / u^* = 1/(0.0035\, U_{10N} - 0.0023),\ 1 \leq U_{10N} \leq 30 \text{ m/s} \tag{31}$$

The wave age (C_p/u^*) is defined as the phase speed of the wave spectral peak (C_p) divided by the wind friction velocity (u^*). Wave age units are in s/m.
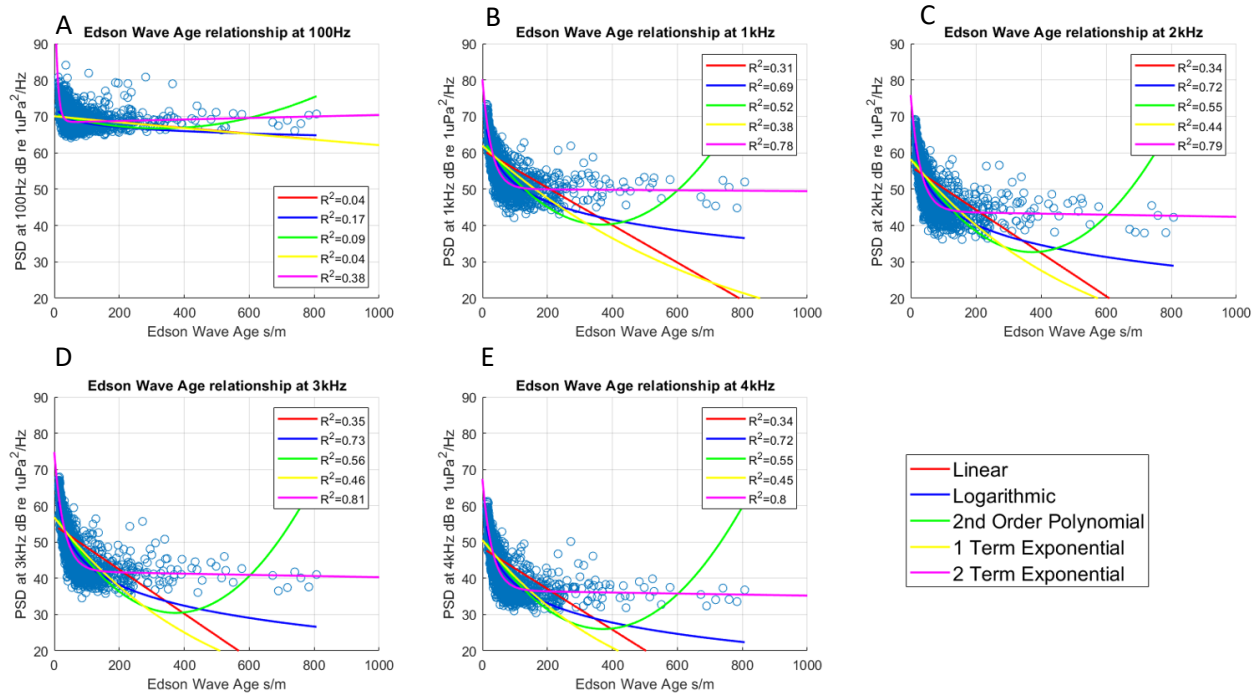
Figure 35: Plot of Edson wave age models at Station 4 linking Edson wave age and hourly minimum sound power levels taken between Jan and June 2016. Figure A) wind *PSD* at 100 Hz frequency bin, B) 1 kHz, C) 2 kHz, D) 3 kHz, E) 4 kHz.
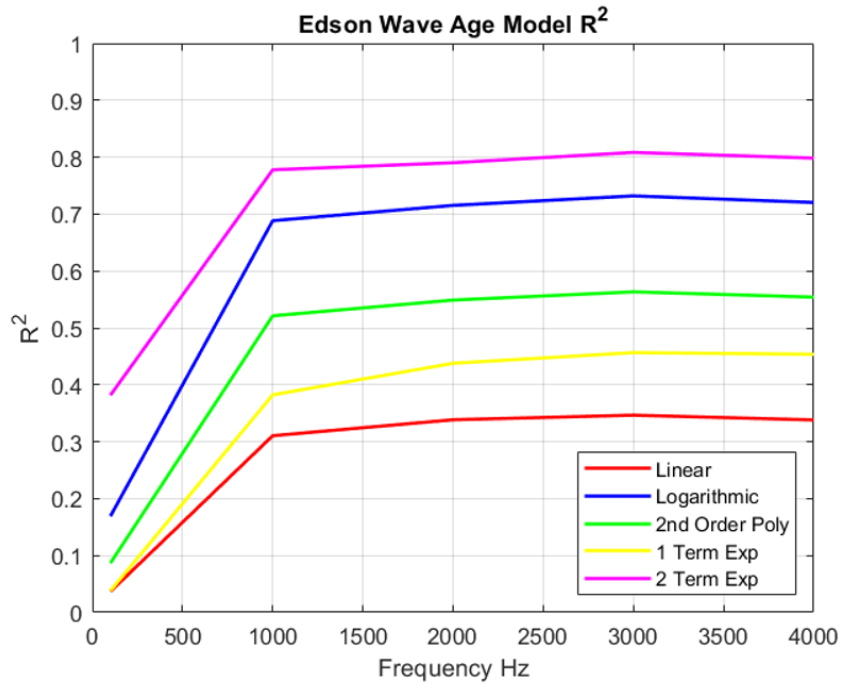
Figure 36: Summary of Station 4 Edson wave age model R^2.

From Figures 35 and 36, the two-term exponential model is the best correlator to the data for the Edson wave age. Most compelling, the Edson wave age is a strong parameter in predicting noise source level. In comparison to horizontal wind speed magnitude, at 100 Hz, wave age correlates 2% better; and from 1 to 4 kHz 5% better. This represents a significant increase in model correlative and source level predicting ability.

It is evident that from 1 to 4 kHz, local wind speed is the primary driver of ambient noise by providing the horizontal stress on the ocean's surface that forms and breaks waves causing them to act as noise sources. Edson wave age, taking into consideration the neutral wind speed derived from wave phase speed and wind friction velocity, has proven to be a strong predictor of ambient noise in the ocean, above horizontal wind speed alone. A unique feature of Edson wave age is its reliance on the two-term exponential function to generate high R^2 values. No other regression function within this parameter can achieve this level of correlation because of its reciprocal relationship with wind speed, shown as Eqn (31).
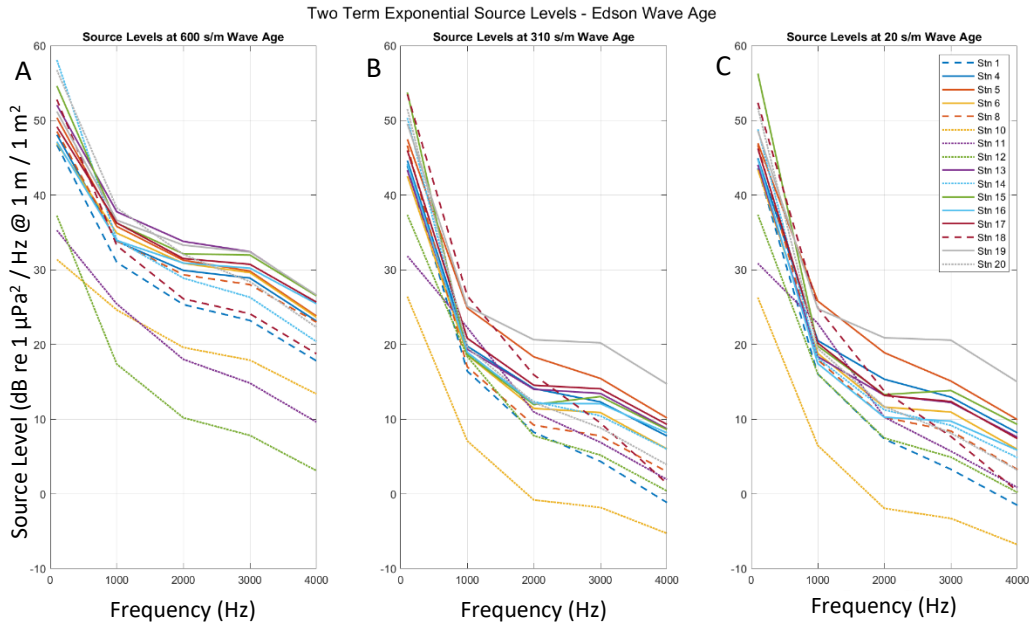
Figure 37: *NSL/A* based on Edson wave age, two-term exponential regression for all stations A) 600 s/m, B) 310 s/m, C) 20 s/m slowness respectively. Solid lines are slope stations, dashed lines are shelf stations with less than 10% surface ice coverage, dotted lines are shelf stations with greater than 10% surface ice coverage.

4.1.5 Neutral Wind Speed Magnitude 10 m Above Sea Level

The neutral wind parameter is calculated from the surface stress and the corresponding roughness length by assuming that the air is neutrally stratified. The neutral wind is slower than the actual wind in stable conditions, and faster in unstable conditions (*ERA5*, 2022). A state of neutrality occurs when there is 0 convective/buoyant contribution to mixing at the air sea interface.
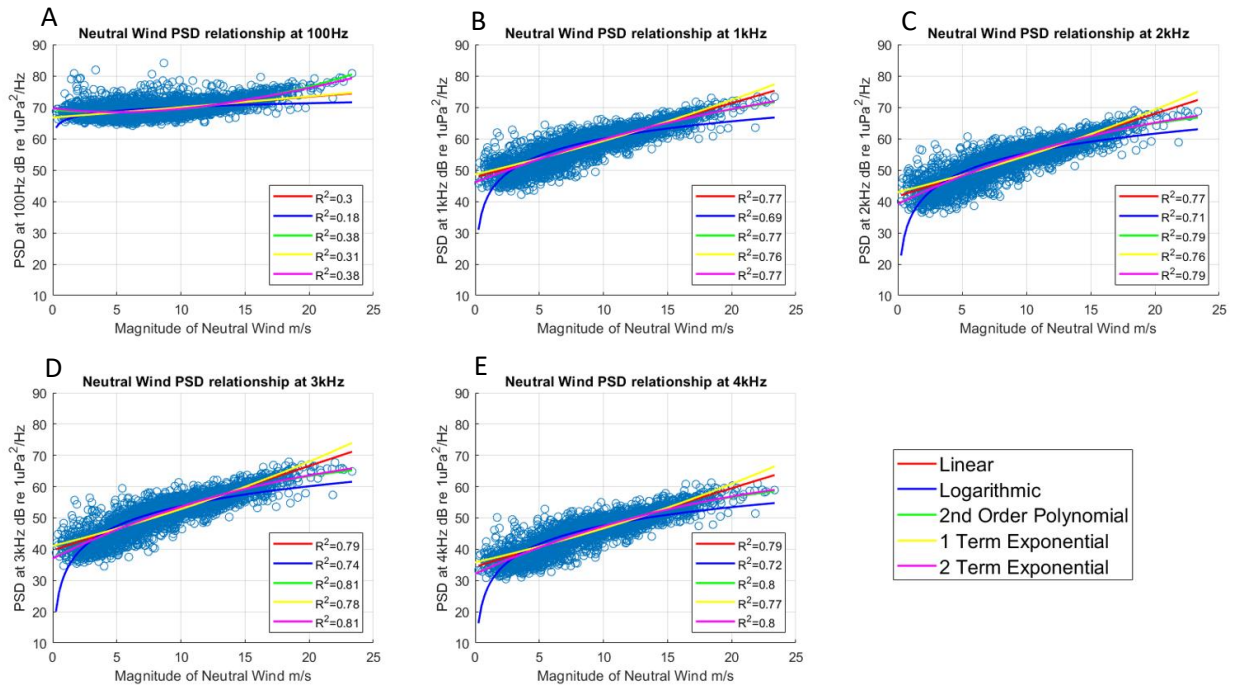
Figure 38: Neutral wind *PSD* models at Station 4 linking neutral wind speed magnitude 10 m above sea level and hourly minimum sound power levels taken between Jan and June 2016. Figure A) wind *PSD* at 100 Hz frequency bin, B) 1 kHz, C) 2 kHz, D) 3 kHz, E) 4 kHz.
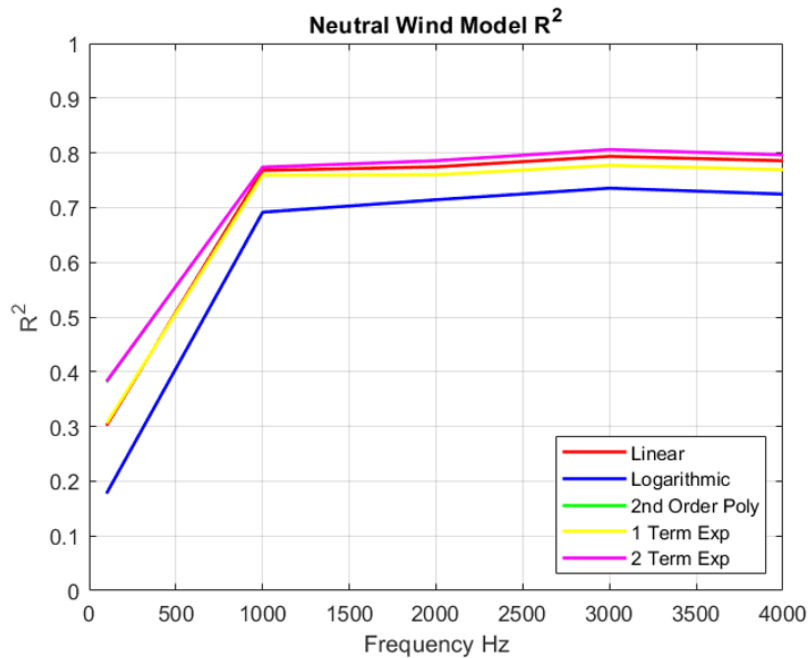
Figure 39: Summary of Station 4 neutral wind model R^2.

Reference Figures 38 and 39, while the highest R^2 values in the neutral wind essentially match the highest R^2 values in the Edson wave age, the Edson wave age parameter requires the two-term exponential function for these values. The next closest function in terms of R^2, the logarithmic function, varies between 7 and 9% lower R^2 than the two-term exponential function from 1 kHz to 4 kHz. While the horizontal wind speed produces lower correlation values with the received level data than the Edson wave age and neutral wind speed, the horizontal wind speed R^2 values between 1 kHz and 4 kHz are within 3% of the highest R^2 values except for the logarithmic function. The fact that all functions but one are generating similar results indicates that neutral wind data depends less on model type. Because the linear function performs similarly to the two-term exponential function, there is a direct relationship between increase in neutral wind speed and *PSD* which is more easily interpretable. Similarly, the neutral wind parameter regressions are all within 3% of the highest R^2 values except for the logarithmic function, from 1 k Hz to 4 kHz. Even at 100 Hz, the neutral wind parameter displays the same combination of strengths when compared with the horizontal wind speed and Edson wave age parameters.
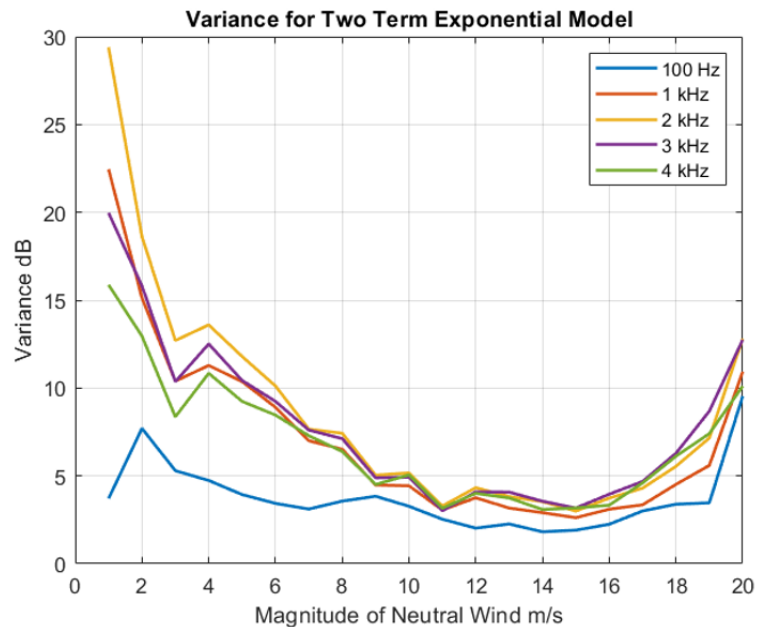
Figure 40: Variance of Station 4 neutral wind model data, two-term exponential regression.

Reference Figure 40, not including the 100 Hz frequency bin, the variance of neutral wind speed displays similar characteristics to horizontal wind speed. At 100 Hz, model variance is low; this is because the 100 Hz data cloud does not vary greatly in *PSD* compared to the other frequency bins. At the other frequency bins, it can be seen that the *PSD* varies mostly at the model extremities and consolidates within 1 dB of one

another between 8 and 16 m/s wind speed. This level of consolidation matches that for horizontal wind speed magnitude. It should be noted that two-term exponential variance for horizontal wind speed is scaled between 0 and 22 dB where the same function for neutral wind is scaled from 0 to 30 dB. However, excluding the 100 Hz frequency bin, neutral wind variance at all frequency bins is at or below 3 dB from 4 to 20 m/s where horizontal wind speed variance is less than or equal to 3 dB from 5 to 19 m/s. That is to say, both datasets behave similarly with respect to the two-term exponential model with slight advantages to the neutral wind model variance at and above 4 m/s wind speed. At slower wind speeds, variance substantially increases which indicates that other acoustical factors begin to manifest. Intuitively, this makes sense as lower wind speeds make less noise and noise from other sources is recorded at the hydrophone.
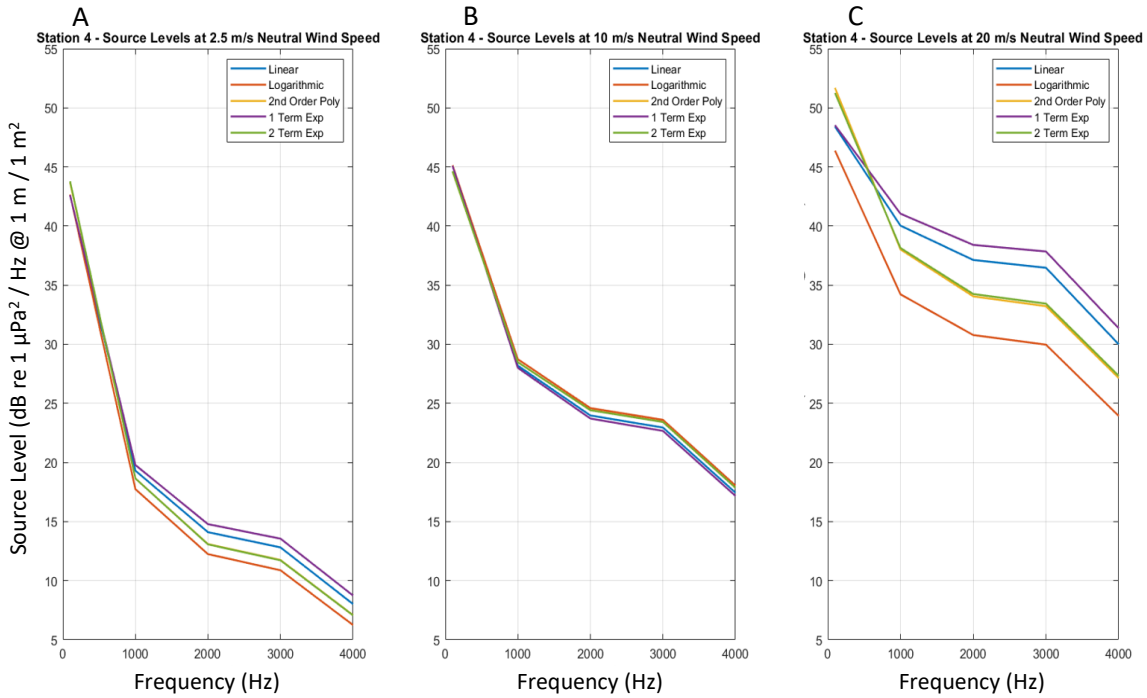
Figure 41: Plot of Station 4 neutral wind estimated source levels at A) 2.5 m/s, B) 10 m/s, and C) 20 m/s wind speed respectively.

Figure 41 indicates that the regression models produce similar results at low and medium wind speeds where at higher wind speeds, the models begin to differ in predictive ability. The two-term exponential and 2nd order polynomial functions produce a similar, high-quality result at low, medium, and high wind speeds.
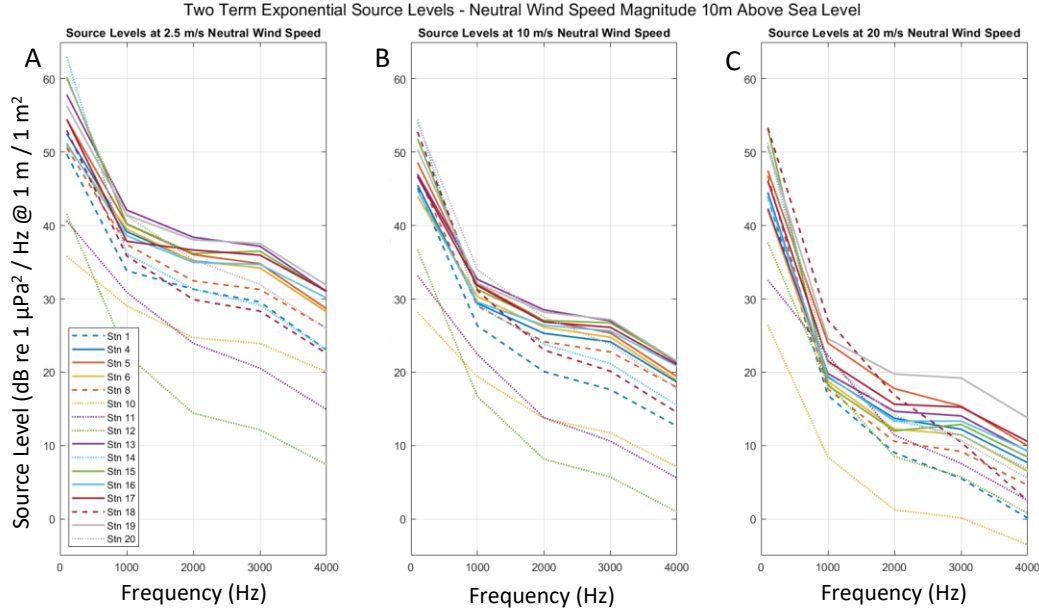
Figure 42: *NSL/A* based on neutral wind speed magnitude 10 m above sea level, two-term exponential regression for all stations A) 2.5 m/s neutral wind speed, B) 10 m/s neutral wind speed, C) 20 s/m neutral wind speed respectively. Solid lines are slope stations, dashed lines are shelf stations with less than 10% surface ice coverage, dotted lines are shelf stations with greater than 10% surface ice coverage.

4.1.6 Charnock Parameter

The Charnock parameter accounts for increased aerodynamic roughness as wave heights grow due to increasing surface stress (ERA5, 2022). The dimensionless Charnock parameter is denoted as α and calculated as

$$\alpha = \hat{\alpha} \Big/ \sqrt{1 - \frac{\tau_w}{\tau}} \,, \tag{32}$$

where τ is the kinematic stress representing the stress of air flow over waves. Values of τ are sea state dependent. τ_w is the stress induced by gravity waves or the "wave stress". In the case of a young wind sea where τ_w becomes the order of the total stress in the surface layer, the value of α is considerably enhanced resulting in an efficient momentum transfer from air to water (*ECMWF* Wave Model, 2022). A greater value of the Charnock parameter corresponds to a greater aerodynamic roughness length over surface waves as wave heights grow due to increasing surface stress.
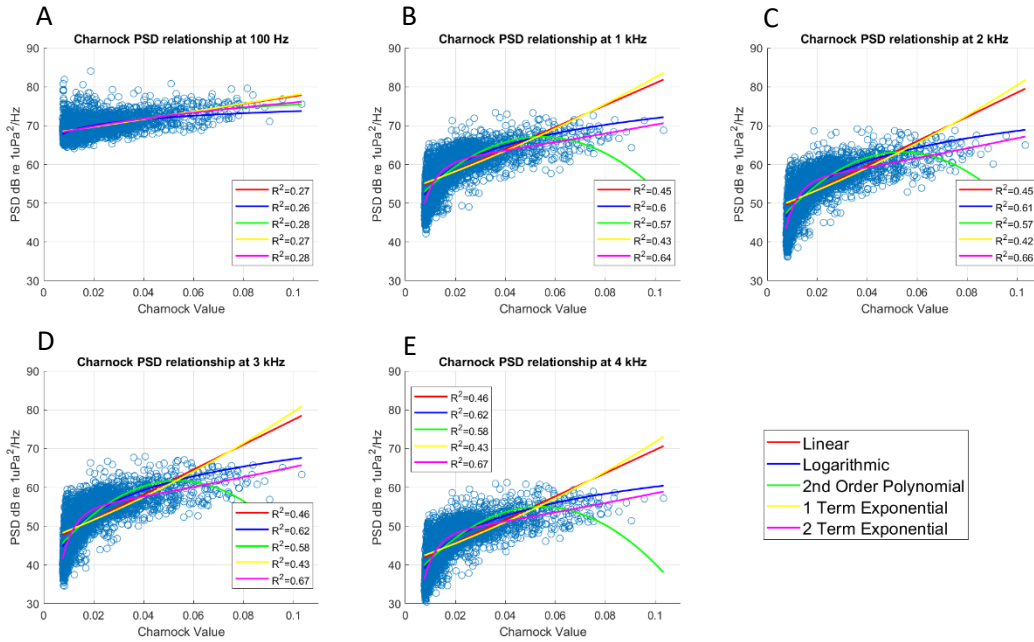
Figure 43: Charnock parameter *PSD* models at Station 4 linking dimensionless Charnock parameter and hourly minimum sound power levels taken between Jan and June 2016. Figure A) Charnock *PSD* at 100 Hz frequency bin, B) 1 kHz, C) 2 kHz, D) 3 kHz, E) 4 kHz.
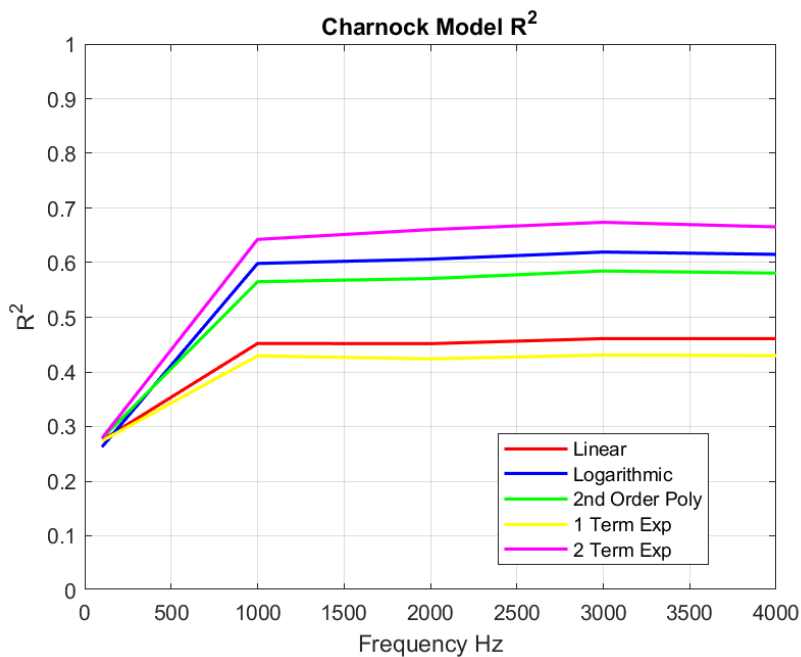
Figure 44: Summary of Station 4 Charnock model R².

Reference Charnock *PSD* models at Figure 43, the data follows a logarithmic distribution although the logarithmic regression function is the second highest performer behind the two-term exponential as with the other parameters. From 1 to 4 kHz, Charnock ranges from R^2 0.64 to 0.67 and cannot compete with the wind based parameters or weighted composite parameters for model accuracy. At 100 Hz, Charnock performs poorly due to the impact of shipping power at this frequency. At Figure 45, Charnock variance expresses a spike between 0.09 and 0.1 at all frequencies however there are so few data points at the upper instances of this metric that the spike is an illusion of variable high and low acoustical power factors. The range in R^2 for all regression functions for all frequencies spans R^2 of mid 0.40 to R^2 of mid 0.60. This is not the greatest range in R^2 that has been seen but it is interesting that no individual regression function performs in a similar fashion to another, or that the regressions are all generating slightly different answers. This is likely because there is a weak relationship between the Charnock parameter and *PSD*; as is seen in Figure 43.
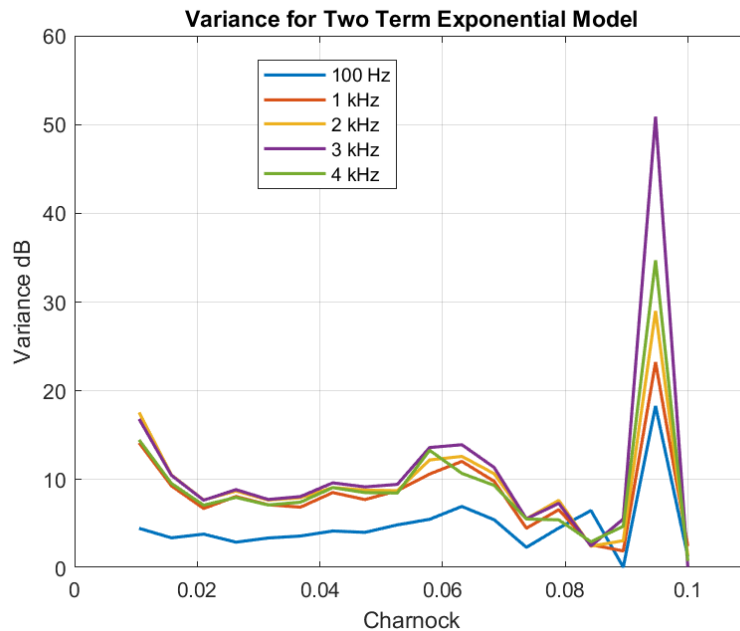
Figure 45: Variance of Station 4 Charnock model data, two-term exponential regression.

The Charnock parameter is unique in that it is developed by referencing neither wind nor wave explicitly but by the stress mechanism that induces wave development from wind. It is an intermediary in that respect and the corresponding R^2 from 1 to 4 kHz reflects this. For example, R^2 modelling places Charnock parameter above *SWH* but below wind wave. Charnock parameter R^2 is inferior to all wind related parameter R^2 at each respective frequency including wave age. It was hypothesized that a parameter directly incorporating wind stress components may offer a unique and robust relationship to hourly minimum sound power levels however Charnock, and by

extrapolation wind stress, does not model well for any regression function and is thus not strongly relatable to hourly minimum sound power level as an individual parameter.
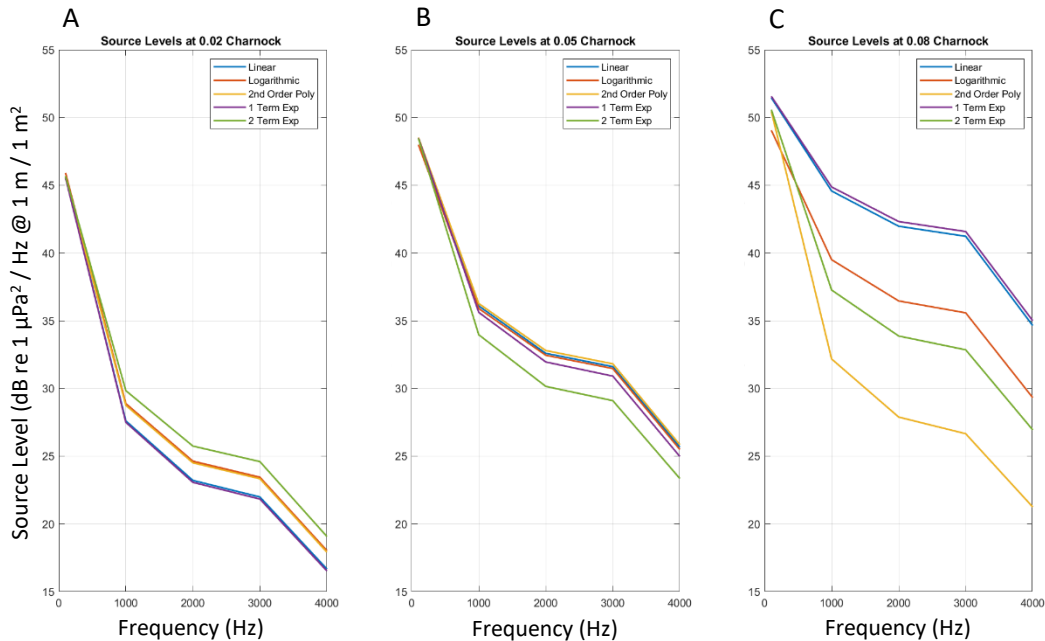
Figure 46: Plot of Station 4 Charnock estimated source levels at A) 0.02 Charnock, B) 0.05 Charnock, and C) 0.08 Charnock respectively.

Figure 46 indicates that the regression models produce similar *NSL/A* results at low and medium values of Charnock where at higher values Charnock, the models vary widely. The two-term exponential and 2nd order polynomial functions produce nearly the exact same low-quality result at low, medium, and high values of Charnock.

4.2 Equally Weighted Composite Neutral Wind 10 m Above Sea Level Plus Significant Height of Combined Wind Waves and Swell

The next parameter is a newly devised equally weighted composite parameter which cultivates the strengths of the neutral wind parameter and the significant wave height parameter. It is apparent that the noise generating acoustic mechanisms of neutral wind and significant wave height do not entirely overlap. Conceptually, the wind or neutral wind is a local phenomenon located above the hydrophone that generate local chop or "wind wave" on the surface. The *SWH* parameter contains significant wind energy imported from regions distant to the hydrophone. To wit, *SWH* is not a subset of local wind conditions, and its acoustical contributions are not necessarily related to the characteristics of the local wind. By combining the acoustic contributions from neutral wind and *SWH* (or wind and *SWH*), a more complete

attribution of sound generating information may be made, modelled, and forecasted. If the cleanest ambient noise field is to be modelled, the model must be free of transient effects including rain, traffic, mammals, ice, etc. In this thesis, the author has gone to lengths to minimize the presence of transient acoustical events in the models and this effort has resulted in remarkable R^2 values using the two-term exponential regression. The addition of the *SWH* term to the equally weighted composite parameter strengthens the models as *SWH* is in some respect almost always present in the coastal and deep-water regions of the ocean. Therefore, it is logical that *SWH* would have the same impact in both coastal and deep waters.

The models at Figure 47 were developed using a three-step process. First, each neutral wind data point and each *SWH* data point were normalized to its respective max over the 6-month study period; second, the respectively normalized data points corresponding to the same date/time group were added together. The normalization process serves to place the neutral wind and the *SWH* parameters on a common scale prior to summation. No information about the magnitude of the neutral wind speed or height of the *SWH* can be determined by examining the x-axis at Figure 47 as at one instant, a weak neutral wind and large *SWH* may add to a similar value as a strong neutral wind and small *SWH*. The x-axis limit is at 2 as the maximum normalized neutral wind value is 1, as is the maximum normalized *SWH* value. Third, the added, respectively normalized neutral wind and *SWH* data points were plotted versus the *PSD* with the corresponding date / time group. Regressions ensued.
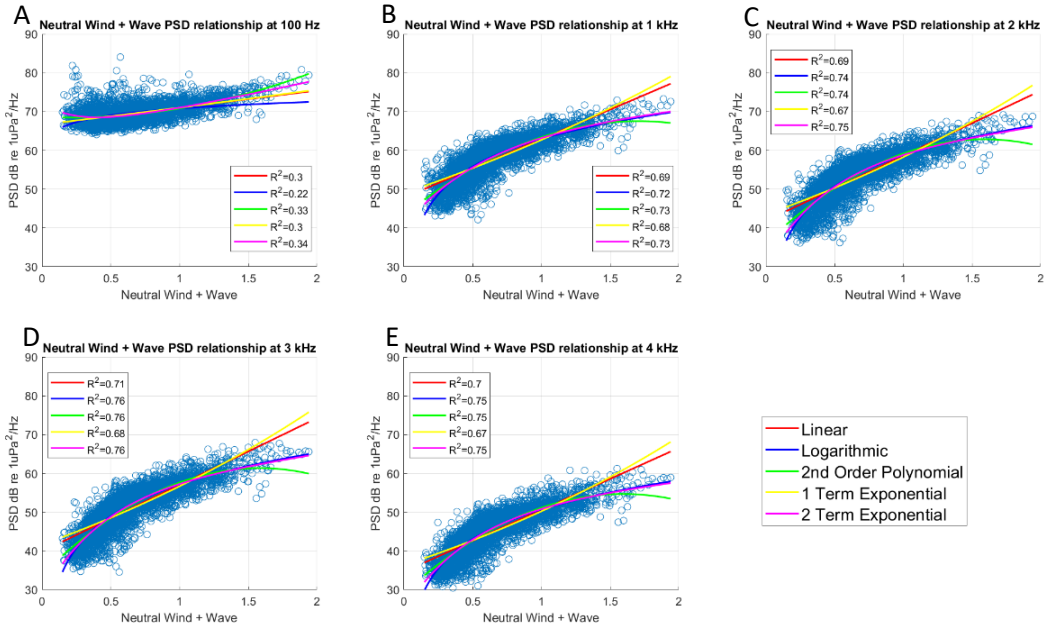
Figure 47: Neutral wind plus *SWH PSD* models at Station 4 linking neutral wind speed magnitude 10 m above sea level plus significant wave height and hourly minimum sound power levels taken between Jan and June 2016. The x-axis is to be interpreted as added values of neutral wind (normalized to max) + *SWH* (normalized to max). Figure A) neutral wind plus wave *PSD* at 100 Hz frequency bin, B) 1 kHz, C) 2 kHz, D) 3 kHz, E) 4 kHz.

Variance for Two Term Exponential Model
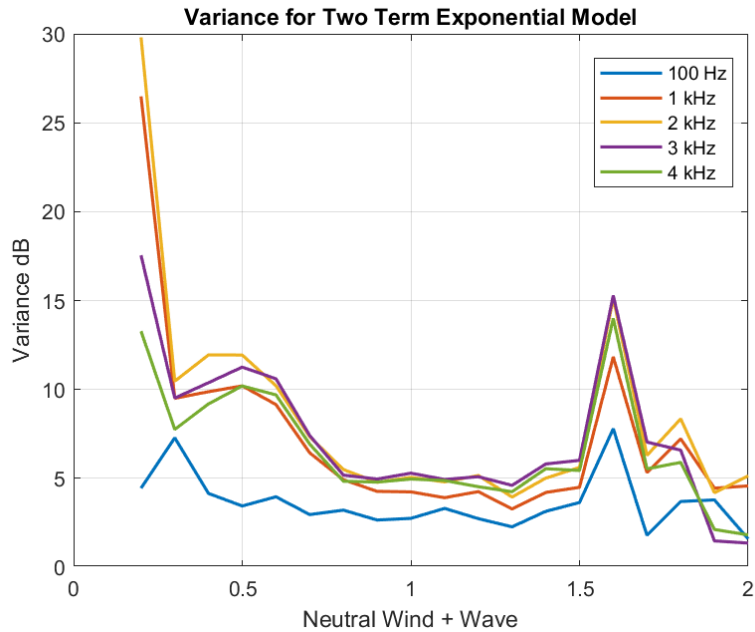
Figure 48: Variance of Station 4 neutral wind plus wave model data, two-term exponential regression.

At Figure 48, as this equally weighted composite parameter is a combination of two separate parameters, its variance is similarly reflected in the variance of its individual constituents.

Figure 49 indicates that the regression models produce extremely similar results at moderate values of neutral wind plus *SWH*. At low and high values, the models begin to differ in predictive ability as the linear and logarithmic models cluster together in one region, and the remaining models cluster at a different region.
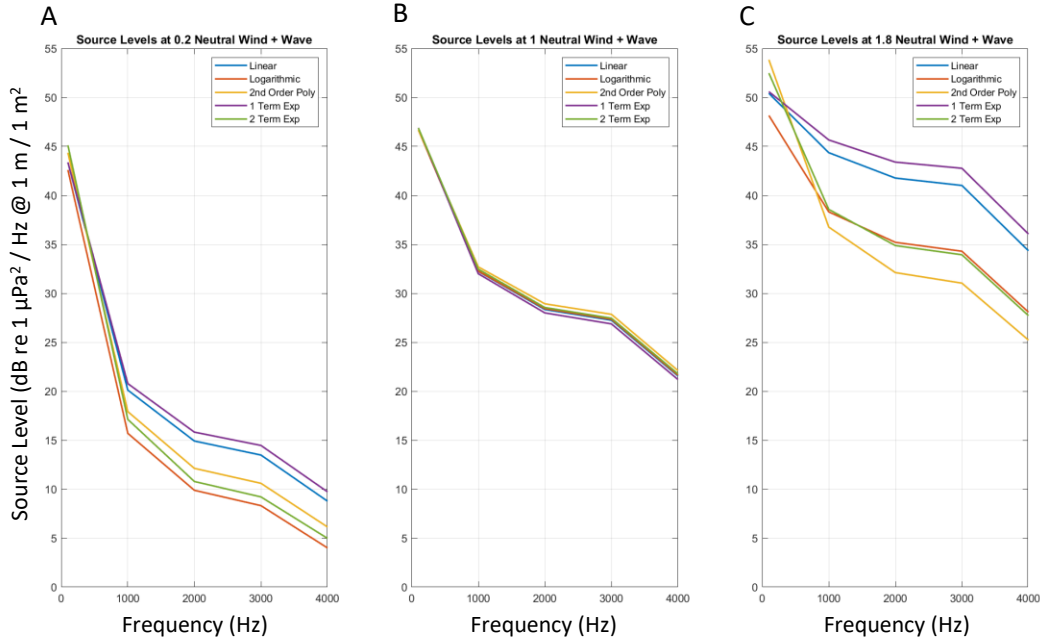
Figure 49: Plot of Station 4 neutral wind plus wave estimated source levels at equally added values of neutral wind (normalized to max) + *SWH* (normalized to max) totalling A) 0.2, B) 1, and C) 1.8 respectively.

4.3 Weighted Composite Parameters

4.3.1 Weighted Composite Neutral Wind 10 m Above Sea Level Plus Significant Height of Combined Wind Waves and Swell

If one were to compare Figure 38 (neutral wind) to Figure 47 (equally weighted, respectively normalized neutral wind + *SWH*), it would appear that neutral wind speed is the superior parameter by an order of 0.04 to 0.05 R^2 across all frequencies when modelling using the two-term exponential function. What is deceptive about Figure 47 is that the plot is generated using equally weighted, respectively normalized to max (over 6-month study period) parameters. X-axis values are derived using Eqn (33).

$$a*(Normalized\ Parameter\ 1) + b*(Normalized\ Parameter\ 2),\ where\ a = b = 1 \qquad (33)$$

However, this type of weighting does not describe the contributive relationship of the normalized parameters, only that they are equally weighted and the R^2 is presented thus. The R^2 is not optimized. The R^2 can be optimized by executing a series of model regressions where the weight of each respectively normalized parameter, formerly known as '*a*', is iterated from 0 to 1 in increments of 0.1 against a constantly held value for the second normalized parameter, formerly known as '*b*'.

72

After one such series, the weight of the second normalized parameter, '*b*' is increased by 0.1 and the iterations of '*a*' begin once again, regression models being generated at each increment of 0.1. This occurs until the weight of the second normalized parameter, '*b*', reaches 1; and, 121 total model regressions would have taken place at each individual frequency. For example, in the first set of model iterations, the weight of *SWH* is held at 0 and neutral wind cycles from weight of 0 to 1 in increments of 0.1. For the second set of iterations, the weight of *SWH* is held at 0.1 and the weight of neutral wind is again cycled from 0 to 1 in increments of 0.1 etc.

The two-term exponential models will generate an R^2 value at each iteration. Out of the 121 model regressions per frequency, the highest R^2 value of the set is associated with a specific weight of '*a*' and '*b*'. By such a process, the optimal set of weighted coefficients is revealed for each respective frequency.

Weighted coefficients '*a*' and '*b*' were reparametrized as α and (1-α) where

$$\alpha = \frac{a}{a+b} \text{ and } (1\text{-}\alpha) = \frac{b}{a+b}, \tag{34}$$

where *a* is the normalized value of neutral wind when maximum R^2 manifested and *b* is the normalized value of *SWH* when the maximum R^2 manifested. (α + (1-α)) = 1 and this is an intuitive way to interpret the respective influence of neutral wind and *SWH* (or any composite combination) under conditions of maximum R^2.

The output of such a process is as Eqn (35) where α and (1-α) are the values of the weighted coefficients which yield the optimized R^2 using the two-term exponential function. Values of α and (1-α) will differ for differing frequencies.

$$\alpha*(Parameter\ 1) + (1\text{-}\alpha)*(Parameter\ 2). \tag{35}$$

As per Figure 50, there are multiple instances of maximum R^2 to two decimal places, however the highest value of R^2 to four decimal places corresponds to the optimal weighting; or, the optimal value of α and (1-α) . The values of the weighted coefficients were determined thus.
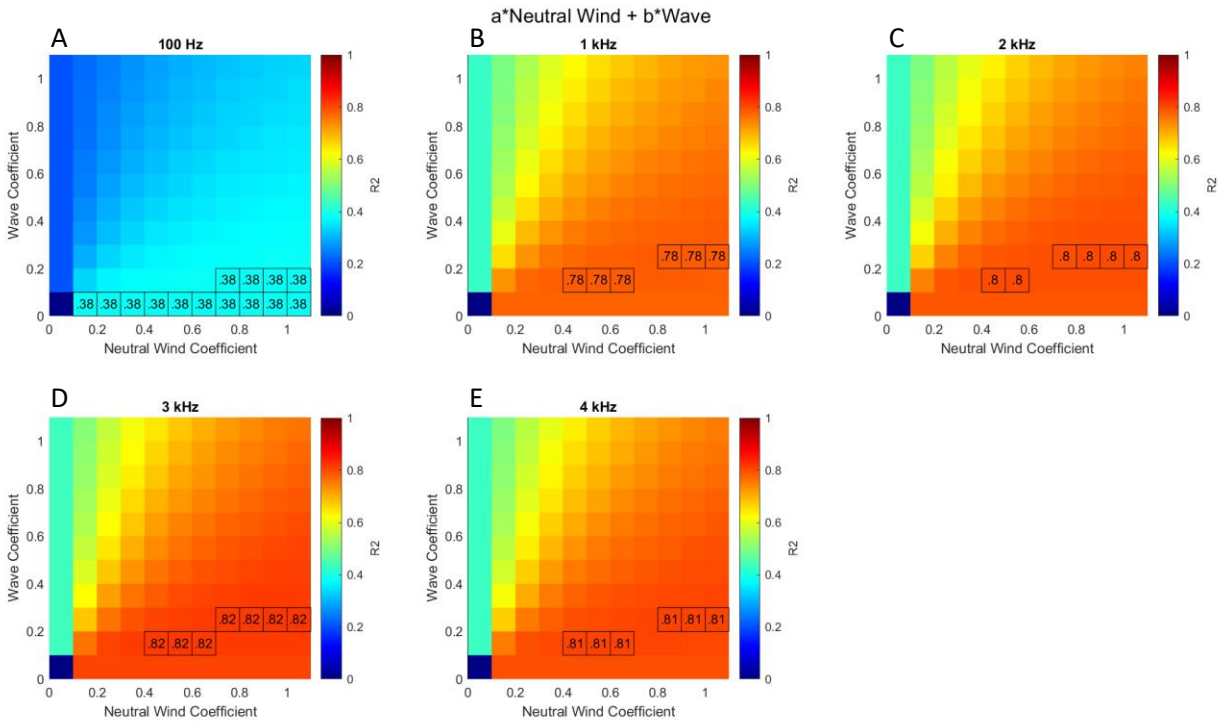
Figure 50: Neutral wind + SWH max R^2 proportionality figures at Station 4 exhibiting the highest R^2 values as a function of respectively normalized, weighted, and summed parameters neutral wind speed magnitude 10 m above sea level and significant wave height. R^2 values were derived using the two-term exponential model. Figure A) neutral wind vs *SWH* proportionality at 100 Hz frequency bin, B) 1 kHz, C) 2 kHz, D) 3 kHz, E) 4 kHz.

Two exceptional cases to the weighting process were Stations 11 and 12 which were covered by surface ice 58% and 62% of the period of study. In those two instances, at 4 kHz, two-term exponential max R^2 was 0.34 and 0.46 respectively and wind played 0 role. Interestingly, when comparing neutral wind plus *SWH* (U_{10N} + *SWH*) with neutral wind plus wind wave (U_{10N} + *WW*) at these two "ice stations", U_{10N} + *SWH* models 0.16 R^2 better at Station 11 and 0.22 R^2 better at Station 12 than when compared with R^2 generated by the U_{10N} + *WW* weighted composite. Or, even simpler, that *SWH* models 0.16 R^2 and 0.22 R^2 better than wind wave at these respective stations. Also, *SWH* R^2 dominated wind wave R^2 at all frequencies studied under conditions of significant surface ice cover and as at 4 kHz, wind played 0 role. This indicates that ambient noise generation under conditions of significant surface ice are likely related to tensile cracking and colliding ice, or at least related to the momentum exchange between *SWH* and ice.

At Figure 50, a fascinating pattern of proportionality emerges at 1 kHz and above where the maximum coefficient of determination occurs at a proportionality of 4 to 6 parts neutral wind to 1-part *SWH*. That is to say that the ambient sound field is optimally modelled by weighting the ambient noise level contributions of neutral wind 4 to 6 times over that of *SWH*. Further, as per Figure 47 at 100 Hz, the R^2 is 0.34 and at Figure 50 at 100 Hz, it is evident that *SWH* plays no significant role; that is to say, whatever relationship exists between the ambient noise field and the parameter neutral wind and *SWH*, *SWH* does not influence the relationship in a significant way. When comparing neutral wind plus *SWH*, neutral wind plus wind wave, and neutral wind the R^2 at 100 Hz is roughly the same for all "non ice stations". R^2 values at 100 Hz for the individual parameters *SWH*, and wind wave are always less than neutral wind. This suggests that neutral wind is the driver for ambient sound at 100 Hz and neither *SWH* nor wind wave play a role.

At Figure 50, if one examines the 4 kHz matrix, there are multiple instances of the highest R^2 of 0.81; however, to 4 decimal places, there is only one top performer. At Station 4, the *PSD* of the top performer can be seen at Figure 51 below and the value of α at each respective frequency is in the caption.
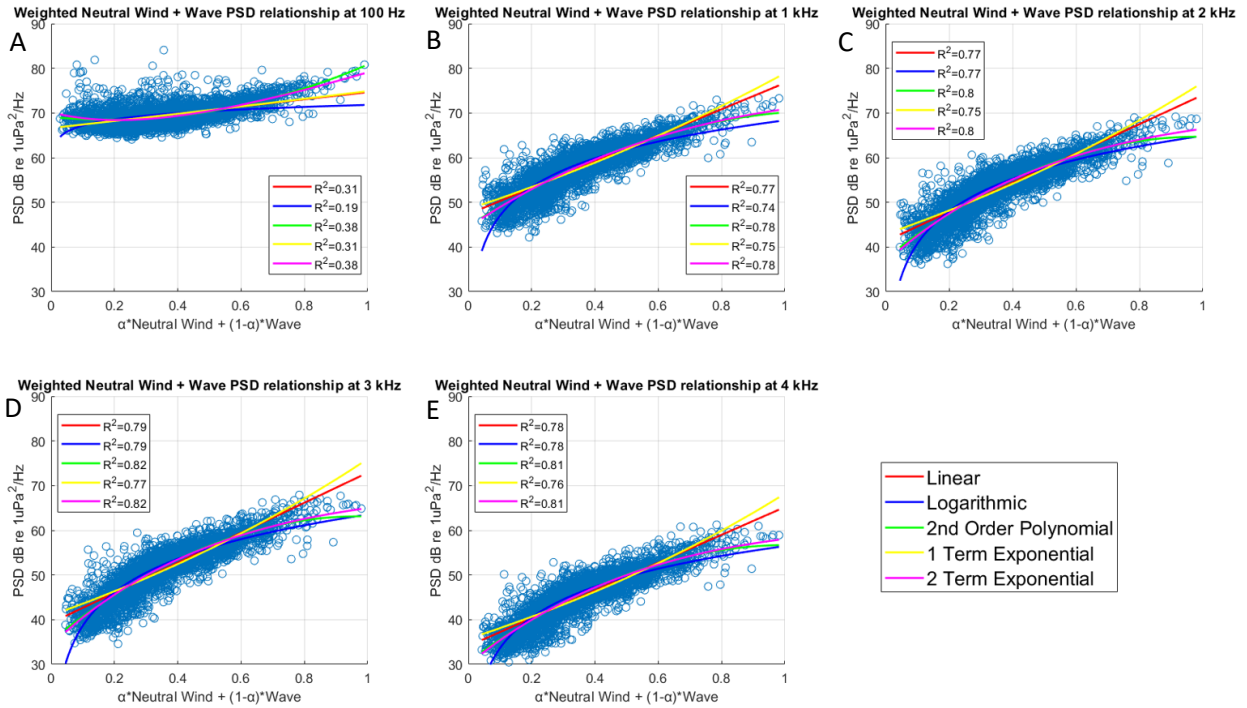
Figure 51: Weighted neutral wind plus *SWH PSD* models at Station 4 expressing value of α*U_{10N} + $(1-\alpha)$*SWH, evaluated at the best performing value of α for the two-term exponential model. Figure A) weighted neutral wind plus wave *PSD* at 100 Hz frequency bin, $\alpha = 0.91$; B) 1 kHz, $\alpha = 0.83$; C) 2 kHz, $\alpha = 0.82$; D) 3 kHz, $\alpha = 0.82$; E) 4 kHz, $\alpha = 0.83$.
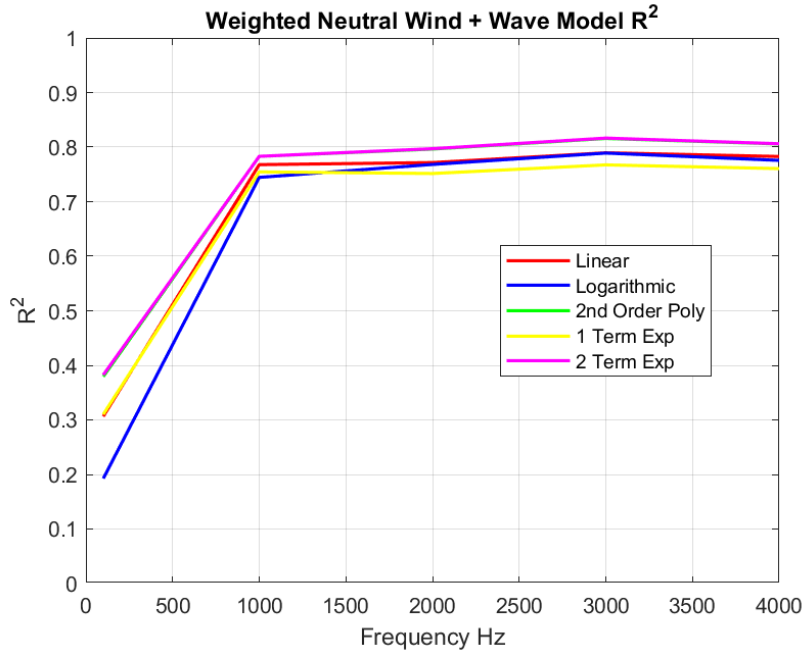
Figure 52: Summary of Station 4 weighted neutral wind plus wave model at the best performing value of α.
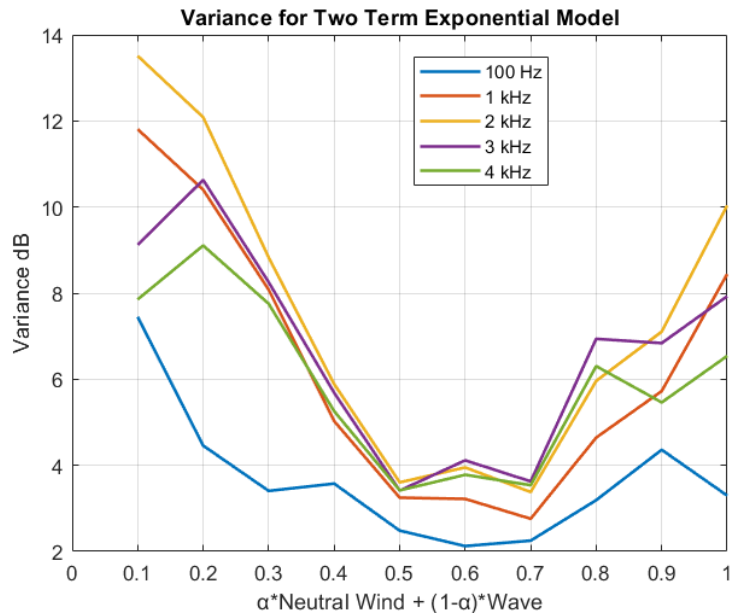
Figure 53: Variance of Station 4 weighted neutral wind plus wave model data, two-term exponential regression.
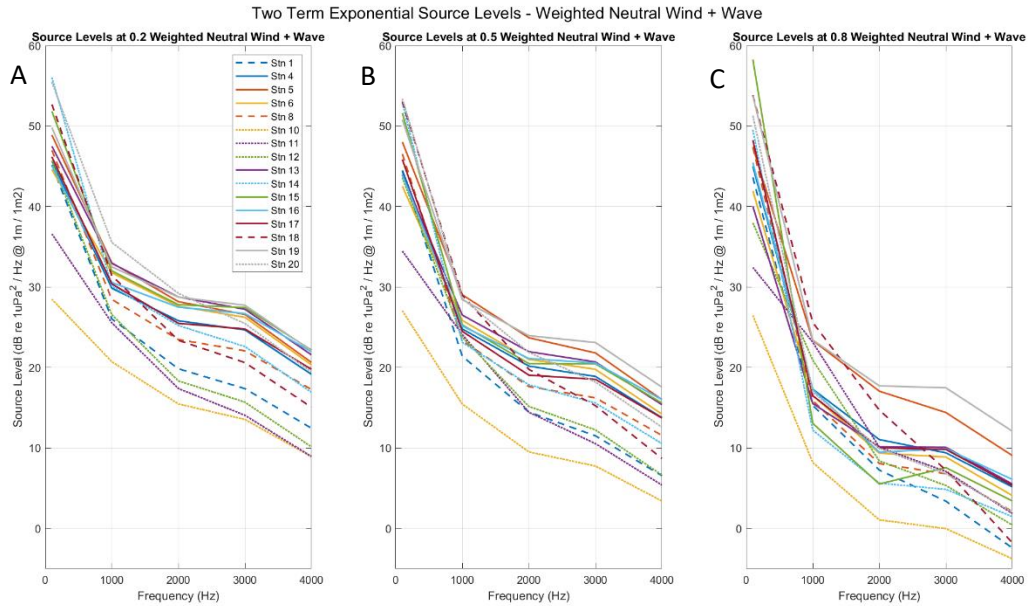
Figure 54: Plot of all stations max two-term exponential R^2 weighted neutral wind plus wave estimated source levels as a function of the respectively normalized, weighted, and added parameters neutral wind speed magnitude 10 m above sea level and *SWH* totalling A) 0.2, B) 0.5, and C) 0.8 respectively.

In Figure 54, the *NSL/A* estimates are built using the best performing R^2 from the best performing parameter. Slope stations are solid lines; shelf stations containing insignificant amounts of mean ice coverage (less than 10%) are dashed lines; and ice stations, or stations containing greater than 10% mean ice coverage are dotted lines.

The weighted U10$_N$ plus *SWH* composite parameter is the choice method for modelling and description of ambient noise fields.

Non-averaged tabulated data (Annex A) comparing weighted neutral wind speed plus *SWH* against weighted neutral wind speed plus wind wave indicates that the *SWH* case can add up to 0.21 R^2 over the wind wave case. This indicates that *SWH* has unique acoustical characteristics that wind wave cannot/does not contribute to an optimized model. Wind wave is never superior to *SWH* in the weighted composite modelling strategy.

4.3.2 Impact of Seismic Exploration and Oil Production on R² Performance of Weighted Composite Neutral Wind 10 m Above Sea Level Plus Significant Height of Combined Wind Waves and Swell
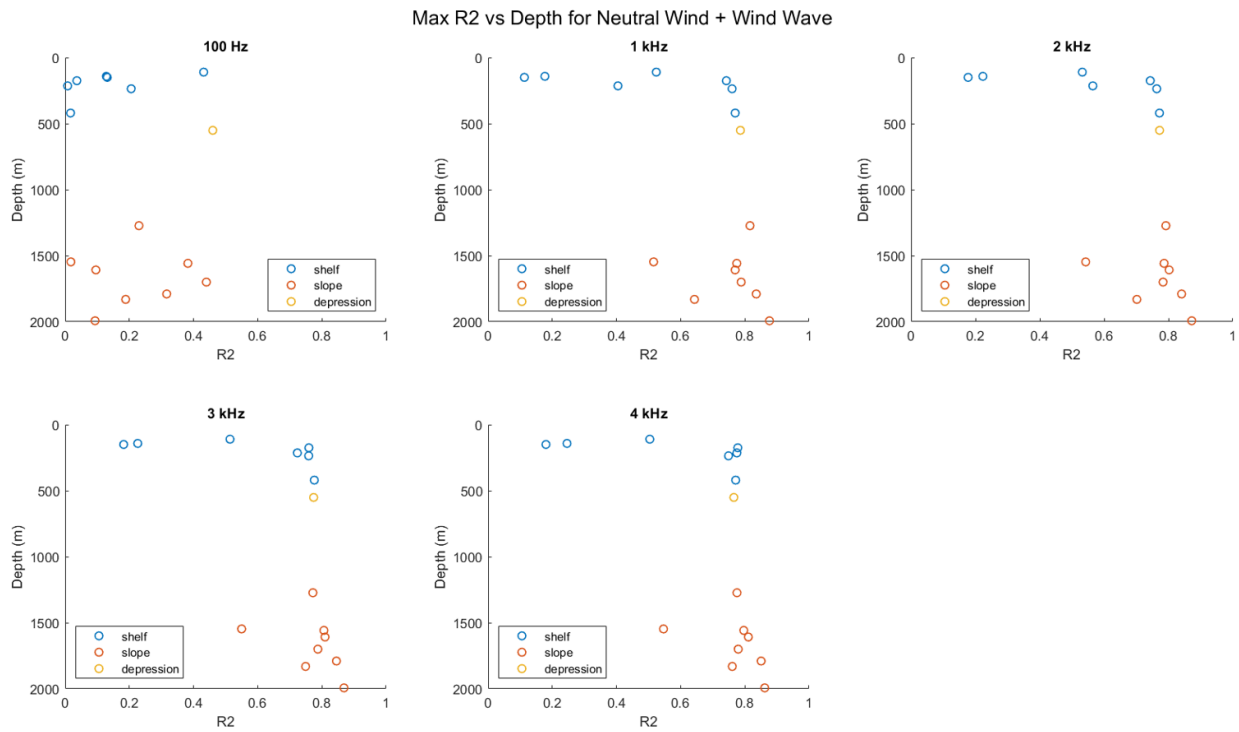
Figure 55: Max R² for all stations vs depth using weighted neutral wind plus wave, two term exponential regression function.
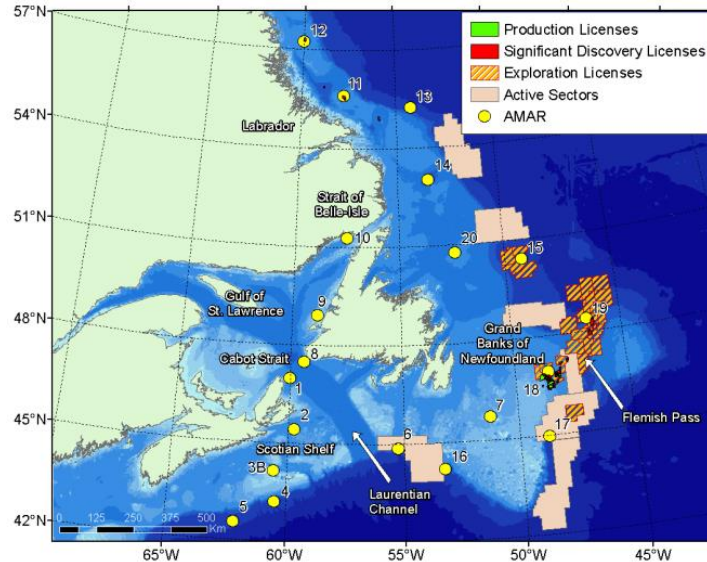
Figure 56: Areas of interest to the oil and gas industry under the jurisdiction of the Canada-Newfoundland and Labrador Offshore Petroleum Board (*CNLOPB)*, in relation to the location of acoustic recorders in this study (reproduced from Delarue et al, 2018).

At Figure 55, the weighted composite function exhibits increasing R^2 with increasing frequency. At 1 and 2 kHz, the shelf stations exhibiting an R^2 at or below 0.6 are ice stations 10, 11, and 12 which are stations with significant instances of ice coverage (greater than 10%); Station 18, a shelf station situated in a region with moderate issuance of seismic exploration and production licences; and Station 19, a slope station situated in a region with significant issuance of seismic exploration licences. The proximity of the exploration and production licences to the acoustic recorders can be seen at Figure 56. According to the Canada Energy Regulator (*CER*, 2022) website, a significant or commercial discovery would be associated with intensive exploration, drilling, and testing, more so than seismic exploration activities. Further, a significant discovery licence does not have an expiry date where a seismic exploration licence does (*CER*, 2022).

Station 18 R^2 improves from 100 Hz, 1 to 4 kHz as 0.014, 0.41, 0.57, 0.73, 0.78. Station 19 fails to express any improvement from 100 Hz, 1 to 4 kHz with R^2 as 0.088, 0.51, 0.54, 0.54, 0.54. As per the jump in R^2 from 2 to 3 kHz, based on the chart in Figure 56, the shelf station (Station 18) is likely affected by seismic exploration and oil production at 100 Hz, 1 and 2 kHz but not at 3 and 4 kHz and the slope station (Station 19) is likely broadly affected by seismic exploration and significant discovery licences from 1 to 4 kHz.

Station 15 is situated in the presence of significant seismic exploration and is on the continental slope at a depth of 1993 m; it is the deepest station in this study. This

station was unaffected by seismic exploration as at 1 kHz: U_{10}, *SWH*, and weighted composite parameter R^2 was 0.86, 0.52, and 0.88 respectively while at 4 kHz: U_{10}, *SWH*, and weighted composite parameter R^2 was 0.84, 0.49, and 0.86 respectively. Conclusions cannot be made as to why slope Stations 15 and 19 exhibit differing model performance however the author speculates that it may be related to the frequency and intensity of seismic exploration activities. To this point, Station 19 is surrounded by significant discovery licences and exploration licences while Station 15 is surrounded only by exploration licences.

The active oil and gas sectors in the vicinity of slope stations 6, 16, and 17 have no significant impact on model performance. Station 6 at 1790 m at 1 kHz expressed 0.80, 0.43, and 0.84 for U_{10}, *SWH*, and weighted composite parameter respectively. At 4 kHz, Station 6 expressed 0.82, 0.41, and 0.85 respectively. Station 16 at 1608 m at 1 kHz expressed 0.73, 0.40, and 0.77 for U_{10}, *SWH*, and weighted composite parameter respectively. At 4 kHz, Station 16 expressed 0.78, 0.41, and 0.82 respectively. Station 17 at 1273 m at 1 kHz expressed 0.79, 0.46, and 0.83 for U_{10}, *SWH*, and weighted composite parameter respectively. At 4 kHz, Station 17 expressed 0.75, 0.44, and 0.79 respectively. Active oil and gas sector activity, either on account of its acoustical frequency output or frequency of occurrence does not degrade model performance in the frequency band of 1 to 4 kHz vs U_{10} or weighted composite parameter when regressed versus hourly minimum sound power levels.

Stations 14 and 20 are of note in the context of the composite neutral wind plus wave parameter as they are both ice stations which exhibited significant improvement in R^2 when compared to their respective individual U_{10} and *SWH* R^2. Station 14 at 1 kHz expressed R^2 of 0.50 and 0.43 for U_{10} and *SWH* respectively but 0.79 using the weighted composite parameter. At 4 kHz, Station 14 expressed R^2 of 0.45 and 0.41 for U_{10} and *SWH* respectively but 0.76 using the weighted composite parameter. Station 20 at 1 kHz expressed R^2 of 0.56 and 0.51 for U_{10} and *SWH* respectively but 0.76 using the weighted composite parameter. At 4 kHz, Station 20 expressed R^2 of 0.53 and 0.50 for U_{10} and *SWH* respectively but 0.76 using the weighted composite parameter. It is worth noting that the ice stations that did not benefit from the weighted composite parameter: Station 10 at a depth of 110 m, Station 11 at a depth of 150 m, and Station 12 at a depth of 142 were shallower than the ice stations that did benefit from the weighted composite parameter: Station 14 at a depth of 551 m, and Station 20 at a depth of 236 m. The ostensible import is that the weighted composite parameter may have the ability to preserve model performance in the presence of sea ice over the continental shelf in depths greater than 200 m.

At 100 Hz, the presence of shipping increases power spectral density variance about the model line which manifests as a substantial decrease in model R^2. In the

absence of significant ice coverage and seismic exploration and oil production, R^2 does not necessarily increase or decrease with hydrophone depth.

4.3.3 Weighted Composite Neutral Wind 10 m Above Sea Level Plus Charnock Parameter
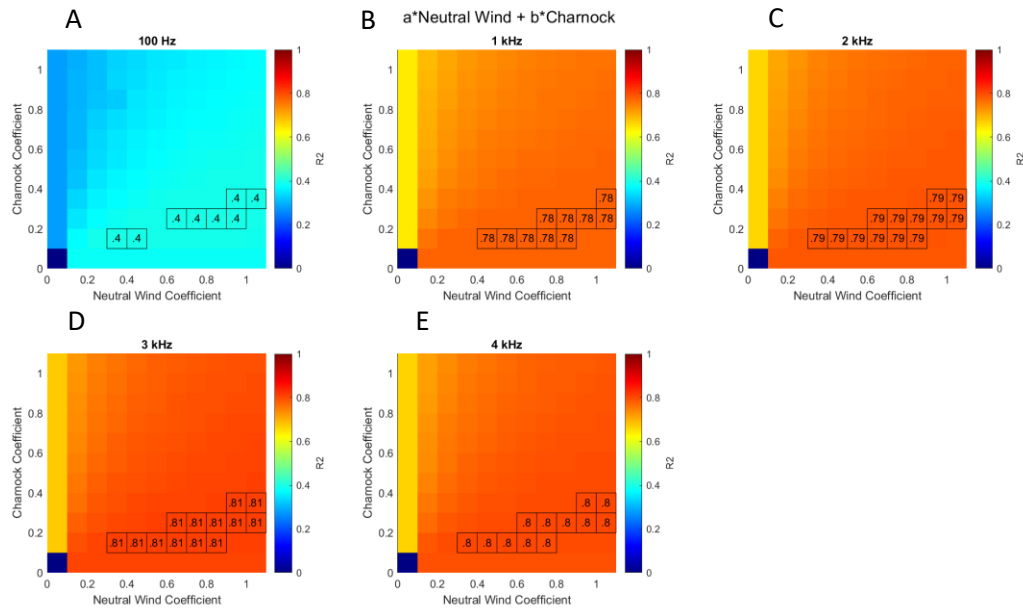
Figure 57: Neutral wind + Charnock max R^2 proportionality figures at Station 4 exhibiting the highest R^2 values as a function of the respectively normalized, weighted, and added parameters neutral wind speed magnitude 10 m above sea level and Charnock using the two-term exponential function. A) neutral wind vs Charnock proportionality at 100 Hz frequency bin, $\alpha = 0.78$; B) 1 kHz, $\alpha = 0.83$; C) 2 kHz, $\alpha = 0.82$; D) 3 kHz, $\alpha = 0.82$; E) 4 kHz, $\alpha = 0.82$.

The Station 4 proportionality figures at Figure 50, neutral wind + *SWH* compared with those at Figure 57, neutral wind + Charnock which demonstrate the max achievable R^2 using the two-term exponential function indicate that these weighted composite parameters perform similarly. However, the former is marginally superior to the latter. Table 2, which expresses averaged R^2 values per frequency over non-ice shelf or slope using the two-term exponential regression proves this fact in a more comprehensive fashion.

The maximum R^2 for neutral wind plus *SWH*, averaged over all non-ice stations, was always equal to or superior to the maximum R^2 for neutral wind plus wind wave using the two-term exponential regression from 100 Hz to 4 kHz. When neutral wind plus *SWH* was superior, it was superior to a maximum extent of R^2 0.01 on either the

shelf or slope. This fine margin of difference indicates that *SWH* is slightly more related to hourly minimum sound power level than wind wave. The Charnock parameter which is an expression denoting the sea state roughness through wave induced stress, exhibits an interesting result when paired with neutral wind as a weighted composite parameter. The maximum R^2 of the weighted neutral wind plus Charnock parameter, averaged over all non-ice stations, was equal the R^2 of the weighted neutral wind plus *SWH* over the shelf at all instances; in the case of the slope, the neutral wind plus *SWH* had an advantage of R^2 0.01. When one examines the maximum R^2 at the individual stations, one finds that the maximum R^2 of weighted neutral wind plus Charnock exceeds the maximum R^2 of weighted neutral wind plus *SWH* by R^2 0.0065 at Station 5 (slope), R^2 0.0018 at Station 8 (shelf), and R^2 0.0047 at Station 19 (slope). While these values are small, the import is that neutral wind and wind stress (Charnock) models have an infrequently occurring superiority unique from that of neutral wind and *SWH* models.

5. Tabulated Results

5.1 Parametric R^2 Performance over Shelf and Slope

Tabulated summaries of parametric R^2 performance based on the two-term exponential regression are in Tables 2 and 3. The first row in dark blue expresses the parameter of which data is presented in the column below it. The first column on the left of the table indicates the frequency corresponding to the parametric data. *SH* refers to continental shelf (shallow), *SL* refers to continental slope (deep). In Table 2, the yellow highlighted columns are to be compared with the red highlighted columns in Table 3. The difference between tables 2 and 3 is contained within the shelf data (*SH*); and only for the highlighted parameters U_{10}, U_{10N}, and weighted composite $U_{10N} + SWH$. U_{10}, U_{10N}, and weighted composite $U_{10N} + SWH$ were given additional study in the form of Table 3 as they were the most promising parameters studied. The difference between the data in Tables 2 and 3 is that Table 2, shelf (*SH*) data is averaged based on 3 shelf stations (Stns 1, 8, 18) which naturally did not have any ice cover during the study period. The Table 3 shelf (*SH*) data expresses data averaged between the non-ice Stations 1, 8, and 18; as well as ice-culled Stations 10, 14, and 20. The process of ice-culling which is described in Section 7, is a process by which if ice is present in the grid above the hydrophone with a concentration of 10% or greater within a given hour, that hour's hydrophone data is culled out of the 6 month hydrophone data set. By this process, the influence of ice on sound propagation and attenuation is deleted and additional useable "ice free" data is made available. Stations 10, 14, and 20 benefitted from this process and Table 3 expresses shelf (*SH*) station R^2 averages for stations 1, 8, 18, 10, 14, and 20. The R^2 values for the weighted composite parameters were the maximum R^2 that manifested after the iterative process described earlier. The values of α are different for each weighted composite parameter, different for each frequency, and different at each station. This can be seen at Table 5.

Table 2: Table summarizing maximum R^2 averages across all <u>non-ice stations</u>. The respective highlighted columns in this table express shelf station data from Stations 1, 8, and 18. Slope station information in this table and Table 3 are the same and correspond to Stations 4, 5, 6, 13, 16, 17, 19.

Freq	U_{10}	Edson Wave Age	U_{10N}	SWH	WW	Char Param	$\alpha*U_{10N} + (1-\alpha)*SWH$	$\alpha*U_{10N} + (1-\alpha)*WW$	$\alpha*U_{10} + (1-\alpha)*SWH$	$\alpha*U_{10N} + (1-\alpha)*Char$
4 kHz SH:	0.75	0.76	0.77	0.45	0.74	0.68	0.77	0.77	0.76	0.77
SL:	0.74	0.74	0.77	0.42	0.74	0.62	0.78	0.77	0.76	0.77
3 kHz SH:	0.73	0.73	0.74	0.45	0.71	0.65	0.75	0.75	0.74	0.75
SL:	0.74	0.74	0.77	0.42	0.74	0.59	0.78	0.77	0.76	0.77
2 kHz SH:	0.67	0.67	0.68	0.42	0.65	0.60	0.69	0.69	0.68	0.69
SL:	0.73	0.73	0.76	0.42	0.73	0.60	0.77	0.76	0.75	0.76
1 kHz SH:	0.62	0.62	0.62	0.41	0.60	0.56	0.64	0.63	0.62	0.64
SL:	0.72	0.72	0.75	0.42	0.72	0.57	0.76	0.75	0.74	0.75
100 Hz SH:	0.01	0.01	0.02	0.01	0.01	0.01	0.02	0.02	0.02	0.02
SL:	0.21	0.21	0.22	0.15	0.20	0.14	0.23	0.22	0.22	0.22

Mean and peak wave periods had nil relationship with recorded acoustic power. Friction velocity had sub R^2 0.20 at all frequencies with recorded acoustic power. These three parameters were not tabulated for this reason. In Table 2, while U_{10N} + SWH is the top performing parameter in terms of R^2, it is computationally complex. U_{10N} as an individual parameter yields similar R^2 values and U_{10N} information is easily extracted from an online database. Even simpler is the U_{10}, parameter which can be measured by handheld anemometer on a ship at sea. The U_{10} values are also similar to those of the U_{10N} + SWH and the ease of measurement of this parameter is its strength. It requires no computer nor sophisticated calculation and the result is good.

The author found the comparison between *WW*, *SWH*, and Charnock as individual parameters with their composite U_{10N} corollary very interesting. *SWH* R^2 from 1 to 4 kHz is poor expressing a range from 0.41 to 0.45, whether on the shelf or slope. This is followed by the better Charnock parameter with a R^2 range from 0.56 to 0.68 whether on the shelf or slope, and the reasonably good *WW* parameter with a R^2 range from 0.60 to 0.74, also whether over the shelf or slope. However, the U_{10N} + *SWH* composite, U_{10N} + Charnock composite, and U_{10N} + *WW* composite holistically achieve the highest R^2 values seen in this study. Interestingly, U_{10N} + *SWH* performs best, followed by U_{10N} + Charnock which is followed by U_{10N} + *WW* with only marginal performance differences between them; however, this is the exact opposite performance trend of *SWH*, Charnock, and *WW* as individual parameters.

Table 3: Table summarizing maximum R^2 averages across all <u>non-ice shelf and slope stations plus ice-culled shelf stations.</u> The respective highlighted columns in this table express shelf station data from Stations 1, 8, 18, 10, 14, and 20. R^2 for slope stations are the same as in Table 2 (significant ice coverage was present only over shelf stations).

Freq	U_{10}	Edson Wave Age	U_{10N}	SWH	WW	Char Param	$\alpha*U_{10N} + (1-\alpha)*SWH$	$\alpha*U_{10N} + (1-\alpha)*WW$	$\alpha*U_{10} + (1-\alpha)*SWH$	$\alpha*U_{10N} + (1-\alpha)*Char$
4 kHz SH:	0.76		0.77				0.77			
SL:	0.74	0.74	0.77	0.42	0.74	0.62	0.78	0.77	0.76	0.77
3 kHz SH:	0.74		0.76				0.76			
SL:	0.74	0.74	0.77	0.42	0.74	0.59	0.78	0.77	0.76	0.77
2 kHz SH:	0.71		0.73				0.73			
SL:	0.73	0.73	0.76	0.42	0.73	0.60	0.77	0.76	0.75	0.76
1 kHz SH:	0.69		0.70				0.70			
SL:	0.72	0.72	0.75	0.42	0.72	0.57	0.76	0.75	0.74	0.75
100 Hz SH:	0.22		0.22				0.22			
SL:	0.21	0.21	0.22	0.15	0.20	0.14	0.23	0.22	0.22	0.22

Table 3 expresses R^2 averages for combined non-ice <u>and</u> ice-culled shelf stations, as well as slope stations during acoustically quiet periods. Data is tabulated for Shelf Stations 1, 8, 18, 10, 14, 20 and Slope Stations 4, 5, 6, 13, 15, 16, 17, 19. The new data in this table compared to Table 2 is exclusively that of the highlighted shelf stations (*SH*) data which consists of average R^2 data for shelf stations 1, 8, 18, 10, 14, and 20. Stations 10, 14, and 20 were culled for ice and the ice free acoustical data was regressed such that it could be included with the naturally non-ice station data for larger data set generalized conclusions.

Table 4: Table summarizing R² range across slope and non-ice shelf stations for weighted composite neutral wind + *SWH*, and, weighted composite neutral wind + Charnock. Data is tabulated for Shelf Stations 1, 8, 18 and Slope Stations 4, 5, 6, 13, 15, 16, 17, 19.

Frequency	Slope Station R^2 Range $\alpha*U_{10N} + (1-\alpha)*SWH$	Shelf Station R^2 Range $\alpha*U_{10N} + (1-\alpha)*SWH$
4 kHz	0.54 – 0.86	0.77 – 0.78
3 kHz	0.54 – 0.87	0.73 – 0.77
2 kHz	0.54 -0.87	0.57 – 0.77
1 kHz	0.51 – 0.88	0.41 – 0.77
100 Hz	0.08 – 0.44	0.01 – 0.03
Frequency	Slope Station R^2 Range $\alpha*U_{10N} + (1-\alpha)*Char$	Shelf Station R^2 Range $\alpha*U_{10N} + (1-\alpha)*Char$
4 kHz	0.55 – 0.86	0.77 – 0.77
3 kHz	0.55 – 0.86	0.72 – 0.77
2 kHz	0.54 – 0.87	0.56 – 0.77
1 kHz	0.51 – 0.87	0.41 – 0.77
100 Hz	0.01 – 0.44	0.00 – 0.03

Parametric R^2 performance in the 1 to 4 kHz band from best to worst is as follows:

1. Weighted neutral wind (U_{10N}) plus significant wave height (*SWH)*

2. Weighted neutral wind (U_{10N}) plus Charnock parameter

3. Weighted neutral wind (U_{10N}) plus wind wave (*WW*)

4. Neutral wind (U_{10N})

5. Weighted horizontal wind (U_{10}) plus significant wave height (*SWH)*

6. Edson wave age

7. Horizontal wind (U_{10})

8. Wind wave (*WW*)

9. Charnock parameter

10. Significant wave height (*SWH*)

However, when ease of measurement, ease of use in computations, strength of R^2, and intuitive quality are considered, U_{10} is the preferred parameter. The difference in

R^2 performance between the leading model (weighted neutral wind plus *SWH*) and U_{10} is less than 0.04, or approximately 5%.

5.2 Optimized Coefficients for Weighted Composite Parameters

Table 5: Table summarizing mean maximum R^2 across slope and non-ice shelf stations for weighted neutral wind + *SWH*, and, weighted neutral wind + Charnock, as well as corresponding values for weight coefficients α and $(1-\alpha)$. Data is tabulated for Shelf Stations 1, 8, 18 and Slope Stations 4, 5, 6, 13, 15, 16, 17, 19.

Freq	$\alpha*U_{10N} + (1-\alpha)*$Char R^2	$\alpha*U_{10N} + (1-\alpha)*$Charnock Mean Weighted Coefficient		$\alpha*U_{10N} + (1-\alpha)*$SWH R^2	$\alpha*U_{10N} + (1-\alpha)*$SWH Mean Weighted Coefficient	
		α	$(1-\alpha)$		α	$(1-\alpha)$
4 kHz SH:	0.77	0.863	0.136	0.77	0.916	0.083
SL:	0.77	0.857	0.142	0.78	0.848	0.151
Mean:	0.77	0.858	0.141	0.78	0.866	0.133
3 kHz SH:	0.75	0.877	0.122	0.75	0.916	0.083
SL:	0.77	0.863	0.136	0.78	0.841	0.158
Mean:	0.76	0.867	0.132	0.77	0.861	0.138
2 kHz SH:	0.69	0.869	0.130	0.69	0.869	0.130
SL:	0.76	0.875	0.124	0.77	0.830	0.169
Mean:	0.74	0.873	0.126	0.75	0.841	0.158
1 kHz SH:	0.64	0.827	0.172	0.64	0.848	0.151
SL:	0.75	0.886	0.113	0.76	0.838	0.161
Mean:	0.72	0.870	0.129	0.72	0.840	0.159
100 Hz SH:	0.02	0.691	0.308	0.02	0.740	0.259
SL:	0.22	0.862	0.137	0.23	0.790	0.209
Mean:	0.16	0.816	0.183	0.17	0.776	0.223

Per Table 2, weighted neutral wind plus *SWH* R^2 outperformed weighted neutral wind plus Charnock from R^2 0.01 on the continental slope and is equal on the continental shelf. Per Table 5, when examining the influence afforded to either of two members of a weighted composite parameter, that is, the value of α and/or $(1-\alpha)$, the weighted neutral wind plus *SWH* indicates that from 1 to 4 kHz, there is an increasing dependence on neutral wind with increasing frequency and therefore a decreasing dependence on *SWH* with increasing frequency. However, in the same band, the weighted neutral wind plus Charnock parameter indicates increasing dependence on neutral wind from 1 to 2 kHz and then a decreasing dependence on neutral wind from 3 to 4 kHz.

The simplified relationship between horizontal wind (U_{10}) and Charnock is such that more wind speed leads to more surface stress resulting in more friction drag, generating higher sea state resulting in an increased Charnock parameter. In effect, there is a direct relationship between the total stress in the surface layer with Charnock parameter.

Neutral wind is unique from horizontal wind in that neutral wind assumes atmospheric stability and the absence of turbulent convective and buoyant contributions to mixing at the air/sea interface. *SWH* represents the average height of the highest third of surface ocean/sea waves generated by wind and swell. It is evident that wind, waves, and Charnock are mechanically related. Wind wave is a subset of the forcing mechanisms of local wind, *SWH* is a representation of the forcing mechanisms of distant and persistent wind effects, and Charnock is related to local stress; or related to the resultant stresses of the local winds upon the local waves, be they wind wave or *SWH* or a combination.

6. Cross Correlations

6.1 Cross Correlation of Environmental Parameters

Understanding the underlying correlation and lead/lag time between two different parameters can help interpret the relative genesis of said parameters which may have implications on the use of the parameter in predicting underwater noise. If one parameter leads another, this indicates that former may generate the latter and the lag may indicate the time required to achieve mature parametric growth as a function of the former acting on the latter.

Ice stations were not culled in this section. It is interesting to see how ice plays a role in eroding parametric correlation coefficients and generally decreasing lead/lag time in the case of two well-correlated parameters under conditions of ice.

Tables 6 to 8 exhibit the maximum correlation value and associated lag for every combination of the tested parameters. The greatest lag times are associated with any parameter crossed with friction velocity however these correlation values are quite low.

Table 6: Parametric cross-correlation of U_{10} vs other parameters.

Parametric Cross Correlation												
Bathymetry and Station Number	U_{10} x SWH		U_{10} x WW		U_{10} x Charnock Parameter		U_{10} x Friction Velocity		U_{10} x Edson Wave Age		U_{10} x U10N	
	Max Corr	Lag (Hrs)	Max Corr	Lag (Hrs)	Max Corr	Lag (Hrs)	Max Corr	Lag (Hrs)	Max Corr	Lag (Hrs)	Max Corr	Lag (Hrs)
Shelf (1,8,18)	0.79	-3.33	0.93	-1	0.78	0	-0.12	4.33	-0.63	0	0.99	0
Slope (4,5,6,13,15,16,17,19)	0.75	-4	0.93	-1	0.71	0	-0.18	-4.25	-0.63	0	0.99	0
Mean	0.77	-3.81	0.93	-1	0.73	0	-0.16	-1.9	-0.63	0	0.99	0
Non-Culled Ice Stations (10,11,12,14,20) *** Not included in mean values	0.77	-3	0.90	-0.6	0.52	-0.2	-0.14	-7	-0.60	0	0.99	0

The intuitive and easily measurable U_{10} is of particular interest in this research. Consider U_{10} x SWH, shelf stations express a shorter lag than slope stations and the presence of ice decreases the lag time but not the correlation when compared to the mean. However, U_{10} x WW, shelf and slope stations express the same lag time of -1 hr and correlation. Ice decreases the lag time and the correlation of this combination. This suggests that ice suppresses wind wave but not SWH (swell). Due to its greater bulk volume, swell has more momentum than wind wave and is therefore less subject to momentum losses on account of the presence of surface ice.

Consider U_{10} x Charnock parameter, its max correlation values are similar to those of U_{10} x *SWH* for the shelf, slope, and mean, however under conditions of ice, this combination expresses a precipitous drop in correlation from 0.73 to 0.52.

In the case of U_{10} x Friction Velocity, its max correlation is poor and its lag cannot be patterned from station to station. Within a +/- 24 hr lag interval, the lag of this combination ranges from -24 to 16. Friction velocity does not correlate well with any parameter and the lag times swing widely in all combinatory cases. Friction velocity also regressed poorly vs hourly minimum sound power levels, cross-correlated poorly with 4 kHz hourly minimum sound power levels and is not a viable parameter for application in the study of underwater ambient noise.

As Edson wave age is proportional to $1/U_{10N}$, its lag property is the same as U_{10} or U_{10N}. However, U_{10} has a mean inverse correlation with Edson wave age with a mean value of -0.63. The inverse nature of the correlation is self evident. The decrease in correlation away from 1 is attributed to the modification of the U_{10N} term by the coefficient and constant at Eqn (31).

The U_{10} x U_{10N} combination expresses 0 lag and the max correlation ranges from 0.994 to 0.995, even in the presence of ice. These two parameters are extremely similar with barely a modicum of difference.

Table 7: Parametric cross-correlation of *SWH* and *WW* vs other parameters.

Bathymetry and Station Number	SWH x WW		SWH x Charnock Parameter		SWH x Friction Velocity		WW x Charnock Parameter		WW x Friction Velocity	
Parametric Cross Correlation										
	Max Corr	Lag (Hrs)	Max Corr	Lag (Hrs)	Max Corr	Lag (Hrs)	Max Corr	Lag (Hrs)	Max Corr	Lag (Hrs)
Shelf (1,8,18)	0.86	2	0.61	6	-0.12	-1.66	0.75	2	-0.12	3.33
Slope (4,5,6,13,15,16,17,19)	0.82	2.25	0.48	7.12	-0.25	5.37	0.65	1.87	-0.19	-0.75
Mean	0.83	2.18	0.51	6.81	-0.22	3.45	0.68	1.90	-0.17	0.36
Non-Culled Ice Stations (10,11,12,14,20) *** Not included in mean values	0.86	1.6	0.24	-0.6	-0.26	-9.4	0.24	-3.4	-0.21	-5.4

Consider *SWH* x *WW* in Table 7. The two are highly correlated however *SWH* lags wind wave by 2 hours over the shelf and 2.25 hours over the slope. This indicates that there may be more immediacy to the relationship over the shelf than over the slope. Additionally, the correlative relationship between this combination is stronger over the shelf than the slope. Interestingly, the presence of ice does not affect the correlation compared to ice free slope stations while it decreases the lag time of the correlation.

WW x Charnock correlate significantly better than *SWH* x Charnock. This indicates that surface stress is more strongly related to wind wave than *SWH*. This makes sense as swell, being a generally large rolling wave compared to the smaller more intermittent 'chop' of wind wave, would be the surface over which surface stress is occurring while the 'chop' of wind wave is the small-scale element which manifests the surface layer stress.

SWH x Friction Velocity, and Wind Wave x Friction Velocity are unremarkable in a correlative sense.

Cross Correlation of Wind Speed Magnitude vs Significant Wave Height
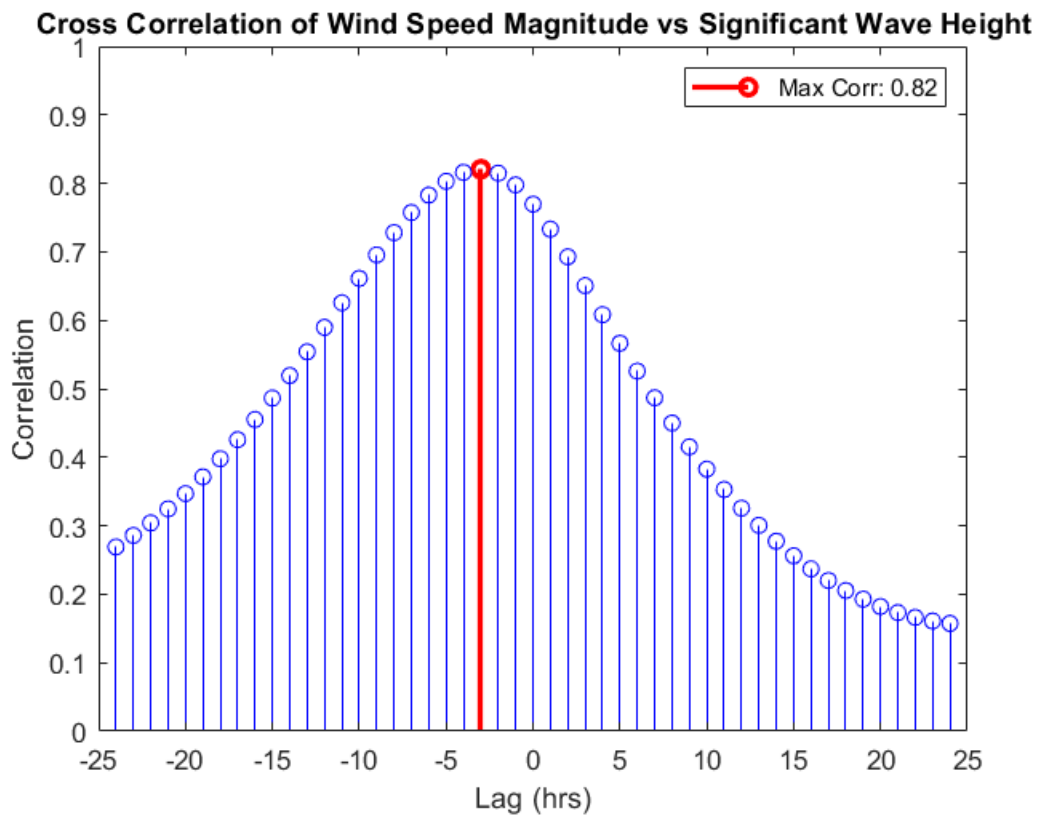
Figure 58: Cross correlation data of horizontal wind speed magnitude 10 m above sea level vs significant wave height at Station 1.

In Figure 58, it can be seen that wind leads wave by 3 hours when the maximum correlation of 0.82 occurs. This indicates that significant wave height is most highly correlated to horizontal wind speed magnitude 10 m above sea level when the wind has had 3 hours to act over a given parcel of ocean. The correlation builds slowly and then drops off with a greater speed than the build phase following peak correlation.
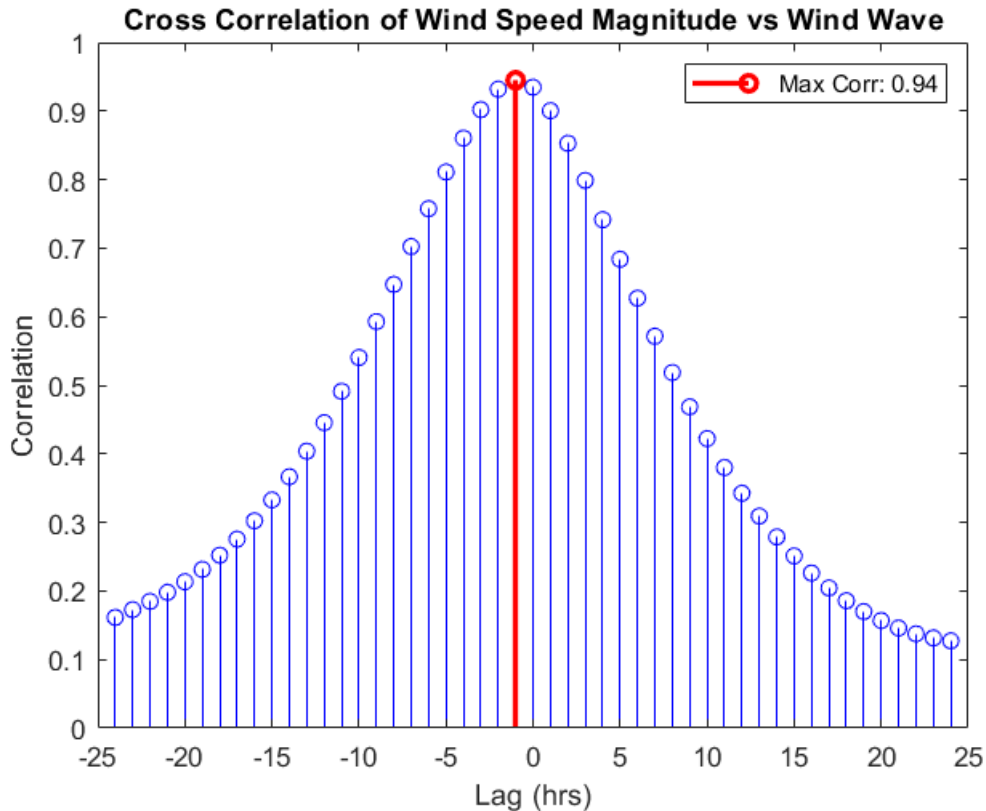
Figure 59: Cross correlation data of horizontal wind speed magnitude 10 m above sea level vs wind wave at Station 1.

Comparing Figures 58 and 59, U_{10} vs wind wave correlates 0.12 better than U_{10} vs *SWH*, and wind leads wind wave by 1 hour where wind leads *SWH* by 3 hours. The short 1-hour lead time validates the idea that wind wave is the result of local wind forces and that *SWH* is the result of long duration, consistently directed wind forces. The reduction in correlation of U_{10} vs *SWH* is related to the idea that a fully developed sea requires a not insignificant amount of time for the wind to act upon that sea and develop the swell. It could be assumed that a wind with consistent speed, direction, and duration would correlate significantly better with *SWH*. The genesis of wind wave is less physically intensive than the genesis of *SWH* and thus requires fewer/lower wind building forces than *SWH* which results in superior and more immediate correlation. This leads into the idea that the force developing waves is surface stress acting on the surface of the ocean. Two available parameters for examination are friction velocity, which is the wind speed at the air/sea interface required to overcome resistance to movement in the surface layer, and Charnock parameter which grows with increasing aerodynamic roughness length.
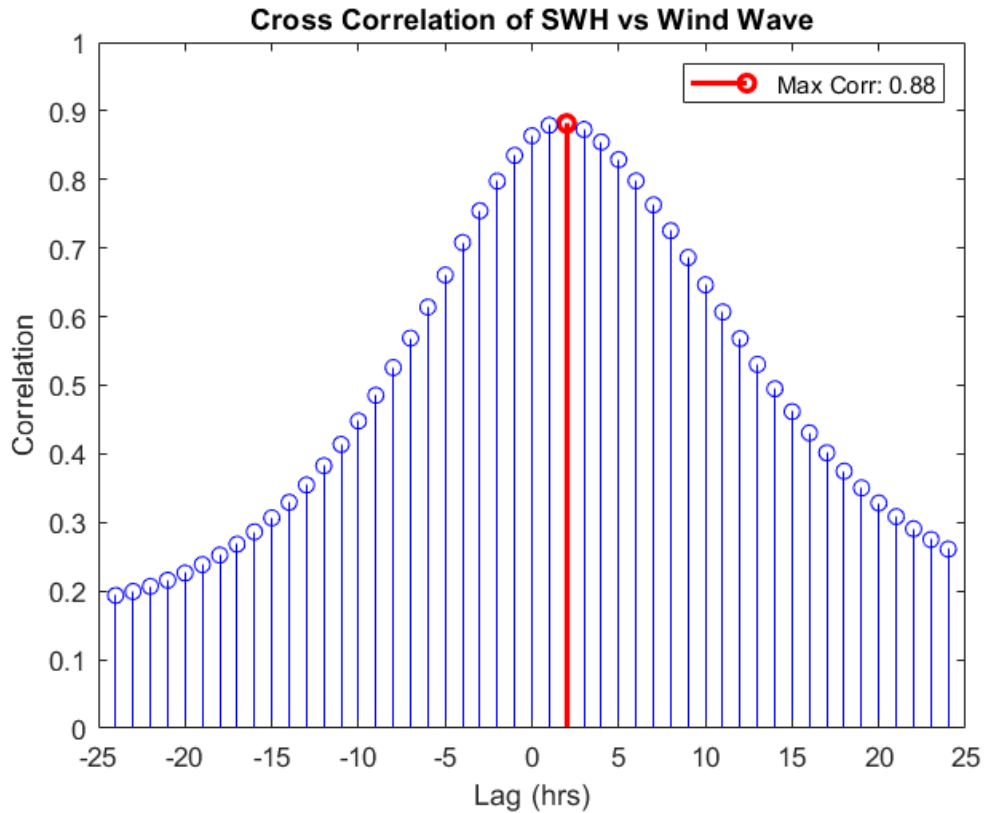
Figure 60: Cross correlation data of *SWH* vs wind wave at Station 1.

In this thesis, *SWH* is defined as the significant height of combined wind waves and swell which is defined as the average height of the highest third of surface ocean/sea waves generated by wind and swell. Wind wave is a significant element in the *SWH* definition and the correlative value expresses this. The high correlation coefficient indicates that either *SWH* has a growth effect on wind wave or a common element, a wind actor is growing both. *SWH* lags wind wave by 3 hours at max correlation.
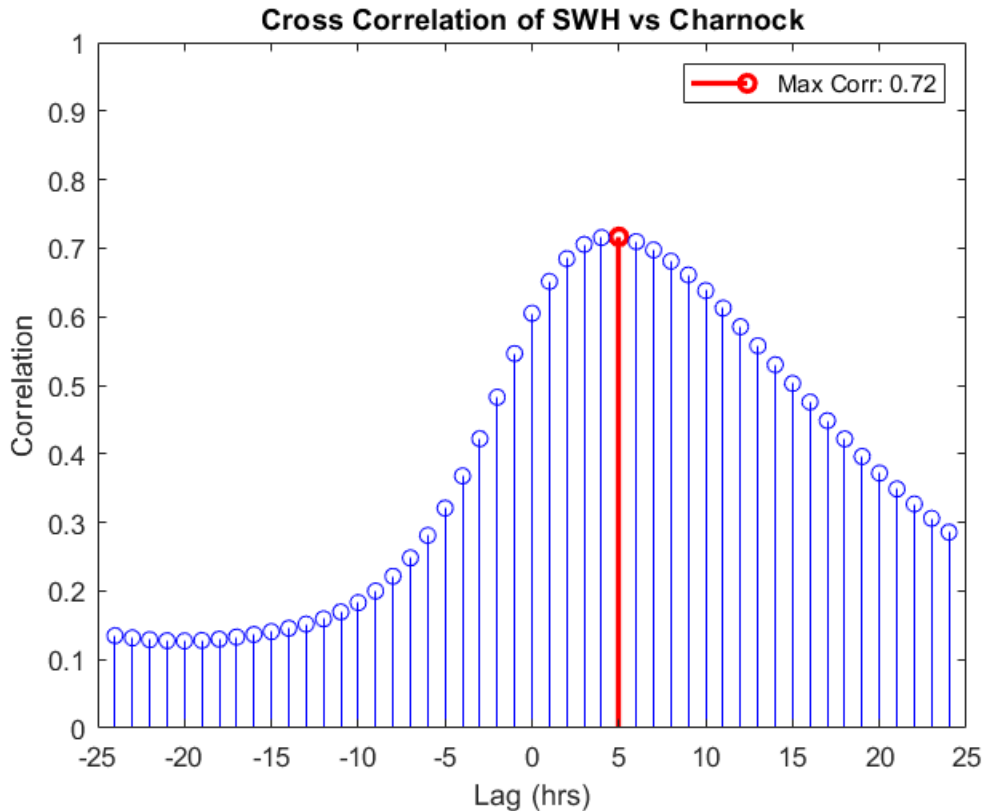
Figure 61: Cross correlation data of *SWH* vs Charnock parameter at Station 1.

In Figure 61, *SWH* lags Charnock by five hours indicating that Charnock, being driven by wind stress in the surface layer requires 5 hours of action over a parcel of water in order to generate a given significant wave height.

6.2 Parametric Cross Correlation with 4 kHz Hourly Minimum Sound Power Levels

It is important to distinguish the differences between a regression between two variables; i.e., a line of best fit, and the cross-correlation between these two variable. They are not the same process, and the results cannot be expected to be similar. Correlation is a quantification of how well two variables relate to each other over a period of time and characterize the magnitude of the relationship between those two variables where with regression, the regression line is determined as the best way to predict Y from X and thus explains the cause-and-effect relationship between two parameters. Notwithstanding, there are some similarities between correlation and regression, including the direction of the correlation (negative correlation provides a negative regression slope).

Table 8: Cross correlation of parameter versus hourly minimum sound power levels at 4 kHz.

Bathymetry and Station Number	U10 x 4 kHz HMSPL		U10N x 4 kHz HMSPL		Charnock x 4 kHz HMSPL		SWH x 4 kHz HMSPL		Wind Wave x 4 kHz HMSPL		Friction Velocity x 4 kHz HMSPL		Edson Wave Age x 4 kHz HMSPL		U10N + SWH x 4 kHz HMSPL	
	Max Corr	Lag (Hrs)	Max Corr	Lag (Hrs)	Max Corr	Lag (Hrs)	Max Corr	Lag (Hrs)	Max Corr	Lag (Hrs)	Max Corr	Lag (Hrs)	Max Corr	Lag (Hrs)	Max Corr	Lag (Hrs)
Shelf (1,8,18)	0.78	1	0.78	1	0.71	0.33	0.76	4	0.84	2	-0.13	-17	-0.34	1	0.79	1
Slope (4,5,6,13,15,16,17,19)	0.71	0.87	0.72	0.87	0.63	0.62	0.69	3.87	0.77	2	-0.15	10.87	-0.30	0.87	0.74	1
Mean	0.73	0.90	0.74	0.90	0.65	0.54	0.71	3.90	0.79	2	-0.14	3.27	-0.31	0.90	0.75	1
Non-Culled Ice Stations (10,11,12,14,20) *** Not included in mean values	0.47	0	0.46	0	0.59	-0.80	0.66	3.80	0.69	2	-0.14	3	-0.17	-0.80	0.67	2.4

Versus 4 kHz hourly minimum sound power levels, wind wave, SWH, U_{10}, U_{10N}, Charnock parameter and composite U_{10N} + SWH correlate better over the shelf than over the slope by R^2 0.05 to 0.08 for non ice stations as seen in Table 8. This indicates that either the shallow acoustical environment is more strongly influenced by surface conditions than a deeper acoustical environment or, that the *ERA5* model produces parameters that more easily predict the acoustic observations. This may be caused by the acoustical environment in deeper water being subject to additional propagation channels which can carry long range acoustical actors (e.g., ship noise). These long-range actors may to some degree mask the local hourly minimum sound power level and deteriorate the correlative relationship between it and the source of those minima, i.e., wind, and its derivatives.

The mean values of wind wave, SWH, U_{10}, U_{10N}, SWH, Charnock parameter and composite U_{10N} + SWH correlate from 0.65 to 0.79. The order of the mean of the top performing parameters is as follows

1.   *WW*: 0.79, 2 hrs

2. U_{10N} + *SWH*: 0.75, 1 hr

3. U_{10N}: 0.74, 0.9 hrs

4. U_{10}: 0.73, 0.9 hrs

5.   *SWH*: 0.71, 3.9 hrs

6.   Charnock Parameter: 0.65, 0.54 hrs

The top performing parameters all lagged 4 kHz hourly minimum sound power levels. U_{10} and U_{10N} lagged by 0.9 hrs, and the wave parameters took more time to correlate to 4 kHz hourly minimum sound power levels: 2 hours for wind wave and 3.9 hours for *SWH*. This indicates that 4 kHz hourly minimum sound power levels tend to

correlate best with the measured wind speed approximately one hour after the hourly minimum sound power levels were recorded; this could be due to time synchronization issues between *ERA5* data set and the JASCO *AMAR* as in reality, the wind should lead the noise by approximately the same amount that the wind leads the wind wave. Similarly, the minima tend to correlate best with measured wave height approximately 2 to 4 hours before the wave heights were measured. Otherwise said, both wind and wave will lag the generation of hourly minimum sound power levels. Charnock parameter had the shortest lag time or most instantaneous relationship with 4 kHz hourly minimum sound power levels at approximately 30 minutes. This indicates that total stress at the air/sea interface has an immediate effect on 4 kHz hourly minimum sound power levels although the relationship is weaker than other parameters which require a developmental delay. The U_{10N} + *SWH* parameter, as seen during regression modelling, performs holistically better than its constituent parameters. Its mean max correlation is R^2 0.75 where that of U_{10N} is 0.74 and *SWH* is 0.71. The composite mean lag time of 1 hr closely resembles the mean lag time of U_{10N} at 0.9 hours and not the mean lag time of *SWH* of 3.9 hours. This is because, as per Table 5, the mean value of α at 4 kHz is 0.866. While the max correlation of the weighted composite parameter experiences a holistic gain above the correlation performance of either respective constituent, the lag time is highly subject to the influence of the α parameter. The lag time of the composite will thus favour the lag time of the more highly weighted of the two constituents but will lie somewhere between the two constituents.

Friction velocity expressed highly variable lead/lag times and did not correlate well with 4 kHz hourly minimum sound power levels in a statistically significant sense. Edson wave age did not correlate well either however its lag time was exactly the same as neutral wind over the shelf and slope, speaking to its status as a derivative of neutral wind.

In the case of stations expressing significant instances of surface ice coverage, correlation coefficients erode in a significant way. That is to say that the presence of ice has a negative impact on the correlation of a meteorological parameter with hourly minimum sound power levels at 4 kHz. This makes sense as the presence of ice modifies the acoustical environment by not only making high power noise and impacting the sound velocity profile of the surface water through cooling, but also by affecting the ability of wind or wave to act over the surface of the water in an uninhibited way. That is to say that if significant ice is present, much like the presence of an island or large persistently present surface object, the ability of wind to produce a

mature sea which necessitates uninhibited wind speed magnitude, fetch, and duration, is not completely possible.
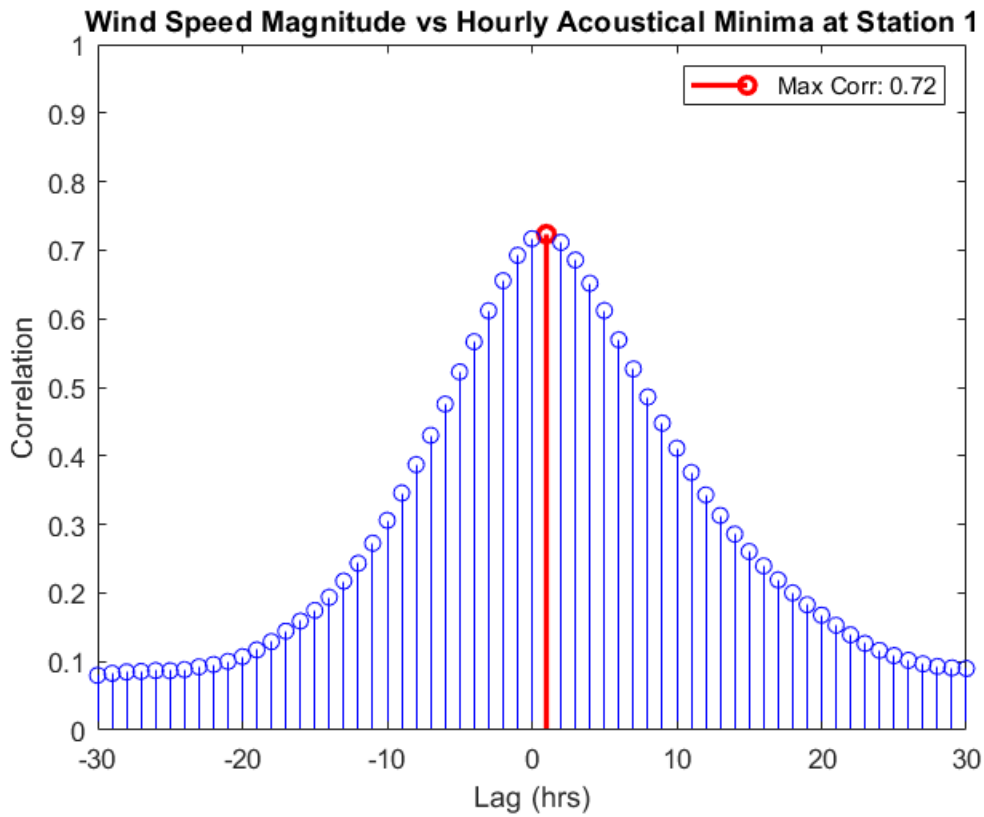
Figure 62: Horizontal wind speed magnitude versus 4 kHz hourly minimum sound power levels at Station 1.

At Figure 62, the correlative growth and decay of wind vs hourly minimum sound power levels are relatively symmetric with respect to lead and lag at both shelf and slope stations. Neutral wind and wind wave correlations express a similar shape.
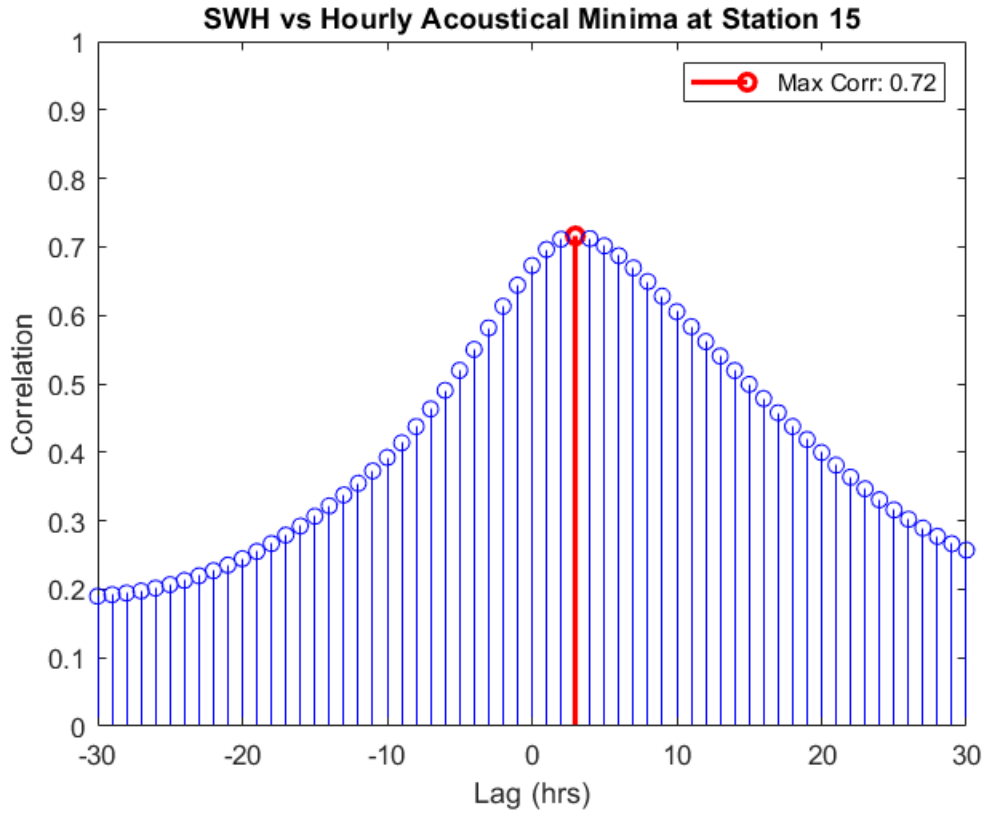
Figure 63: Significant wave height vs 4 kHz hourly minimum sound power levels at Station 15.

At Figure 63, *SWH* slowly correlates to the hourly minimum sound power levels until it peaks at approximately 3 hours lag followed by a more gradual decay in correlation.
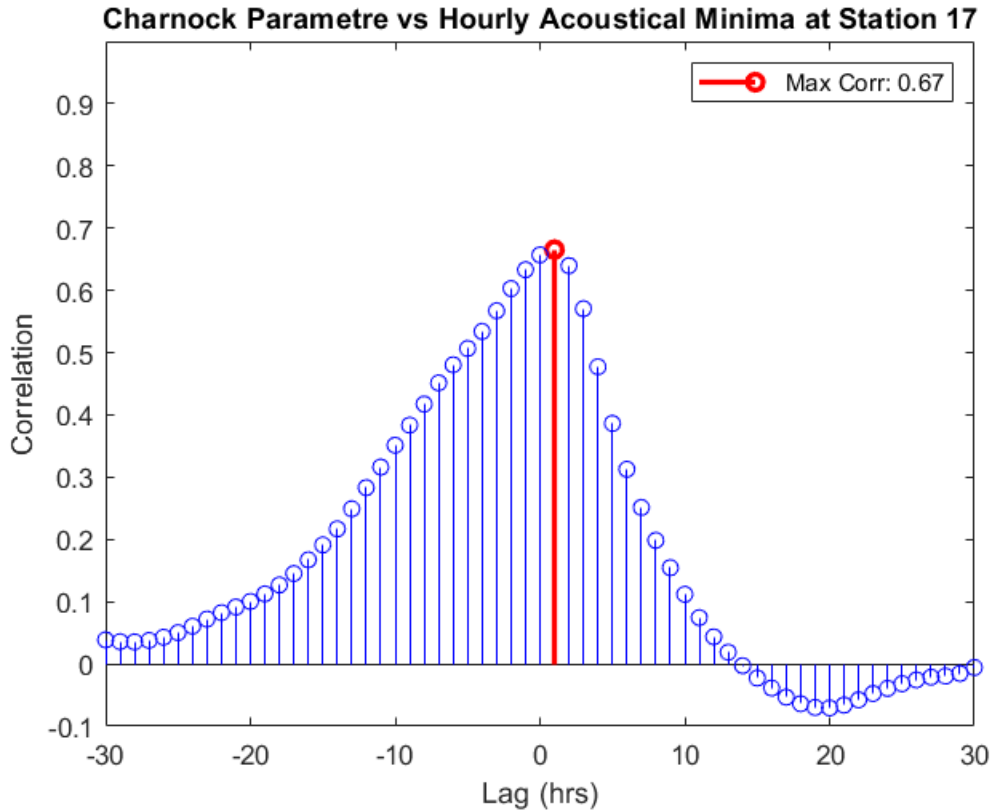
Figure 64: Charnock parameter vs 4 kHz hourly minimum sound power levels at Station 17.

At Figure 64, Charnock parameter gradually increases to peak correlation at 1 hour lag followed by rapid decay and peak negative correlation at 20 hours lag. This shape of this correlation is consistent from station to station although the minimum correlation is not always negative. The minimum correlation tends to occur from 20 to 25 hours lag.
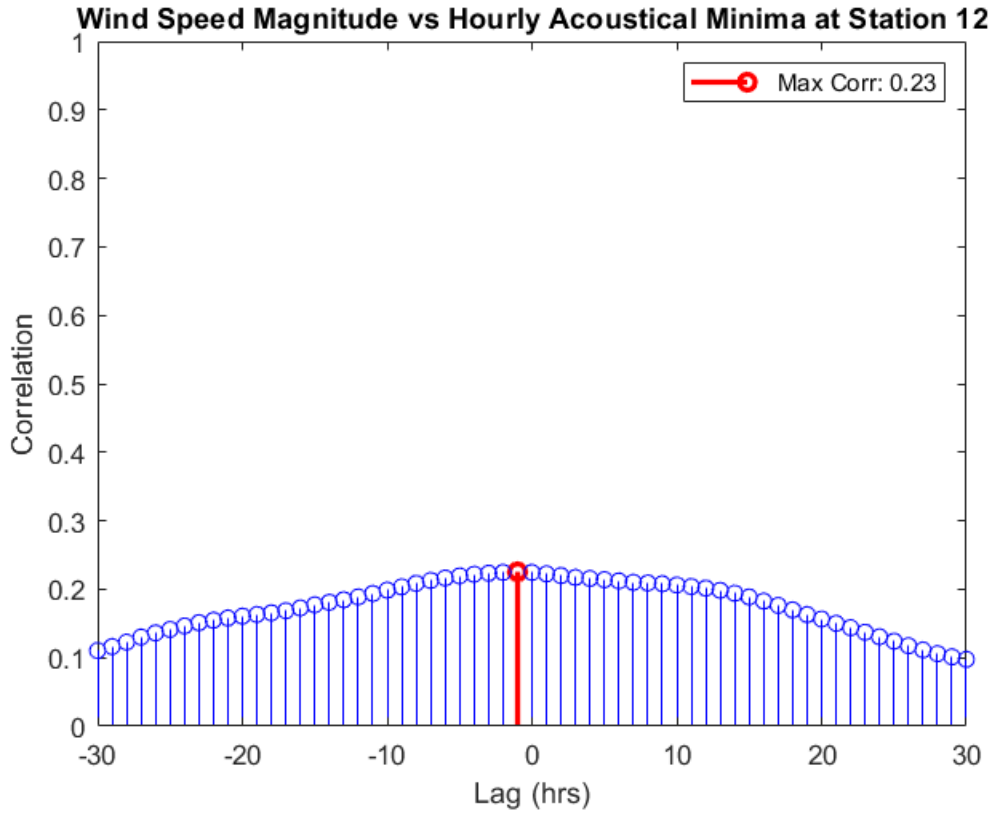
Figure 65: Horizontal wind speed magnitude versus 4 kHz hourly minimum sound power levels at Station 12 with 62% surface ice coverage.

In Figure 65, the deleterious effects of ice on wind versus 4 kHz hourly minimum sound power levels can be seen when compared with the ice-free station at Figure 62.

7. Ice Cull

Of the 16 hydrophones studied, *ERA5* data indicated that 9 of them had instances of sea ice cover during the study period. The parameter is defined as the fraction of a grid box covered by sea ice. Sea ice does not include icebergs nor shore-fast ice sheets. This thesis qualified significant sea ice coverage as an instance when the mean hourly sea ice cover was greater than 10% over the study period. Of the 9 hydrophones stations with sea ice cover, 5 met the qualifier for a significant sea ice coverage and 4 did not. The 5 stations expressing significant sea ice coverage were all on the continental shelf.

7.1 Tabulated Shelf Station R^2 Improvement

In order to include the maximum amount of acoustical and modelling information possible, data was culled in all instances of ice presence over the 5 stations which express significant levels of sea ice coverage. That is to say, the hourly minimum sound power level when sea ice cover was present was deleted from the model regression fit in an attempt to improve model fit. The presence of sea ice does not correlate well with hourly minimum sound power levels as it provides alternate noise generation mechanisms from breaking waves (e.g., ice pan collisions and rubbing, ice cracking, and melting). In the 1 to 4 kHz band, there is a loose linear relation between the concentration of sea ice cover present and the improvement in R^2 which can be expected after culling hourly minimum sound power levels when sea ice was present for the parameters U_{10} and U_{10N}. For insignificant instances of mean sea ice coverage (<10%), R^2 improvement was as shown in Table 9.

Table 9: Stations containing insignificant instances of mean sea ice coverage vs post-ice cull R^2 improvement tabulated using the A) U_{10}, B) U_{10N}, and C) $\alpha*U_{10N} + (1-\alpha)*SWH$ regressions models.

A

Frequency		Surface Ice Coverage <10%	R^2 Improvement Post Ice-Cull Process using U_{10}
4 kHz	Stn 1	0.11%	0.00046
	Stn 18	0.00026%	0
	Stn 13	7.78%	0.079
	Stn 15	1.4%	0.015
3 kHz	Stn 1	0.11%	0.0018
	Stn 18	0.00026%	0
	Stn 13	7.78%	0.077
	Stn 15	1.4%	0.014
2 kHz	Stn 1	0.11%	0.0040
	Stn 18	0.00026%	0
	Stn 13	7.78%	0.076
	Stn 15	1.4%	0.012
1 kHz	Stn 1	0.11%	0.0034
	Stn 18	0.00026%	0
	Stn 13	7.78%	0.069
	Stn 15	1.4%	0.009
100 Hz	Stn 1	0.11%	0.0013
	Stn 18	0.00026%	0
	Stn 13	7.78%	0.038
	Stn 15	1.4%	-0.011

B

Frequency		Surface Ice Coverage <10%	R^2 Improvement Post Ice-Cull Process using U_{10N}
4 kHz	Stn 1	0.11%	0.00071
	Stn 18	0.00026%	0
	Stn 13	7.78%	0.074
	Stn 15	1.4%	0.014
3 kHz	Stn 1	0.11%	0.0023
	Stn 18	0.00026%	0
	Stn 13	7.78%	0.072
	Stn 15	1.4%	0.013
2 kHz	Stn 1	0.11%	0.0050
	Stn 18	0.00026%	0
	Stn 13	7.78%	0.071
	Stn 15	1.4%	0.011
1 kHz	Stn 1	0.11%	0.0040
	Stn 18	0.00026%	0
	Stn 13	7.78%	0.063
	Stn 15	1.4%	0.0091
100 Hz	Stn 1	0.11%	0.0014
	Stn 18	0.00026%	0
	Stn 13	7.78%	0.028
	Stn 15	1.4%	-0.011

C

Frequency		Surface Ice Coverage <10%	R^2 Improvement Post Ice-Cull Process using $\alpha*U_{10N} + (1-\alpha)*SWH$
4 kHz	Stn 1	0.11%	0
	Stn 18	0.00026%	0
	Stn 13	7.78%	0.052
	Stn 15	1.4%	0.012
3 kHz	Stn 1	0.11%	0
	Stn 18	0.00026%	0
	Stn 13	7.78%	0.049
	Stn 15	1.4%	0.01
2 kHz	Stn 1	0.11%	0
	Stn 18	0.00026%	0
	Stn 13	7.78%	0.046
	Stn 15	1.4%	0.0063
1 kHz	Stn 1	0.11%	0
	Stn 18	0.00026%	0
	Stn 13	7.78%	0.036
	Stn 15	1.4%	0.0042
100 Hz	Stn 1	0.11%	0
	Stn 18	0.00026%	0
	Stn 13	7.78%	0.023
	Stn 15	1.4%	-0.011

Two-term exponential R^2 modelling indicates that the $\alpha*U_{10N} + (1-\alpha)*SWH$ parameter expresses higher R^2 than U_{10N} which expresses higher R^2 than U_{10} at all frequencies studied; however, the differences are not necessarily significant. When comparing the R^2 improvement post-ice cull process for stations expressing insignificant instances of sea ice coverage between U_{10} and U_{10N}, there is no emergent pattern

indicating a superior situation as occasionally, R^2 improvement is better with U_{10} and occasionally better with U_{10N}. However, if R^2 improvement is better for a particular parameter, the improvement is better at all frequencies. A*U_{10N} + (1-α)*SWH yields the lowest post ice-cull R^2 improvement of the three parameters at all frequencies. In an absolute sense, the ice-culling process may not be a necessary step in situations where a station contains less than 10% mean sea ice coverage over a study period as the net achievable R^2 improvement is anticipated to be insignificant, i.e., lower than 10%.

For significant instances of mean sea ice coverage (>10%), R^2 improvement was as follows.

Table 10: Stations containing significant instances of mean sea ice coverage vs post ice cull R^2 improvement tabulated using the A) U_{10}, B) U_{10N}, and C) $\alpha*U_{10N} + (1-\alpha)*SWH$ models.

A

Frequency		Surface Ice Coverage >10%	R^2 Improvement Post Ice-Cull Process using U_{10}
4 kHz	Stn 10	14%	0.16
	Stn 14	29%	0.39
	Stn 20	21%	0.28
3 kHz	Stn 10	14%	0.16
	Stn 14	29%	0.37
	Stn 20	21%	0.28
2 kHz	Stn 10	14%	0.15
	Stn 14	29%	0.36
	Stn 20	21%	0.27
1 kHz	Stn 10	14%	0.16
	Stn 14	29%	0.32
	Stn 20	21%	0.25
100 Hz	Stn 10	14%	0.12
	Stn 14	29%	0.26
	Stn 20	21%	0.08

B

Frequency		Surface Ice Coverage >10%	R^2 Improvement Post Ice-Cull Process using U_{10N}
4 kHz	Stn 10	14%	0.18
	Stn 14	29%	0.41
	Stn 20	21%	0.30
3 kHz	Stn 10	14%	0.18
	Stn 14	29%	0.39
	Stn 20	21%	0.29
2 kHz	Stn 10	14%	0.17
	Stn 14	29%	0.38
	Stn 20	21%	0.28
1 kHz	Stn 10	14%	0.17
	Stn 14	29%	0.34
	Stn 20	21%	0.27
100 Hz	Stn 10	14%	0.14
	Stn 14	29%	0.27
	Stn 20	21%	0.08

C

Frequency		Surface Ice Coverage >10%	R^2 Improvement Post Ice-Cull Process using $\alpha*U_{10N} + (1-\alpha)*SWH$
4 kHz	Stn 10	14%	0.10
	Stn 14	29%	0.09
	Stn 20	21%	0.09
3 kHz	Stn 10	14%	0.10
	Stn 14	29%	0.08
	Stn 20	21%	0.08
2 kHz	Stn 10	14%	0.09
	Stn 14	29%	0.08
	Stn 20	21%	0.08
1 kHz	Stn 10	14%	0.09
	Stn 14	29%	0.06
	Stn 20	21%	0.07
100 Hz	Stn 10	14%	0.09
	Stn 14	29%	0.05
	Stn 20	21%	-0.01

When comparing the R^2 improvement post-ice cull process for stations expressing significant instances of sea ice coverage between U_{10} and U_{10N}, U_{10N} always yields a better R^2 improvement at all frequencies. The comparative improvement of U_{10N} over U_{10} varies from R^2 0 to 0.04. $\alpha*U_{10N} + (1-\alpha)*SWH$ yields the lowest post ice-cull R^2 improvement of the three parameters at all frequencies. In an absolute sense, the ice-

culling process is a very necessary step in situations where a station contains more than 10% mean sea ice coverage over a study period as the net achievable R^2 improvement is anticipated to be significant, i.e., greater than 10%. As an example, Station 14, with 29% mean sea ice coverage reaped a highly significant improvement of R^2 0.41 at 4 kHz, decreasing to 0.27 at 100 Hz using the U_{10N} parameter. The lowest performing post ice-cull R^2 improvement, $\alpha*U_{10N} + (1-\alpha)*SWH$, still expressed not insignificant measures of R^2 improvement. For example, Station 14 expressed an R^2 improvement of 0.06 to 0.09 from 1 to 4 kHz.

7.2 Limitations

It should be re-emphasized that from 1 to 4 kHz, there is a loose linear relation between the anticipated R^2 improvement and the mean sea ice coverage over the hydrophone station when using either U_{10} or U_{10N}. Also, as will be seen in Figures 66 and 69, Stations 11 and 12 which expressed 58% and 62% of mean sea ice coverage respectively could not benefit from the ice cull process as too much acoustical data was subtracted from the models and the regressions failed. Somewhere between the 29% mean ice coverage at Station 14 and the 58% ice coverage at Station 11, there exists a threshold where the ice culling process fails to yield a legitimate benefit.

Figure 66: Neutral wind pre / post ice cull process at Station 11 using two-term exponential regression. Figure A) neutral wind *PSD* at 100 Hz frequency bin, B) 1 kHz, C) 2 kHz, D) 3 kHz, E) 4 kHz.

Figure 67: Variance of neutral wind post ice cull data from Station 11, two-term exponential regression.

Figure 68: Mean hourly sea-ice concentration as a function of time at Station 11.
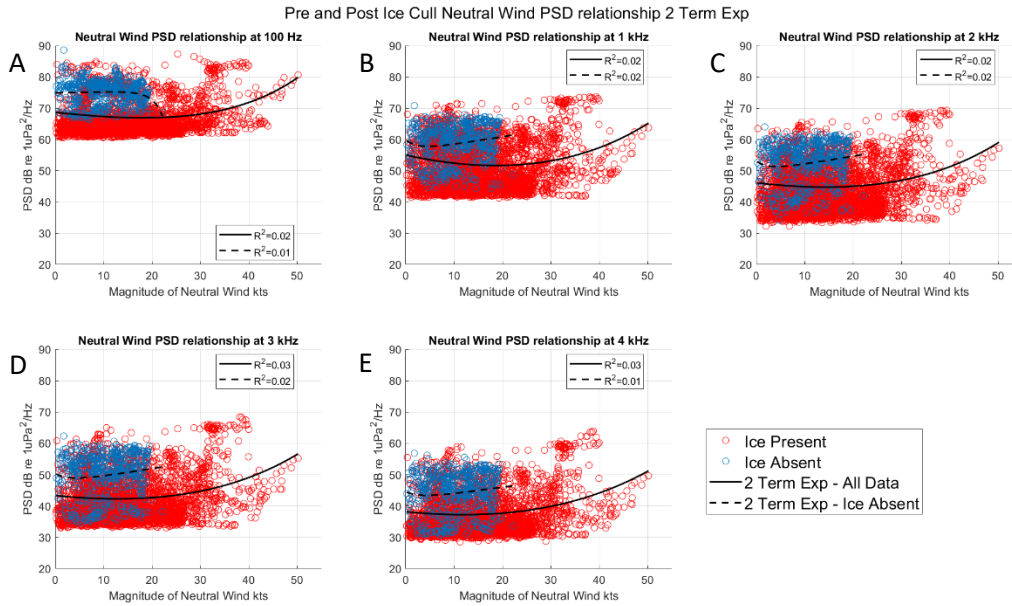
Figure 69: Neutral wind pre / post ice cull process at Station 12 using two-term exponential regression. Figure A) neutral wind *PSD* at 100 Hz frequency bin, B) 1 kHz, C) 2 kHz, D) 3 kHz, E) 4 kHz.
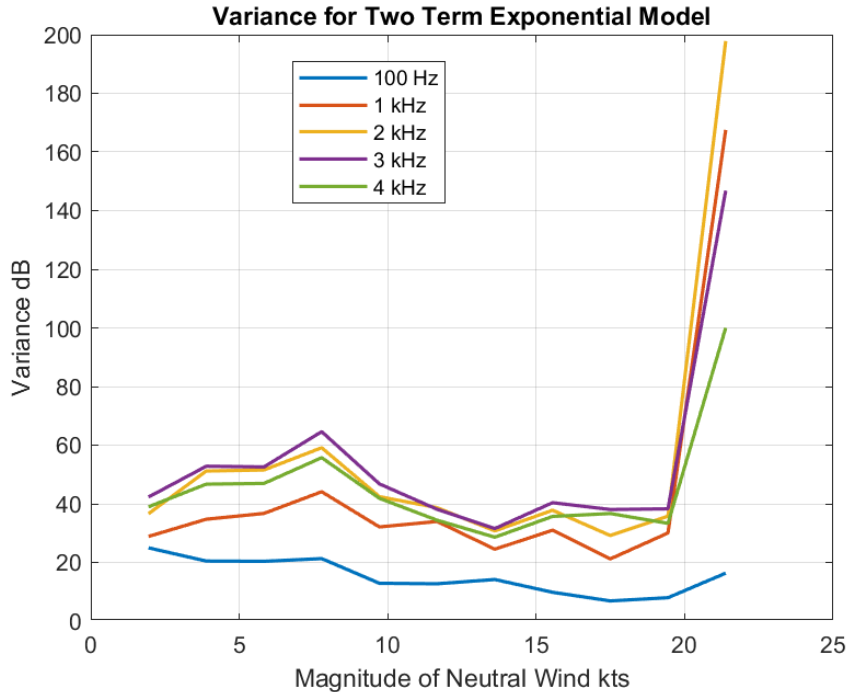
Figure 70: Variance of neutral wind post ice cull data from Station 12, two-term exponential regression.
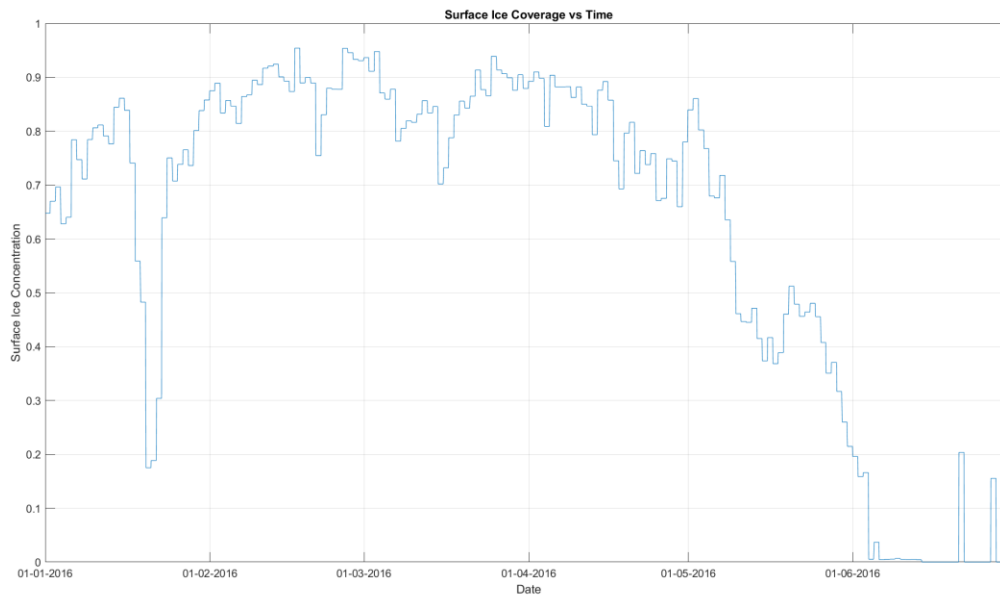
Figure 71: Mean hourly sea-ice concentration as a function of time at Station 12.

Stations 11 and 12 were unique in that they contained greater than 50% mean sea ice coverage over the study period; 58% and 62% respectively. In Figure 66, it is evident that culling greater than 50% of the acoustical data points can render improvements in model regression as at Station 11 although it is an illusion. Examining the two-term exponential ice absent line, low metric wind speeds are associated with higher spectral power than mid-metric wind speeds which is not possible.

7.3 Quintessential Example

Station 14 will illustrate the power of the ice-culling process. This station is located on the continental shelf in 551 m of water and contained 29% mean sea ice cover over the study period.

Pre ice-cull data based on the neutral wind parameter is as follows
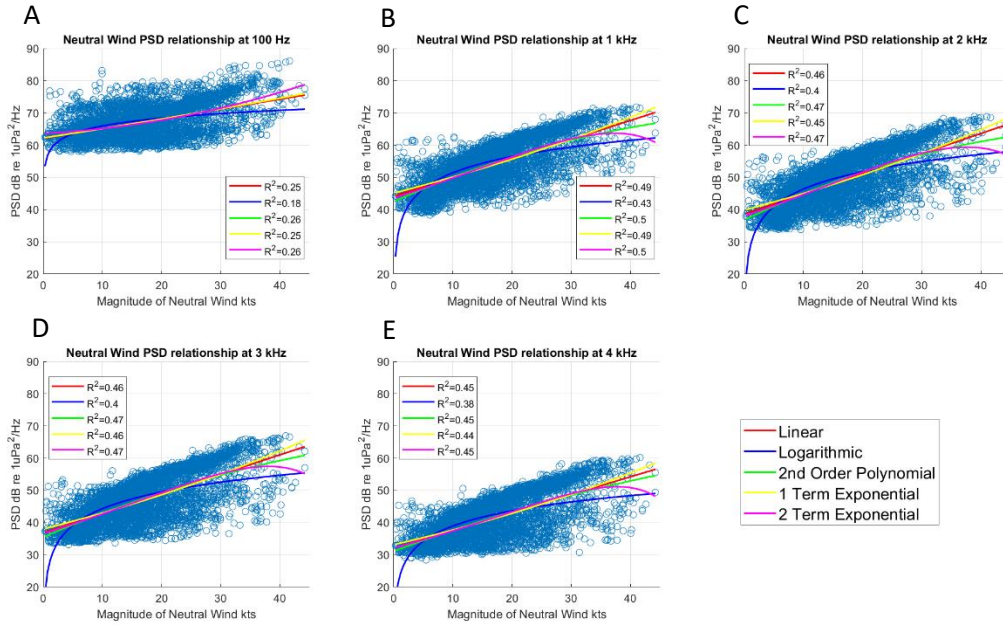
Figure 72: Neutral wind *PSD* models at Station 14 linking neutral wind speed magnitude 10 m above sea level and hourly minimum sound power levels taken between Jan and June 2016. Figure A) neutral wind *PSD* at 100 Hz frequency bin, B) 1 kHz, C) 2 kHz, D) 3 kHz, E) 4 kHz.
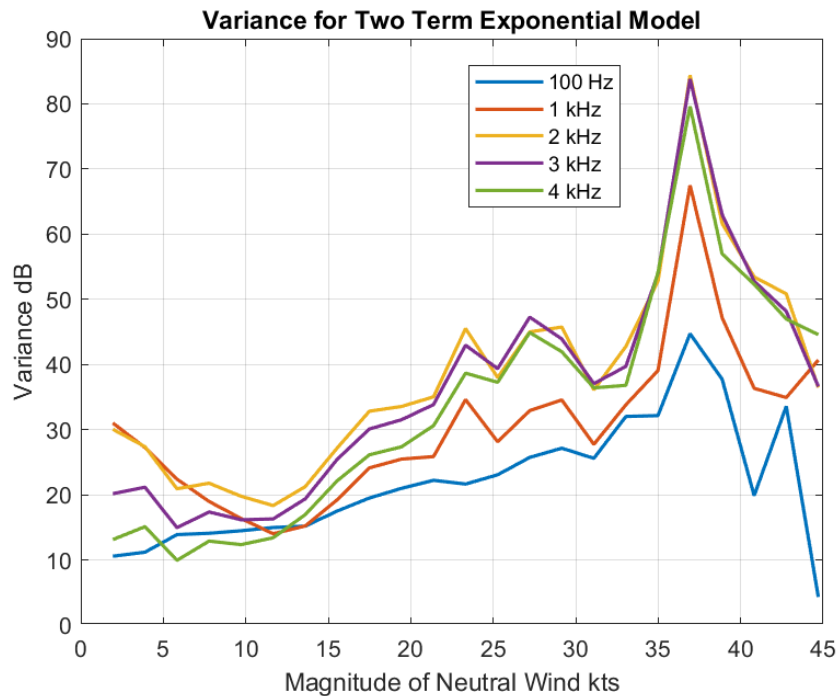
Figure 73: Variance of neutral wind pre ice cull data from Station 14, two-term exponential regression.

Examining the two-term exponential regressions at Figure 72, the R^2 values from 1 to 4 kHz are generally low ranging from R^2 0.5 to R^2 0.45. Under ice-free conditions, R^2 improves with increasing frequency but this is not necessarily the case under conditions of significant mean ice cover. Large variation of hourly minimum sound power levels about the regression line is due to the high-power noise-generating mechanisms inherent in sea ice. Additionally, there appears to be two groups of data that become more distinct as wind speeds increase. This is seen by the presence of a wedge-shaped data gap commencing at approximately 30 kts at all frequencies.

The pre / post ice cull data is as follows
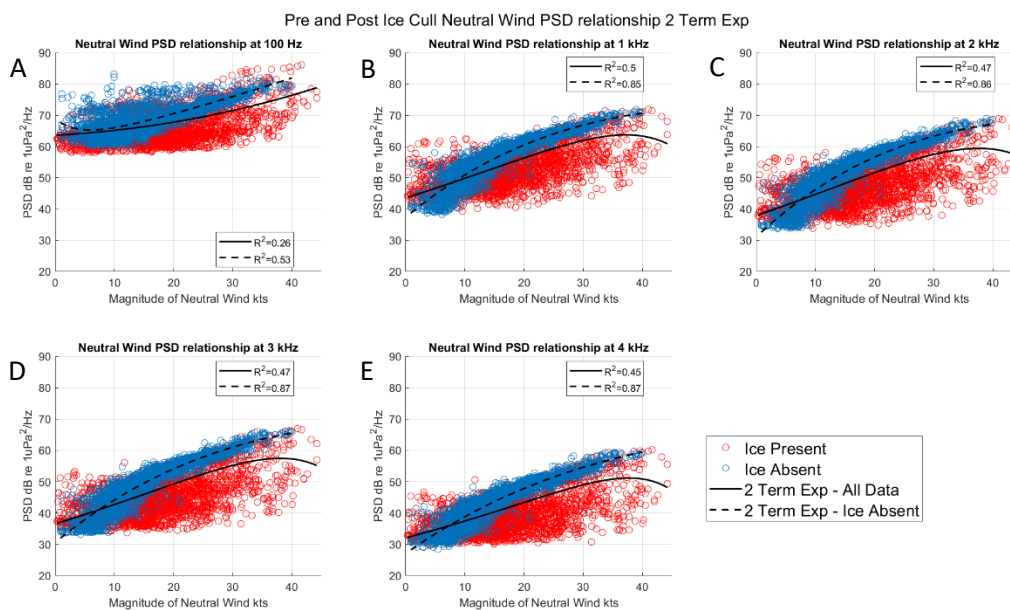
Figure 74: Neutral wind pre / post ice cull process at Station 14 using two-term exponential regression. Figure A) neutral wind *PSD* at 100 Hz frequency bin, B) 1 kHz, C) 2 kHz, D) 3 kHz, E) 4 kHz.

By culling all instances of hourly minimum sound power levels which correspond to the presence of sea-ice, the characteristic bi-mechanistic shape of the ice-free station appears. Manifestly, high power *PSD* values become apparent at higher wind speeds, and high-power *PSD* values at lower wind speeds are absent. Exceptional R^2 values materialize, in particular at 100 Hz. This is due to the fact that ice represents a navigation hazard to most shipping (shipping without ice-strengthened hulls), and thus shipping prefers to sail around it. As the shipping avoids the ice and therefore the active listening area of the hydrophone, the hydrophone is able to make unadulterated low-frequency recordings. The culling of hourly minimum sound power levels

corresponding to ship presence via *AIS* data over the effective listening area of any hydrophone would likely yield a similar result. Consequently, a side-effect of the ice-culling process is the ability to extract higher quality, low frequency power spectra; in effect the best estimates of *NSL/A* at 100 Hz. Within this thesis at 100 Hz, the Station 14 R^2 of 0.52 is by far the best low frequency regression result and the regression line appears to trace the low frequency flat 'S' as seen in Figure 74A. It is hypothesized that up to a certain threshold of mean sea-ice cover, R^2 at all frequencies within this frequency band would progressively improve with increasing sea-ice cover as this would be associated with progressively decreasing shipping density. The threshold would correspond to the threshold where the ice culling process fails to yield a legitimate benefit as described at the beginning of the section and too much acoustical data is subtracted from the data set causing the regression to fail.
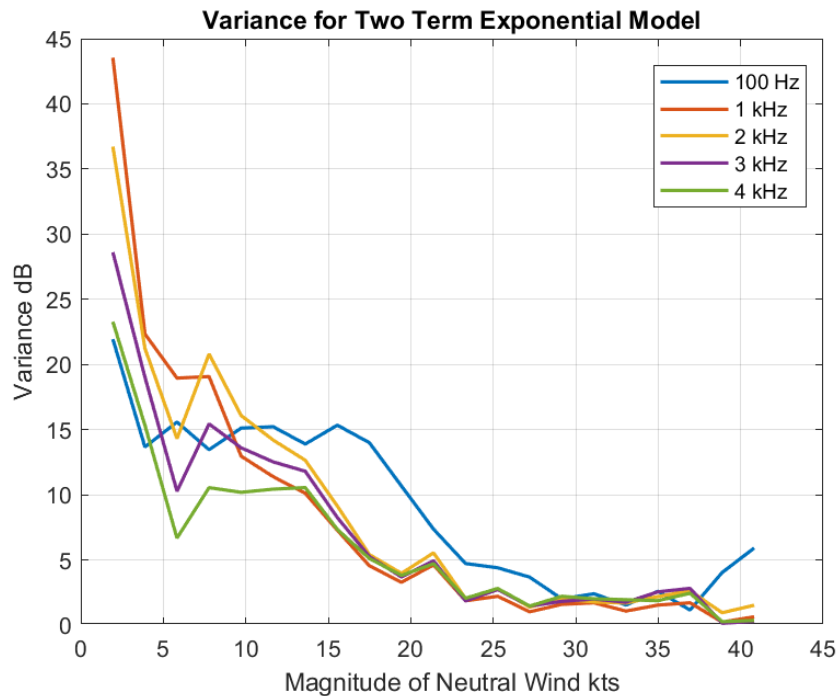
Figure 75: Variance of neutral wind post ice cull data from Station 14, two-term exponential regression.
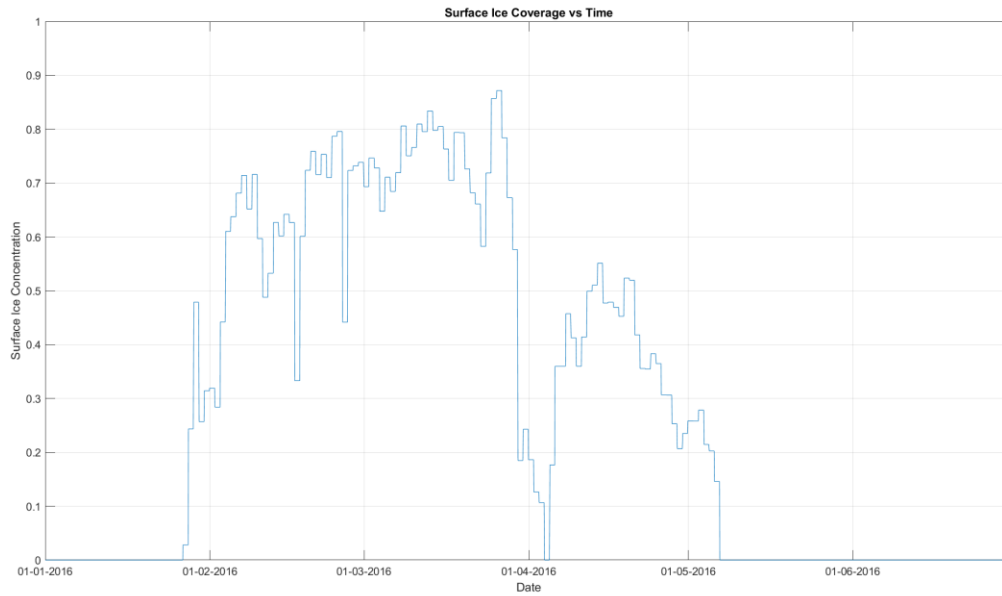
Figure 76: Mean hourly sea-ice concentration as a function of time at Station 14.

Table 11: Post ice-cull tabulated R^2 using two-term exponential regression and U_{10N} parameter for stations expressing significant instances of sea-ice coverage.

Frequency		Surface Ice Coverage >10%	Post Ice-Cull R^2 U_{10N}
4 kHz	Stn 10	14%	0.59
	Stn 14	29%	0.86
	Stn 20	21%	0.84
3 kHz	Stn 10	14%	0.60
	Stn 14	29%	0.86
	Stn 20	21%	0.84
2 kHz	Stn 10	14%	0.61
	Stn 14	29%	0.85
	Stn 20	21%	0.84
1 kHz	Stn 10	14%	0.61
	Stn 14	29%	0.85
	Stn 20	21%	0.83
100 Hz	Stn 10	14%	0.52
	Stn 14	29%	0.53
	Stn 20	21%	0.22

7.4 Low Frequency Discussion

Although there are only three useable examples of significant ice coverage which leverage the ice-cull process, the 100 Hz results express strong R^2 for two of the three examples.
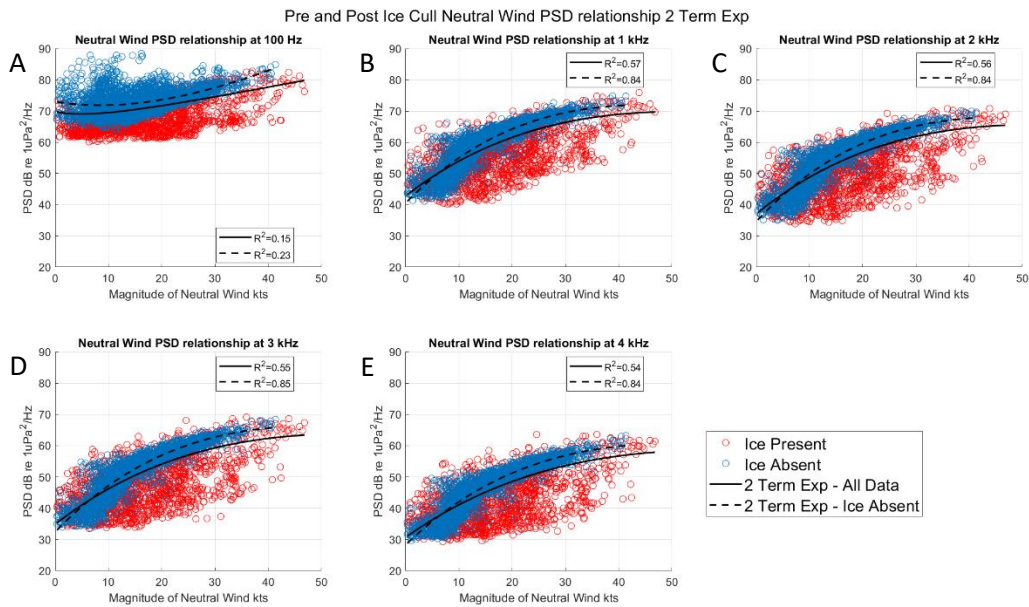
Figure 77: Neutral wind pre / post ice cull process at Station 20 using two-term exponential regression. Figure A) neutral wind *PSD* at 100 Hz frequency bin, B) 1 kHz, C) 2 kHz, D) 3 kHz, E) 4 kHz.
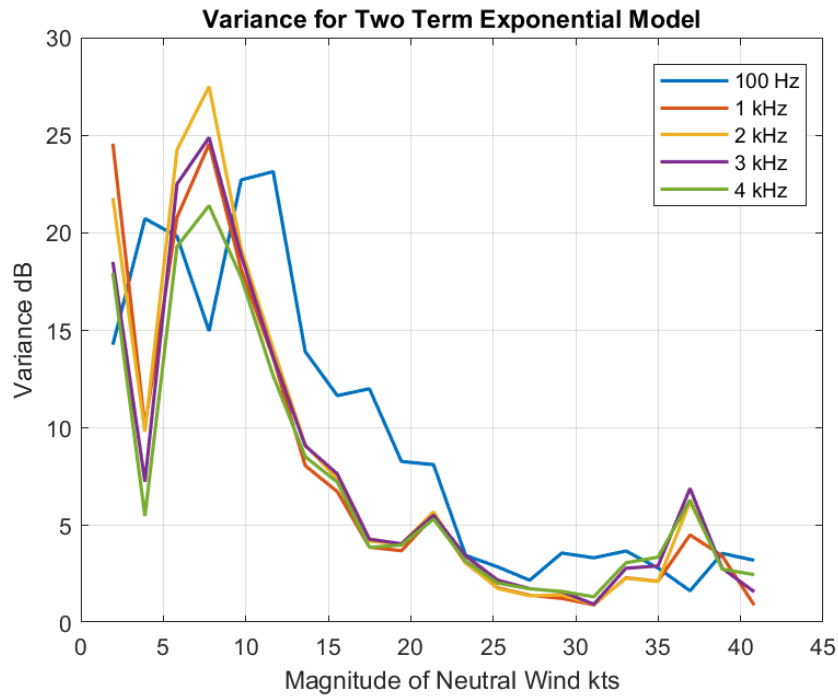
Figure 78: Variance of neutral wind post ice cull data from Station 20, two-term exponential regression.
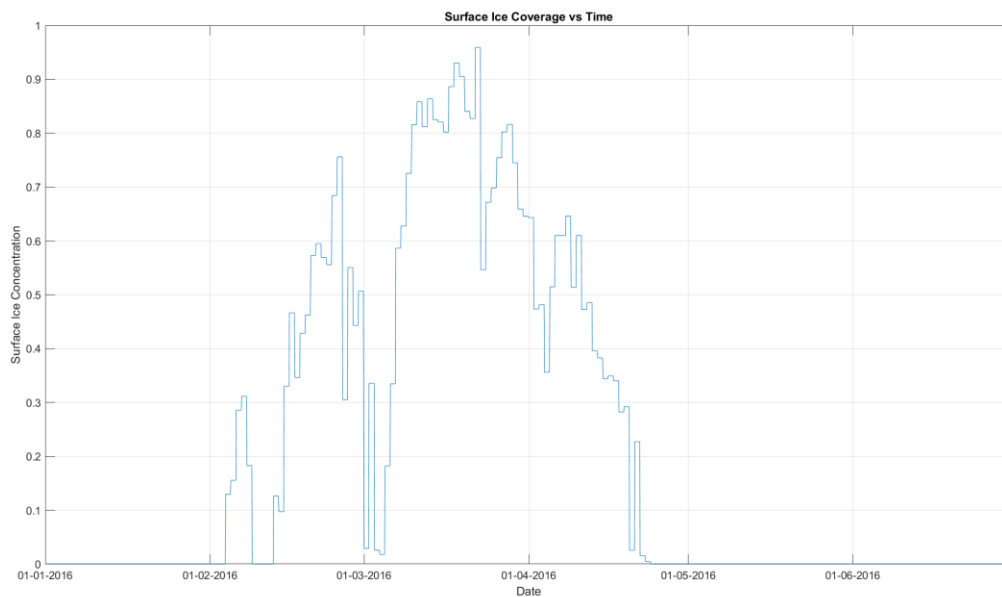
Figure 79: Mean hourly sea-ice concentration as a function of time at Station 20.

Even with 21% mean sea-ice coverage, Station 20 was subjected to the influence of high fishing activity as shown in Figure 80.
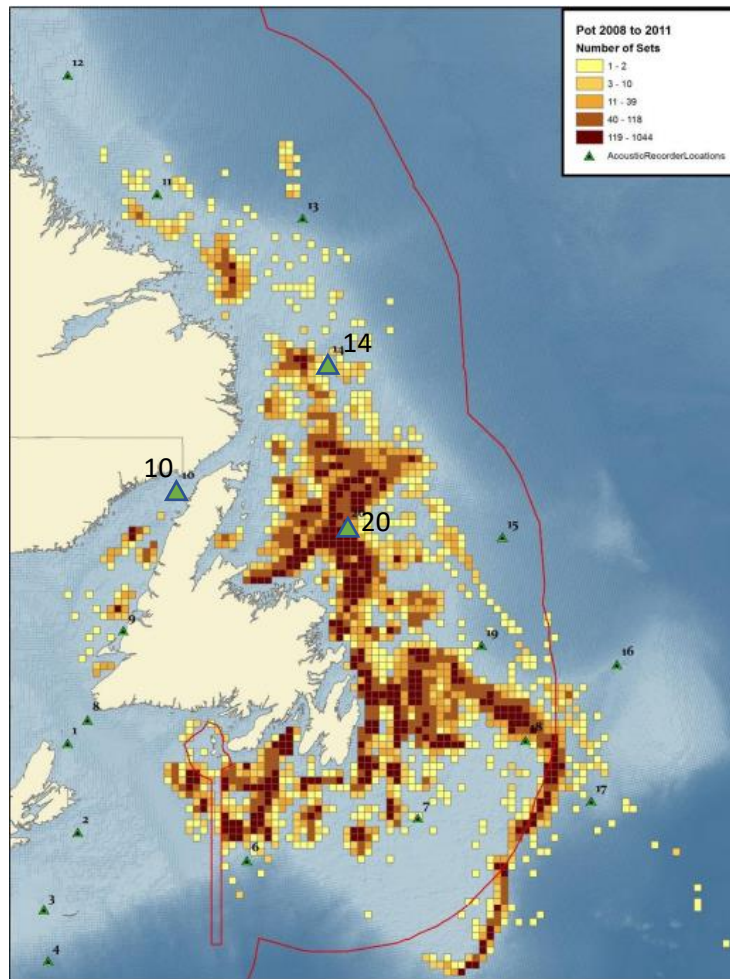
Figure 80: Fishing effort (2008–2011) for pots in areas under the jurisdiction of Department of Fisheries and Oceans Canada (*DFO*) Newfoundland-Labrador. The acoustic recorders are displayed as green triangles (reproduced from Delarue et al, 2018).

Stations 10, 14, and 20 are located within the Newfoundland and Labrador lobster fishing region. Station 10 is located within Lobster Fishing Area (*LFA*) 14B and Stations 14 and 20 are located within *LFA* 3. In these two areas, the 2016 lobster season spanned May to July inclusive (*DFO*, 2017). As the hydrophones recordings used in this study were from Jan to June of 2016, it is evident that the 100 Hz frequency would have been impacted by this activity.

Station 10 expressed low R^2 at all frequencies except for 100 Hz, and as per the high variation in Figure 82, there were high power noise generators operating at low and middle neutral wind speeds from 1 to 4 kHz which eroded the R^2. Station 10 is located within the Gulf of St Lawrence at the mouth of the Straits of Belle Isle and is

approximately 45 km from Newfoundland to the Southeast and 18 km from Quebec to the North. It is suspected that the lower R^2 from 1 to 4 kHz is due to the presence of shipping during non-ice months and the fact the ice severs the relationship between acoustical noise in the ocean and wind. At 100 Hz, although there is a significant improvement in R^2, this is somewhat suspect as the significant consistency in power spectra at low and middle wind speeds is very narrow and therefore models well. It is believed that this is the noise floor of the hydrophone at 100 Hz.
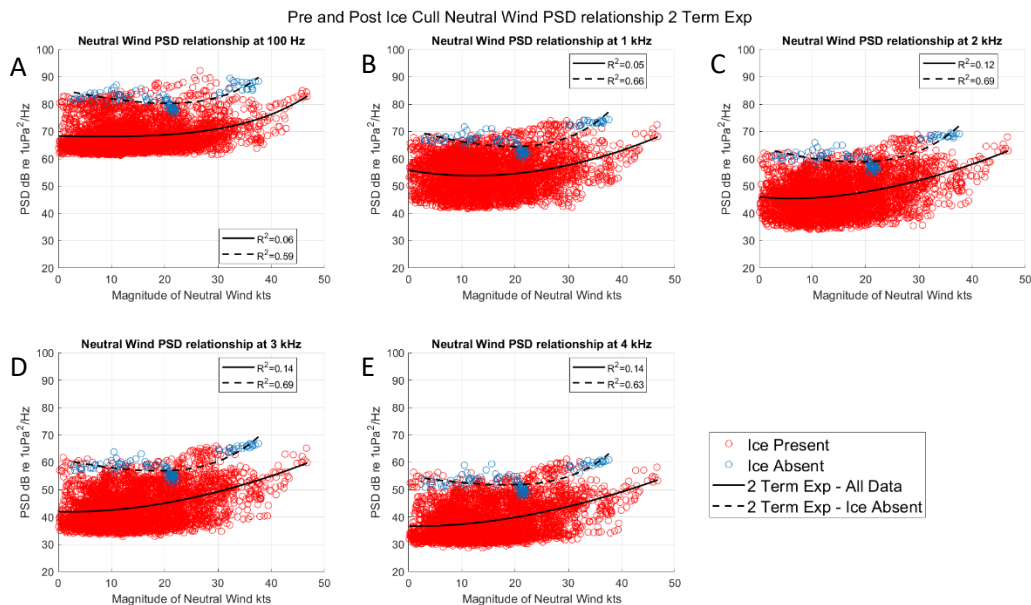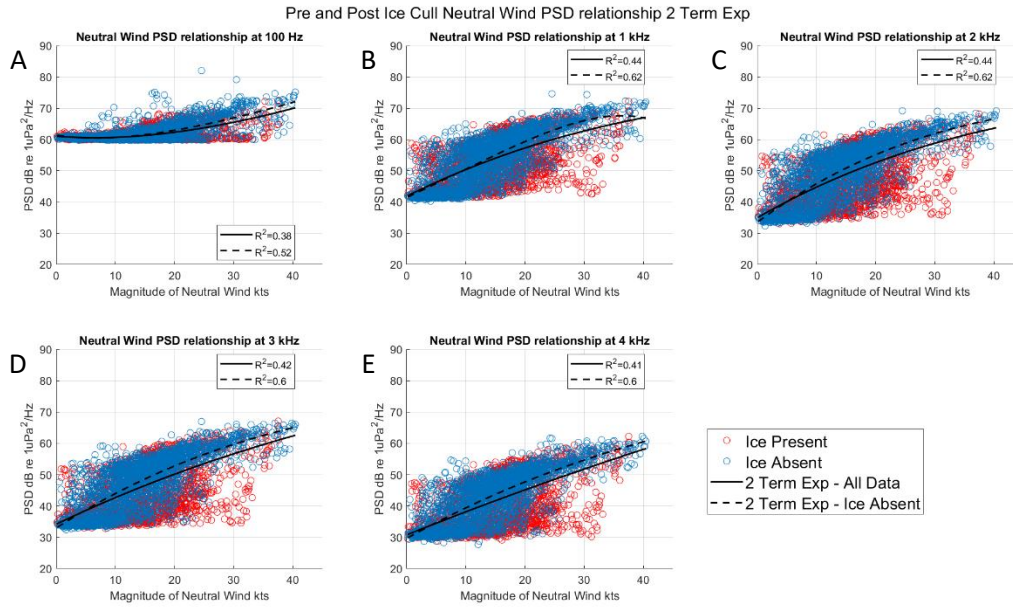

Figure 81: Neutral wind pre / post ice cull process at Station 10 using two-term exponential regression. Figure A) neutral wind *PSD* at 100 Hz frequency bin, B) 1 kHz, C) 2 kHz, D) 3 kHz, E) 4 kHz.
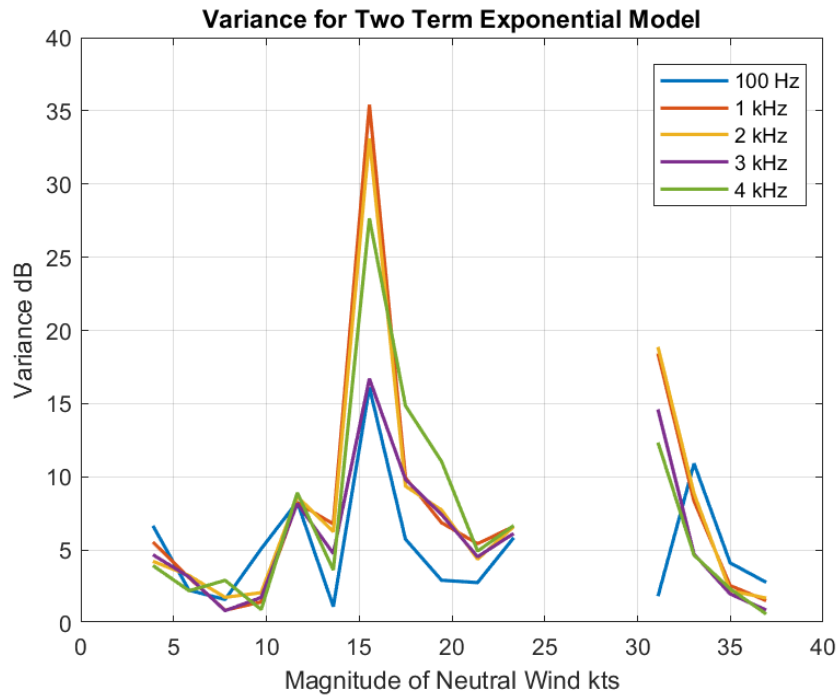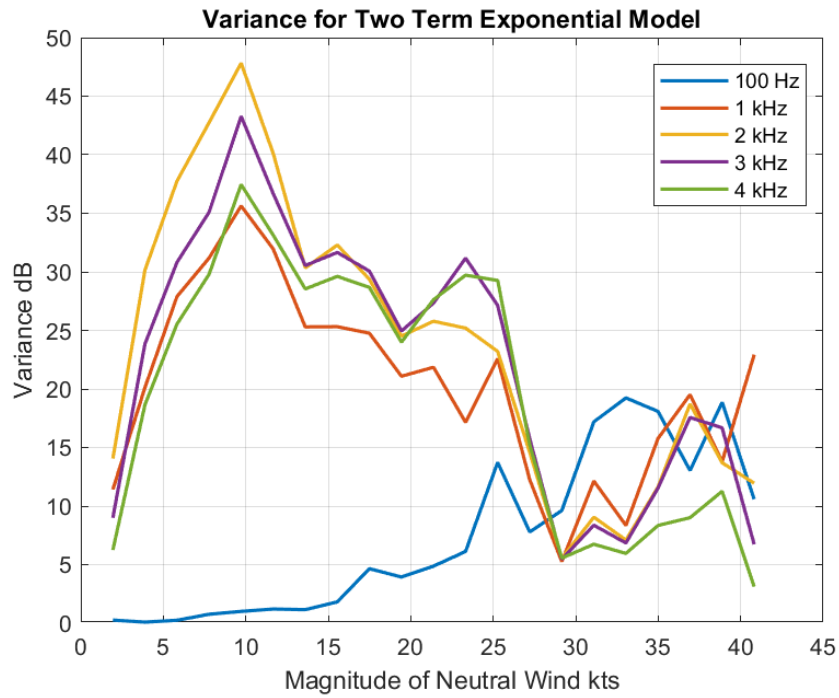
Figure 82: Variance of neutral wind post ice cull data from Station 10, two-term exponential regression.
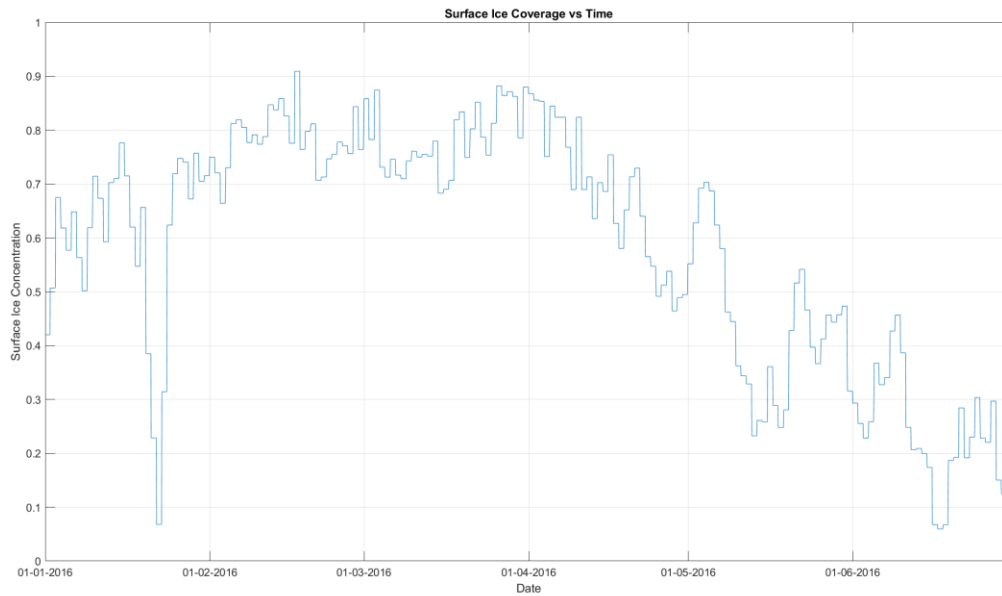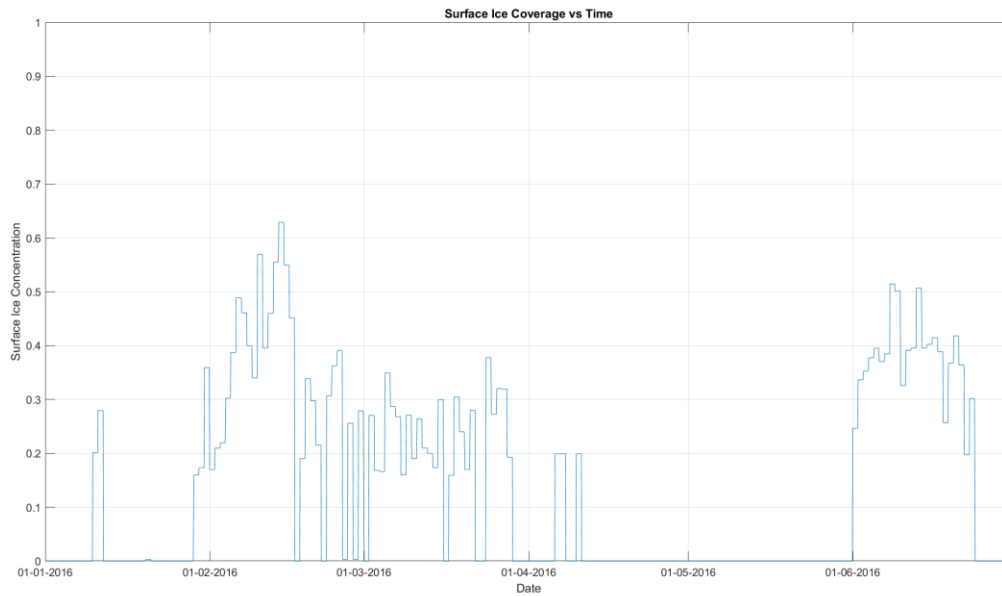

Figure 83: Mean hourly sea-ice concentration as a function of time at Station 10.

7.5 Tabulated Shelf Station R² Minima, Maxima, and Mean Statistics

Tabulated R² data for the shelf stations is presented in the following four tables:

Table 12: Min, max, and mean of R² for U_{10} parameter. Yellow stations did not undergo a process of ice-culling; red stations did undergo a process of ice-culling.

Horizontal Wind 10m Analysis: Shelf Stations 1, 8, 18 (Non-Ice)   10, 14, 20 (Ice- Culled)

Frequency	Non-Ice Shelf Station R² Stats U_{10} Stations 1, 8, 18	Non-Ice and Ice-Culled Shelf Station R² Stats U_{10} Stations 1, 8, 18, 10, 14, 20
4 kHz	Min = 0.75 Max = 0.76 Mean = 0.75	Min = 0.61 Max = 0.85 Mean = 0.76
3 kHz	Min = 0.69 Max = 0.75 Mean = 0.73	Min = 0.61 Max = 0.84 Mean = 0.74
2 kHz	Min = 0.53 Max = 0.74 Mean = 0.67	Min = 0.53 Max = 0.83 Mean = 0.71
1 kHz	Min = 0.38 Max = 0.75 Mean = 0.62	Min = 0.38 Max = 0.82 Mean = 0.69
100 Hz	Min = 0.00 Max = 0.03 Mean = 0.01	Min = 0.00 Max = 0.52 Mean = 0.22

Table 13: Min, max, and mean of R^2 for U_{10N} parameter. Yellow stations did not undergo a process of ice-culling; red stations did undergo a process of ice-culling.

Neutral Wind Analysis: Shelf Stations 1, 8, 18 (Non-Ice)   10, 14, 20 (Ice- Culled)

Frequency	Non-Ice Shelf Station R² Stats U_{10N} Stations 1, 8, 18	Non-Ice and Ice-Culled Shelf Station R² Stats U_{10N} Stations 1, 8, 18, 10, 14, 20
4 kHz	Min = 0.77 Max = 0.77 Mean = 0.77	Min = 0.59 Max = 0.86 Mean = 0.77
3 kHz	Min = 0.72 Max = 0.75 Mean = 0.75	Min = 0.60 Max = 0.86 Mean = 0.76
2 kHz	Min = 0.56 Max = 0.77 Mean = 0.69	Min = 0.56 Max = 0.85 Mean = 0.73
1 kHz	Min = 0.40 Max = 0.76 Mean = 0.63	Min = 0.40 Max = 0.85 Mean = 0.70
100 Hz	Min = 0.00 Max = 0.03 Mean = 0.01	Min = 0.00 Max = 0.53 Mean = 0.22

Table 14: Mix, max, and mean of R^2 for $\alpha*U_{10N} + (1-\alpha)*SWH$ parameter. Yellow stations did not undergo a process of ice-culling; red stations did undergo a process of ice-culling.

Weighted U_{10N} + SWH Analysis: Shelf Stations 1, 8, 18 (Non-Ice)   10, 14, 20 (Ice- Culled)

Frequency	Non-Ice Shelf Station R² Stats Weighted U_{10N} + SWH Stations 1, 8, 18	Non-Ice and Ice-Culled Shelf Station R² Stats Weighted U_{10N} + SWH Stations 1, 8, 18, 10, 14, 20
4 kHz	Min = 0.77 Max = 0.78 Mean = 0.77	Min = 0.61 Max = 0.86 Mean = 0.77
3 kHz	Min =0.73 Max = 0.77 Mean = 0.75	Min = 0.61 Max = 0.86 Mean = 0.76
2 kHz	Min = 0.57 Max = 0.77 Mean = 0.69	Min = 0.57 Max = 0.85 Mean = 0.73
1 kHz	Min = 0.41 Max = 0.77 Mean = 0.64	Min = 0.41 Max = 0.85 Mean = 0.70
100 Hz	Min = 0.01 Max = 0.03 Mean = 0.02	Min = 0.01 Max = 0.53 Mean = 0.22

Table 15: Condensed mean R^2 table for the three tested parameters. Yellow stations did not undergo a process of ice-culling; red stations did undergo a process of ice-culling.

Freq	U_{10}	U_{10}	U_{10N}	U_{10N}	$\alpha*U_{10N} + (\alpha-1)*SWH$	$\alpha*U_{10N} + (\alpha-1)*SWH$
4 kHz SH:	0.75	0.76	0.77	0.77	0.77	0.77
3 kHz SH:	0.73	0.74	0.75	0.76	0.75	0.76
2 kHz SH:	0.67	0.71	0.69	0.73	0.69	0.73
1 kHz SH:	0.62	0.69	0.63	0.70	0.64	0.70
100 Hz SH:	0.01	0.22	0.01	0.22	0.02	0.22

From Table 15, it can be seen that R^2 of the models improves with increasing frequency in both the non ice-culled and, non ice-culled <u>and</u> ice-culled cases. However, the magnitude of improvement increases with decreasing frequency. Because the spectral signature of shipping is most pronounced in the lower frequencies, the side-effect discussed above is put into play and the lower frequencies receive a boost of 0.04 R^2 at 2 kHz, 0.06 to 0.07 R^2 at 1 kHz, and 0.20 to 0.21 R^2 at 100 Hz for all parameters tested.

8. *NSL/A* Comparison versus Kewley (1990)

8.1 Two Mechanism Fit

Kewley endorsed the idea that local low- and high-speed wind regimes associate with differing least square fit slopes in a given data set. He used a two-mechanism fit model in his research where the x-axis was wind speed on a log scale and the y-axis was in decibels. The logarithmic scale would have a linearizing effect on data behaving in an exponential fashion. The success of the two-mechanism fit is closely related to the success of the two-term exponential model explored in this thesis. The fact that the two-term exponential function has modelled the data most accurately proves that Kewley and others who used the two-mechanism fit, as well as this author with the two-term exponential model were using an ideal modelling methodology. For discussion, a horizontal wind speed regression is shown from this thesis
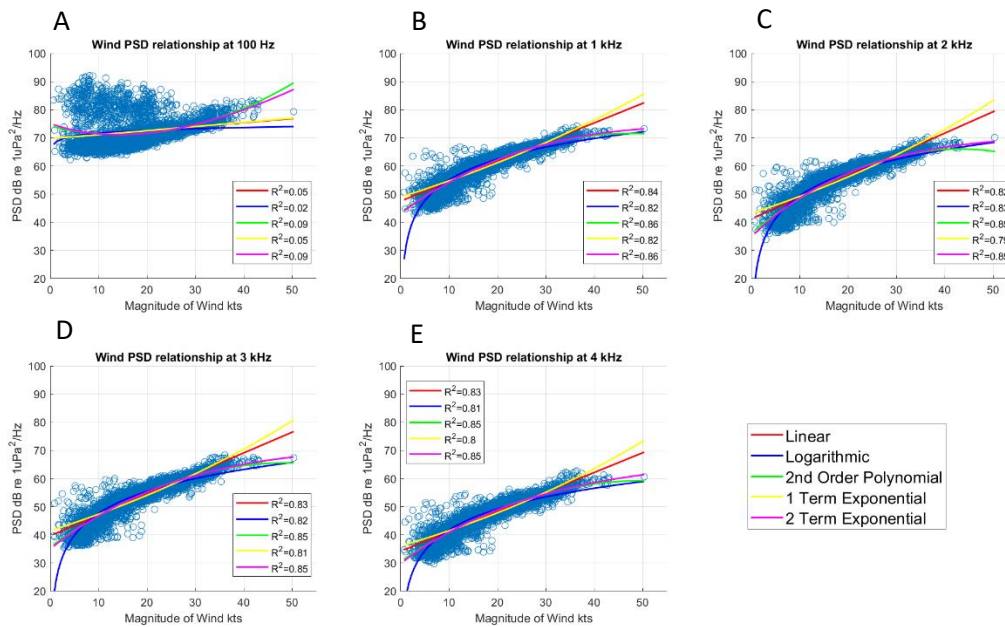
Figure 84: Wind *PSD* models linking horizontal wind speed magnitude 10 m above sea level and hourly minimum sound power levels taken between Jan and June 2016 at Station 15. Figure A) wind *PSD* at 100 Hz frequency bin, B) 1 kHz, C) 2 kHz, D) 3 kHz, E) 4 kHz.

And an example regression from Kewley (Kewley, 1990) is shown for comparison
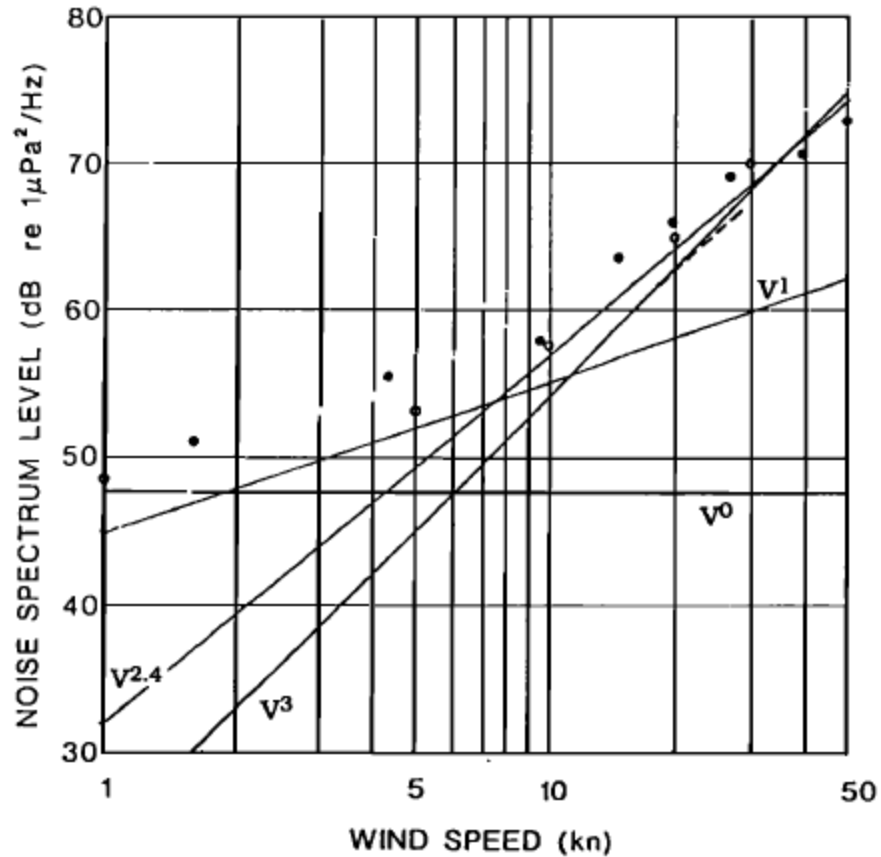
Figure 85: Wind speed dependence of ambient noise level at 500 Hz. ○ North Pacific deepest hydrophone data – Morris; ● North Atlantic deepest hydrophone data – Perrone; - - - the 446 Hz regression fit of Shooter and Gentry. Lines for the two-mechanism fit (V^1 and V^3) and the Crouch and Burt method (V^0 and $V^{2.4}$) are shown (reproduced from Kewley, 1990).

8.2 Speed Regions and the Low Frequency Flat 'S'

The two-mechanism fit example from Kewley leverages two low frequency bands, 500 Hz and 446 Hz. A comparison vs the 100 Hz band in this thesis is possible if one disregards the high variance, low density scatter cloud above 70 dB from 0 to 25 kts. The result is similarly shaped data. Kewley speaks to two mechanism lines falling along what appear to be two sets of data with one of the data sets existing in the range of 1 to 10 kts and the other in excess of this speed band. The Beaufort wind scale indicates that wave crests begin to break at 10 kts (5.1 m/s) and Kewley indicates two speed-dependent regions separated by a wind speed of 8 to 10 m/s or 16 to 20 kts. Mechanistically, it is clear in Figure 85 that after 10 kts, the slope of the noise level becomes steeper. This effect is seen in Figure 84A, if one disregards the high variance

data described above. It is interesting that Kewley's 500 Hz and 446 Hz data, and this author's 100 Hz data articulate a concave shape where this author's 1 to 4 kHz band data articulates a convex shape. Given the muting of sound power at higher wind speeds, it is hypothesized that sub 1 kHz frequencies would articulate a flat 'S' curved power spectral distribution from 0 to 50 kts; that is to say, three speed-dependent regions.

The "break point" effect is more easily seen at higher frequencies, i.e., the 1 to 4 kHz range in Figures 84B through 84E. Above 30 kts, a plateauing of the scatter cloud manifests as bubbles driven below the surface begin to attenuate and mute the noise present within the water column and a horizontal power spectral density limit is achieved (Farmer and Lemon, 1984). Before the break point, it is debateable if the scatter distribution expresses a linear or curved characteristic because there is such high variance – the truth of the matter is not clear. However, after the break point, the scatter expresses an undeniable radius of curvature between 10 and 50 kts. In the 1 to 4 kHz band, it is recommended that further study on this subject experiment with a pre-break point linear, post-break point 1 term exponential model. A bi-linear regression would not model well post-break point. In the sub 1 kHz band, it is recommended that model experimentation follow a 0 to 10 kt linear, 10 to 33 kt two-term exponential, and 33 to 50 kt linear regression. There appear to be three regions of fit (three speed regions) in the sub 1 kHz band. This would be more easily seen if high power sources were culled from the data through a process of *AIS* culling (ship traffic noise culling) beyond the maximum extent of the hydrophone listening area. This process would be challenged by distantly ducted shipping noise, but it is a reasonable position from which to begin.

For example, at Figure 86, Vagle (Vagle et al, 1990) presents two listening radii for a low and a high frequency source as a function of depth for an ambient sound hydrophone, such as the *WOTAN* instrument in the absence of refraction. Farmer and Vagle (1988) developed such figures assuming that the hydrophone is omnidirectional, the ocean surface is cylindrically symmetrical, whose listening area increases with instrument depth and decreases with acoustic frequency (Farmer and Vagle, 1988). The listening radius will vary with *SVP*, ambient noise, and receiver directionality. Let us hypothetically assume one wished to execute model regressions at the 3 kHz band for a hydrophone at a depth of 800 m. The listening radius of a hydrophone at this band is approximately 1200 m. It is recommended that instances of hourly minimum sound power levels corresponding to the presence of *AIS* ship traffic as well as the presence of sea ice within a 1200 m radius of the hydrophone be culled from the data set in order to refine the quality of the hourly minimum sound power levels. At the 3 kHz band, the process of ice culling on hourly minimum sound power levels would have much greater impact on the quality of the regressions than *AIS* culling but at sub 1 kHz

frequencies, it is suspected that the process of ice and *AIS* culling could collectively yield significant enhancement to the models.
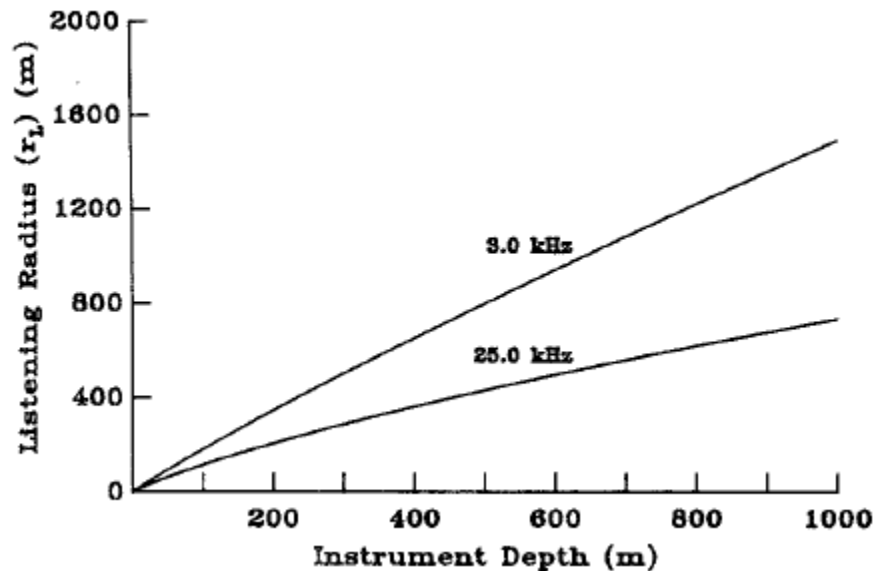
Figure 86: Listening radius of *WOTAN* instrument as a function of depth for 3 and 25 kHz (reproduced from Vagle et al, 1990).

8.3 *NSL/A* Kewley versus Kovaloff

Comparisons between Kewley's compiled *NSL/A* figure (Kewley, 1990) and three cases from this thesis will follow. For reasons of equality, horizontal wind speed magnitude 10 m above sea level was selected as the parameter of comparison vs Kewley. Kovaloff's 3 – 4 kHz *NSL/A* lines are likely affected by the anti-aliasing roll off leading to the sharp drop in values. All *NSL/A* figures assumed a 50 cm bubble cloud penetration depth. The *NSL/A* low, medium, and high metric plots based on horizontal wind speed magnitude 10 m above sea level for all stations are found at Figure 87.
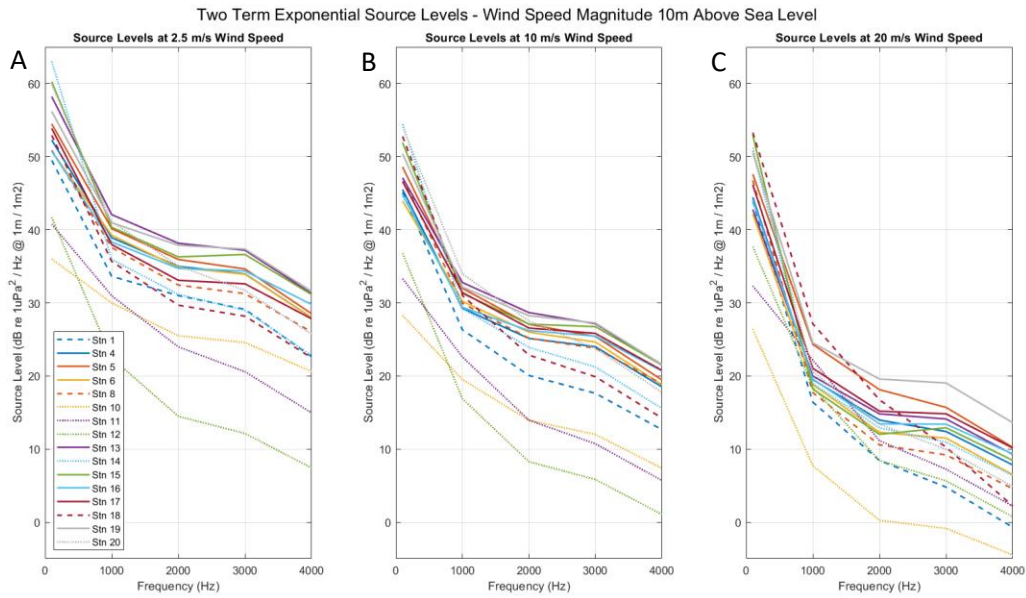
Figure 87: *NSL/A* based on horizontal wind speed magnitude 10 m above sea level, two-term exponential regression for all stations A) 2.5 m/s, B) 10 m/s, C) 20 m/s wind speed respectively. Solid lines are slope stations, dashed lines are shelf stations with less than 10% surface ice coverage, dotted lines are shelf stations with greater than 10% surface ice coverage.
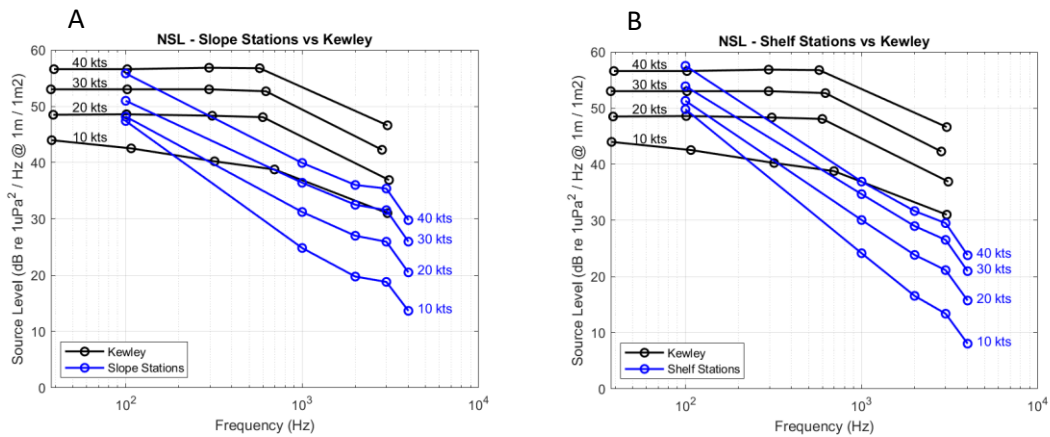
Figure 88: *NSL/A* Kewley vs Kovaloff continental slope and shelf side-by-side comparison. Figure A) Kovaloff continental slope data at 10 kts, 20 kts, 30 kts, 40 kts wind speed (Stations 4, 5, 6, 13, 15, 16, 17, 19). Figure B) Kovaloff continental shelf data at 10 kts, 20 kts, 30 kts, 40 kts wind speed for stations containing insignificant surface ice coverage (Stations 1, 8, 18) and ice-culled stations (Stations 10, 14, 20).

The side-by-side comparison of Kovaloff's slope vs Kovaloff's shelf (including ice culled) stations is presented at Figure 88. At 100 Hz, *NSL/A* on the slope are marginally lower than on the shelf likely because of decreased shipping density and therefore contamination although these levels are defined by such contamination and are not reliable. At 1 kHz, slope and shelf levels are within 1 dB of one another except at 40 kts wind speed where shelf *NSL/A* is 3 dB lower than on the slope. At 2 kHz, shelf *NSL/A* are 3 to 4 dB lower than on the slope across all wind speeds. At 3 kHz, shelf *NSL/A* are 5 to 6 dB lower than on the slope across all wind speeds. In summary, at 1 kHz, slope and shelf station *NSL/A* are very similar except at high wind speeds, and at 2 and 3 kHz, the *NSL/A* over the shelf are generally lower.
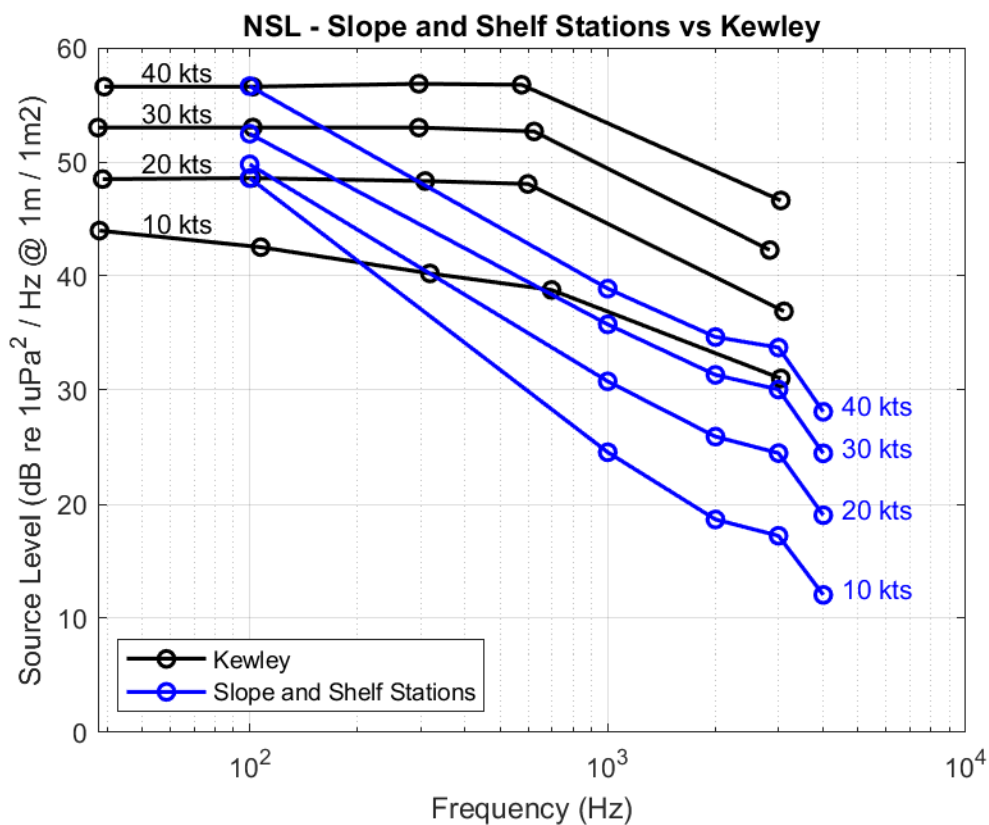
Figure 89: *NSL/A* Kewley vs Kovaloff total continental slope <u>and</u> shelf data at 10 kts, 20 kts, 30 kts, 40 kts wind speed for slope stations (Stations 4, 5, 6, 13, 15, 16, 17, 19) <u>and</u> shelf stations containing insignificant surface ice coverage (Stations 1, 8, 18) <u>and</u> ice-culled stations (Stations 10, 14, 20).

The comparison of Kewley vs Kovaloff total Slope and Shelf is presented at Figure 89. This is the most generalized comparison which combines Kewley's consolidated Atlantic and Pacific data with Kovaloff's consolidated Slope and Shelf data from the Canadian East Coast. Conclusions cannot be made on the 100 Hz data as both

Kewley and Kovaloff estimates are contaminated by shipping. Kovaloff's 1 to 3 kHz *NSL/A* data is significantly lower than Kewley's *NSL/A* data.

9. Applications

Step 1: Let us assume that a Canadian Patrol Frigate is operating in an *ASW* threat environment, with bathymetry similar to that in the vicinity of hydrophone Station 4; the *SVP* is equally similar. The sonic layer depth is 200 m and the threat is suspected of hiding beneath it. The *ASW* team wishes to optimize *SNR* when the towed sonar array is streamed to 220 m. The *ASW* team is searching for a 1 kHz tonal. The ship's Navigating Officer measures a wind speed of 20 kts. He consults Figure 88B. At 1 kHz and 20 kts wind speed, the corresponding ambient noise source level is 30 dB re 1 μPa^2 / Hz @ 1 m / m^2. This is indicative of the estimated ambient sound source power due to surface wind at a shelf location. In practice, this procedure would likely be done by a computer program.

Step 2: To determine *PSD* due to ambient noise at an arbitrary depth within the water column, 220 m for example, the prior steps must be executed. Next, a propagation loss model from the surface to the suspected submarine depth (220 m) should be executed to determine the *TL*. This would be conducted exploiting reciprocity with the source at the submarine depth. The resulting *TL* should be added to the *NSL/A* to give the ambient noise *PSD* at the arbitrary depth. Sensors may be thusly calibrated.

9.1 Procedural Flow Chart

Context

The reader is in a Frigate searching for an enemy submarine using a towed SONAR array

This procedure may used to estimate background noise levels at a specified depth

1. a) Require Figure 88 NSL/A Table or equivalent

1. b) Require submarine tonal for prosecution within 1 to 4 kHz band

2. Measure U_{10}

3. Determine NSL/A based on Step 2 and Figure 88

4. Execute TL propagation model using reciprocity from depth of towed SONAR array to surface using to frequency to be prosecuted

5. Obtain RL at depth of towed SONAR array by adding TL from Step 4 to NSL/A determined at Step 3

6. Use background noise estimate to inform detection threshold

10. Conclusions

A foundational aspect of this thesis is that hourly minimum sound power levels are the best representation of ocean ambient noise due to surface weather in any given hour and that high power noise factors such as shipping, precipitation, and/or marine mammal calls are either not present in these minima or that their transient nature results in minimal impact during regression modelling. If however a ship or oil rig was located above the hydrophone using dynamic positioning or a fishing fleet was operating in a localized area for an extended period of time, the long-term recordings over the hydrophone would be biased by these sources. It is suspected that the methods of Kewley (1990), Vagle (1990), and others did not adequately remove such high-power instances.

It is assumed that the meteorological parameters harvested from *ERA5* and the acoustical recordings extracted from JASCO *AMAR* hydrophones are accurate. Discrepancies in *NSL/A* estimates between stations are attributed to the uncertainty in the *TL* model which, in this study, cannot account for a dynamically changing sound velocity profile, real world scatterers and attenuators, and unknown ocean bottom layering and density variation. However, should this information be available, the *TL* model could be enhanced, thus improving the estimate of *NSL/A*.

Evaluating modelled transmission loss from 10 km vs 20 km, and 20 km vs 25 km, it was concluded that a 20 km maximum range was the preferred range to study considering that almost all energy, 89 to 97% from 100 Hz to 4 kHz, would be present and accounted for in the transmission loss software integrations. While examining out to longer ranges would yield more accurate results, for practical reasons, 20 km facilitated a reasonable balance of accuracy versus computational time.

In the determination of which bubble cloud penetration depth is most accurate in terms of predicting transmission loss and therefore a more realistic source level term, *TL* and *NSL/A* estimates were made from 100 Hz to 4 kHz at source level depths 25 cm, 50 cm, 75 cm, 100 cm, 125 cm, and 150 cm at a shallow shelf station and a deep slope station. Based on the results of Prosperetti and Buckingham, lower frequencies ~100 Hz would be generated at deeper bubble cloud penetration depths, higher frequencies ~ 1 to 4 kHz would be generated at shallower bubble cloud penetration depths, and the corresponding *NSL/A* values would be directly related to the depth of the water column. That is to say, shelf (shallow) columns express more transmission loss and slope (deep) columns express less transmission loss.

This thesis concluded that of five tested regression functions, the two-term exponential function models hourly minimum sound power levels in the 1 to 4 kHz band the best across all of 13 tested parameters. Although Kewley and others have leaned on a bi-linear model when regressing U_{10}, and it is possible that the two-term exponential function over fits the data in the 1 to 4 kHz band, it is equally possible that a bi-linear regression under fits the data. It is possible that in wind speeds lower than the 30 kt break point, the regressions express a liner shape but certainly a one-term exponential would be required to regress the established departure from linearity at the break point. Until lower variance hydrophone recordings become available, this issue will be left to posterity.

By cross correlating meteorological parameters with each other as well as 4 kHz hourly minimum sound power levels, insights into the relative correlations and lag relationships were found.

A newly devised weighted neutral wind plus wave composite parameter illuminated the distribution of responsibility in ambient underwater acoustical genesis. Respective parameters were normalized to max and iterated against each other in increments or weights of 0.1, from 0.0 to 1.0 in order to determine the maximum modellable R^2. As per Table 5, from 1 to 4 kHz, at the maximum R^2 is roughly 90% weighted to neutral wind and roughly 10% weighted to *SWH*. Experimentation was made with weighted neutral wind plus Charnock parameter with extremely similar values of maximum R^2. However, in the case of weighted neutral wind plus Charnock parameter, hourly minimum sound power levels are roughly 85% weighted to neutral wind and roughly 15% weighted to *SWH* in the 1 to 4 kHz band.

This thesis concluded parametric R^2 performance in the 1 to 4 kHz band from best to worst:

1. Weighted neutral wind (U_{10N}) plus significant wave height (*SWH*)

2. Weighted neutral wind (U_{10N}) plus Charnock parameter

3. Weighted neutral wind (U_{10N}) plus wind wave (*WW*)

4. Neutral wind (U_{10N})

5. Weighted horizontal wind (U_{10}) plus significant wave height (*SWH)*

6. Edson wave age

7. Horizontal wind (U_{10})

8. Wind Wave (*WW*)

9. Charnock parameter

10. Significant wave height (*SWH)*

Critical points are that mean wave period and peak wave period had no relationship with hourly minimum sound power level and friction velocity expressed R^2 less than 0.2 across all frequencies. Edson wave age is an inversion of U_{10N} and never performs as well as U_{10N} during regressions or cross correlations. For ease of measurement, ease of use in computations, strength of R^2, and intuitive quality, U_{10} is the preferred parameter.

At Figure 84A, the Station 15 *PSD* model may illuminate the wind/wave driven shape of power spectral generation in the 100 Hz band. A flat 'S' curve is clearly evident below the low-density, high-power data between 0 and 30 kts. In the sub 1 kHz band, it is recommended that model experimentation follow a 0 to 10 kt linear, 10 to 33 kt two-term exponential, and 33 to 50 kt linear regression. There appear to be three regions of fit (three speed regions) in the sub 1 kHz band.

Of the 16 hydrophones studied, *ERA5* data indicated that 9 of them had instances of sea ice cover during the study period. In order to include the maximum amount of acoustical and modelling information possible, the author culled all instances of ice presence over the 5 stations which express significant (>10%) instances of sea ice coverage. By culling all instances of hourly minimum sound power levels which correspond to the presence of sea-ice, the characteristic bi-mechanistic shape of the ice-free station appears and exceptional R^2 values materialize, in particular at 100 Hz. This is due to the fact that ice represents a navigation hazard to most shipping (shipping without ice-strengthened hulls), and thus shipping prefers to sail around it. As the shipping avoids the ice and therefore the active listening area of the hydrophone, the hydrophone is able to make unadulterated low-frequency recordings. The culling of hourly minimum sound power levels corresponding to ship presence via *AIS* data over the effective listening area of any hydrophone would likely yield a similar result. Consequently, a side-effect of the ice-culling process is the ability to extract higher quality, low frequency power spectra.

From Table 15, it can be seen that R^2 modelling improves with increasing frequency in both the non-ice culled and, non-ice culled <u>and</u> ice culled cases. However, the magnitude of improvement increases with decreasing frequency. Because the spectral signature of shipping is most pronounced in the lower frequencies, the side-effect discussed above is put into play and the lower frequencies receive a boost of 0.04

R^2 at 2 kHz, 0.06 to 0.07 R^2 at 1 kHz, and 0.20 to 0.21 R^2 at 100 Hz for all parameters tested.

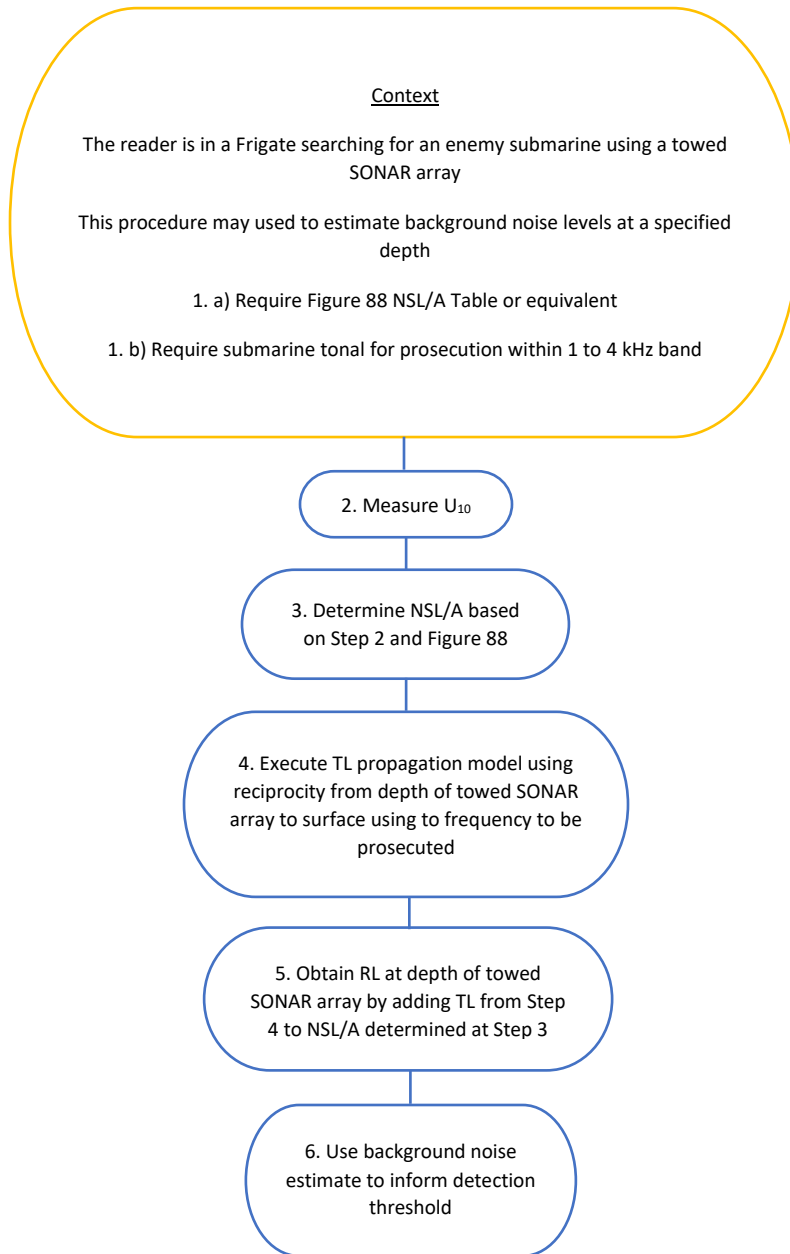A generalized *NSL/A* comparison was executed between Kewley and Kovaloff Slope and Shelf using U_{10} as a common parameter. Conclusions cannot be made on the 100 Hz data as both Kewley and Kovaloff estimates are contaminated by shipping. Kovaloff's 1 to 3 kHz *NSL/A* data is significantly lower than Kewley's *NSL/A* data. Kovaloff's results indicate a decrease in *NSL/A* by 10 to 15 dB in the 1 to 3 kHz band from 10 to 40 kts compared to Kewley. This is attributed to the harvest of hourly minimum sound power levels for regression.

Annex A: Non-Averaged Tabulated R² Data

100 Hz

Station	Depth	Bathy Type	Ice	Ice Conc	Wind R2	Wave R2	WW R2	Char R2	Fric Vel R2	U10N R2	Waveage R2	max U10 + SWH R2	U10 + SWH (a)	U10 + SWH (b)	U10 + SWH (α)	U10 + SWH (α-1)	max U10N + SWH R2	U10N + SWH (a)	U10N + SWH (b)	U10N + SWH (α)	U10N + SWH (α-1)	max U10N + WW R2	U10N + WW (a)	U10N + WW (b)	U10N + WW (α)	U10N + WW (α-1)
1	175	'shelf'	'-'	0.00	0.03	0.03	0.04	0.03	0.00	0.04	0.03	0.03	0.50	0.00	1.00	0.00	0.04	0.40	0.00	1.00	0.00	0.04	0.40	0.00	1.00	0.00
4	1558	'slope'	'-'	0.00	0.36	0.20	0.35	0.28	0.03	0.38	0.36	0.36	0.60	0.10	0.86	0.14	0.38	1.00	0.10	0.91	0.09	0.36	0.10	0.30	1.00	0.00
5	1831	'slope'	'-'	0.00	0.18	0.14	0.16	0.13	0.02	0.19	0.19	0.19	0.80	0.30	0.73	0.27	0.19	0.70	0.20	0.78	0.22	0.19	0.30	0.00	1.00	0.00
6	1790	'slope'	'-'	0.00	0.30	0.21	0.29	0.21	0.03	0.32	0.31	0.31	0.70	0.10	0.88	0.13	0.32	1.00	0.10	0.91	0.09	0.31	0.30	0.00	1.00	0.00
8	420	'shelf'	'-'	0.00	0.02	0.01	0.01	0.01	0.00	0.02	0.02	0.02	1.00	0.00	1.00	0.00	0.02	0.50	0.00	1.00	0.00	0.02	0.50	0.00	1.00	0.00
10	110	'shelf'	'ice'	0.14	0.40	0.33	0.36	0.32	0.00	0.38	0.45	0.45	0.50	0.00	1.00	0.00	0.38	0.30	0.00	1.00	0.00	0.40	0.40	0.50	1.00	0.00
11	150	'shelf'	'ice'	0.59	0.06	0.23	0.14	0.26	0.09	0.06	0.24	0.24	0.10	0.40	0.20	0.80	0.06	0.20	1.00	0.17	0.83	0.06	0.50	0.00	0.00	1.00
12	142	'shelf'	'ice'	0.63	0.02	0.39	0.13	0.20	0.08	0.00	0.43	0.43	0.10	0.40	0.20	0.80	0.06	0.20	0.50	0.17	0.83	0.00	0.50	0.00	0.00	1.00
13	1700	'slope'	'-'	0.08	0.43	0.38	0.41	0.32	0.07	0.44	0.44	0.44	0.20	0.80	0.73	0.27	0.44	1.00	0.00	1.00	0.17	0.44	0.30	0.50	1.00	0.00
14	551	'depression'	'ice'	0.29	0.26	0.38	0.43	0.48	0.12	0.26	0.44	0.48	0.60	0.40	1.00	0.08	0.26	0.26	0.50	0.43	0.48	0.26	1.00	0.00	1.00	0.00
15	1993	'slope'	'-'	0.01	0.09	0.08	0.08	0.05	0.03	0.09	0.09	0.09	0.40	0.00	1.00	0.27	0.09	0.09	0.00	0.41	0.05	0.09	0.20	0.00	1.00	0.00
16	1608	'slope'	'-'	0.00	0.09	0.03	0.08	0.05	0.02	0.10	0.09	0.09	0.10	0.00	1.00	0.10	0.10	0.10	0.00	0.13	0.05	0.10	0.60	0.00	1.00	0.00
17	1273	'slope'	'-'	0.00	0.22	0.11	0.21	0.12	0.01	0.23	0.22	0.22	1.00	0.00	1.00	0.00	0.23	1.00	0.00	1.00	0.00	0.23	0.00	0.60	1.00	0.00
18	214	'shelf'	'-'	0.00	0.00	0.01	0.01	0.01	0.01	0.01	0.00	0.02	0.10	0.50	0.91	0.09	0.01	0.00	0.70	0.22	0.78	0.01	0.00	0.00	1.00	0.00
19	1547	'slope'	'-'	0.00	0.02	0.09	0.01	0.01	0.10	0.02	0.02	0.09	0.50	0.10	0.17	0.83	0.02	0.20	0.10	0.17	0.83	0.09	0.90	0.00	0.00	1.00
20	236	'shelf'	'ice'	0.21	0.15	0.19	0.19	0.35	0.10	0.15	0.24	0.24	0.20	0.70	0.22	0.78	0.15	0.20	0.90	0.18	0.82	0.21	0.50	0.20	0.71	0.29

1 kHz

Station	Depth	Bathy Type	Ice	Ice Conc	Wind R2	Wave R2	WW R2	Char R2	Fric Vel R2	U10N R2	Waveage R2	max U10 + SWH R2	U10 + SWH (a)	U10 + SWH (b)	U10 + SWH (α)	U10 + SWH (α-1)	max U10N + SWH R2	U10N + SWH (a)	U10N + SWH (b)	U10N + SWH (α)	U10N + SWH (α-1)	max U10N + WW R2	U10N + WW (a)	U10N + WW (b)	U10N + WW (α)	U10N + WW (α-1)
1	175	'shelf'	'-'	0.00	0.73	0.46	0.71	0.67	0.02	0.74	0.73	0.73	0.40	0.00	1.00	0.00	0.74	0.10	0.00	0.00	0.00	0.74	0.20	0.00	1.00	0.00
4	1558	'slope'	'-'	0.00	0.73	0.43	0.75	0.64	0.04	0.77	0.74	0.74	0.70	0.20	0.78	0.22	0.78	0.10	0.10	0.17	0.17	0.77	1.00	0.20	0.83	0.17
5	1831	'slope'	'-'	0.00	0.61	0.35	0.63	0.42	0.01	0.64	0.61	0.61	0.60	0.10	0.86	0.14	0.64	0.10	0.10	0.09	0.09	0.64	0.60	0.00	1.00	0.00
6	1790	'slope'	'-'	0.00	0.81	0.44	0.82	0.68	0.05	0.83	0.82	0.82	0.30	0.10	0.75	0.25	0.85	0.20	0.20	0.22	0.22	0.84	0.90	0.40	0.69	0.31
8	420	'shelf'	'-'	0.00	0.75	0.49	0.75	0.69	0.04	0.77	0.76	0.76	0.70	0.10	0.88	0.13	0.77	0.10	0.10	0.09	0.09	0.77	0.10	0.00	1.00	0.00
10	110	'shelf'	'ice'	0.14	0.46	0.38	0.37	0.41	0.00	0.44	0.46	0.54	0.90	0.00	1.00	0.00	0.53	0.10	0.10	0.13	0.13	0.52	0.70	0.00	1.00	0.00
11	150	'shelf'	'ice'	0.59	0.06	0.14	0.12	0.13	0.06	0.05	0.06	0.14	0.10	1.00	0.09	0.91	0.14	0.10	0.20	1.00	1.00	0.11	0.00	0.10	0.00	1.00
12	142	'shelf'	'ice'	0.63	0.02	0.35	0.15	0.14	0.11	0.00	0.00	0.35	0.00	0.40	0.00	1.00	0.35	0.00	0.40	1.00	1.00	0.18	0.00	0.00	0.00	1.00
13	1700	'slope'	'-'	0.08	0.75	0.56	0.75	0.66	0.03	0.78	0.75	0.79	0.90	0.40	0.69	0.31	0.79	0.20	0.10	0.29	0.29	0.79	0.30	0.10	0.75	0.25
14	551	'depression'	'ice'	0.29	0.51	0.43	0.69	0.59	0.16	0.50	0.50	0.78	1.00	0.20	0.83	0.17	0.88	0.10	0.20	0.13	0.13	0.88	0.10	0.10	0.90	0.10
15	1993	'slope'	'-'	0.01	0.86	0.52	0.86	0.75	0.11	0.88	0.87	0.87	1.00	0.20	0.83	0.17	0.90	0.20	0.20	0.13	0.13	0.88	0.60	0.10	0.86	0.14
16	1608	'slope'	'-'	0.00	0.74	0.40	0.74	0.58	0.02	0.77	0.74	0.75	0.70	0.20	0.78	0.22	0.78	0.20	0.20	0.18	0.18	0.77	0.60	0.00	1.00	0.00
17	1273	'slope'	'-'	0.00	0.79	0.47	0.79	0.55	0.02	0.82	0.80	0.82	1.00	0.30	0.77	0.23	0.83	0.20	0.20	0.22	0.22	0.82	0.10	0.00	1.00	0.00
18	214	'shelf'	'-'	0.00	0.38	0.29	0.35	0.33	0.07	0.40	0.38	0.40	0.80	0.60	0.57	0.43	0.42	0.40	0.40	0.36	0.36	0.40	0.60	0.00	1.00	0.00
19	1547	'slope'	'-'	0.00	0.51	0.25	0.49	0.30	0.07	0.52	0.51	0.51	0.20	0.00	1.00	0.00	0.52	0.00	0.00	0.00	0.00	0.52	0.90	0.00	1.00	0.00
20	236	'shelf'	'ice'	0.21	0.56	0.52	0.71	0.67	0.02	0.57	0.56	0.76	0.60	0.20	0.75	0.25	0.77	0.70	0.20	0.22	0.22	0.76	0.90	0.50	0.64	0.36

2 kHz

Station	Depth	Bathy Type	Ice	Ice Conc	Wind R2	Wave R2	WW R2	Char R2	Fric Vel R2	U10N R2	Waveage R2	max U10 + SWH R2	U10 + SWH (a)	U10 + SWH (b)	U10 + SWH (α)	U10 + SWH (α-1)	max U10N + SWH R2	U10N + SWH (a)	U10N + SWH (b)	U10N + SWH (α)	U10N + SWH (α-1)	max U10N + WW R2	U10N + WW (a)	U10N + WW (b)	U10N + WW (α)	U10N + WW (α-1)
1	175	'shelf'	'-'	0.00	0.73	0.45	0.71	0.67	0.02	0.74	0.73	0.73	1.00	0.10	0.91	0.09	0.74	0.70	0.00	1.00	0.00	0.73	0.70	0.00	1.00	0.00
4	1558	'slope'	'-'	0.00	0.74	0.43	0.76	0.66	0.04	0.79	0.74	0.76	1.00	0.30	0.77	0.23	0.80	0.90	0.20	0.82	0.18	0.74	0.80	0.20	0.80	0.20
5	1831	'slope'	'-'	0.00	0.66	0.36	0.68	0.46	0.01	0.70	0.67	0.67	0.80	0.10	0.89	0.11	0.70	1.00	0.00	0.91	0.09	0.67	0.40	0.00	1.00	0.00
6	1790	'slope'	'-'	0.00	0.81	0.41	0.82	0.71	0.05	0.84	0.82	0.82	0.70	0.20	0.78	0.22	0.85	0.80	0.20	0.80	0.20	0.82	0.10	0.30	0.25	0.75
8	420	'shelf'	'-'	0.00	0.75	0.48	0.75	0.70	0.04	0.77	0.76	0.75	0.70	0.10	0.88	0.13	0.77	1.00	0.00	0.91	0.09	0.75	1.00	0.00	1.00	0.00
10	110	'shelf'	'ice'	0.14	0.47	0.39	0.38	0.43	0.00	0.44	0.46	0.55	0.70	0.00	1.00	0.00	0.53	1.00	0.00	0.83	0.17	0.46	1.00	0.00	1.00	0.00
11	150	'shelf'	'ice'	0.59	0.13	0.28	0.18	0.18	0.07	0.12	0.13	0.30	0.10	0.70	0.13	0.87	0.29	0.10	0.70	0.11	0.89	0.13	0.20	0.00	1.00	0.00
12	142	'shelf'	'ice'	0.63	0.02	0.45	0.21	0.18	0.11	0.02	0.02	0.45	0.00	0.90	0.00	1.00	0.45	0.00	0.90	0.00	1.00	0.02	1.00	0.30	1.00	0.00
13	1700	'slope'	'-'	0.08	0.75	0.53	0.74	0.67	0.04	0.77	0.74	0.78	0.50	0.20	0.71	0.29	0.77	0.50	0.20	0.75	0.25	0.74	1.00	0.00	1.00	0.00
14	551	'depression'	'ice'	0.29	0.47	0.41	0.67	0.62	0.16	0.47	0.47	0.77	0.60	0.10	0.86	0.14	0.77	0.60	0.10	0.88	0.12	0.47	0.40	0.10	0.88	0.13
15	1993	'slope'	'-'	0.01	0.85	0.50	0.86	0.76	0.10	0.87	0.86	0.86	1.00	0.20	0.83	0.17	0.86	1.00	0.20	0.90	0.10	0.86	0.70	0.00	0.36	0.64
16	1608	'slope'	'-'	0.00	0.77	0.41	0.77	0.62	0.03	0.80	0.77	0.79	0.30	0.10	0.75	0.25	0.79	0.30	0.10	0.75	0.25	0.77	0.80	0.10	0.91	0.09
17	1273	'slope'	'-'	0.00	0.77	0.46	0.76	0.60	0.02	0.79	0.77	0.80	0.70	0.30	0.70	0.30	0.80	0.70	0.30	0.71	0.29	0.77	1.00	0.10	1.00	0.00
18	214	'shelf'	'-'	0.00	0.54	0.35	0.52	0.44	0.07	0.56	0.54	0.56	0.90	0.50	0.64	0.36	0.56	0.90	0.50	0.78	0.22	0.54	0.70	0.10	0.77	0.23
19	1547	'slope'	'-'	0.00	0.54	0.29	0.51	0.40	0.09	0.54	0.54	0.54	0.50	0.00	1.00	0.00	0.54	0.50	0.00	1.00	0.00	0.54	1.00	0.00	1.00	0.00
20	236	'shelf'	'ice'	0.21	0.55	0.51	0.71	0.67	0.03	0.56	0.55	0.77	0.60	0.20	0.75	0.25	0.77	0.60	0.20	0.80	0.20	0.55	0.90	0.50	0.64	0.36

3 kHz

Station	Depth	Bathy Type	Ice	Ice Conc	Wind R2	Wave R2	WW R2	Char R2	Fric Vel R2	U10N R2	Waveage R2	max U10 + SWH R2	U10 + SWH (a)	U10 + SWH (b)	U10 + SWH (α)	U10 + SWH (α-1)	max U10N + SWH R2	U10N + SWH (a)	U10N + SWH (b)	U10N + SWH (α)	U10N + SWH (α-1)	max U10N + WW R2	U10N + WW (a)	U10N + WW (b)	U10N + WW (α)	U10N + WW (α-1)
1	175	'shelf'	'-'	0.00	0.75	0.47	0.72	0.68	0.02	0.76	0.75	0.75	1.00	0.10	0.91	0.09	0.76	0.40	0.00	1.00	0.00	0.40	0.40	0.00	1.00	0.00
4	1558	'slope'	'-'	0.00	0.76	0.44	0.77	0.67	0.04	0.81	0.76	0.78	1.00	0.30	0.77	0.23	0.81	0.90	0.20	0.82	0.18	0.70	0.70	0.10	0.88	0.13
5	1831	'slope'	'-'	0.00	0.71	0.39	0.71	0.49	0.01	0.75	0.72	0.72	0.80	0.10	0.89	0.11	0.75	1.00	0.10	0.91	0.09	0.50	0.50	0.00	1.00	0.00
6	1790	'slope'	'-'	0.00	0.82	0.41	0.83	0.71	0.05	0.84	0.82	0.83	0.40	0.10	0.80	0.20	0.85	0.50	0.10	0.83	0.17	1.00	0.30	0.30	0.77	0.23
8	420	'shelf'	'-'	0.00	0.76	0.47	0.75	0.71	0.04	0.76	0.76	0.76	0.90	0.10	0.90	0.10	0.78	1.00	0.00	1.00	0.00	1.00	0.00	0.00	1.00	0.00
10	110	'shelf'	'ice'	0.14	0.46	0.39	0.38	0.42	0.00	0.42	0.45	0.54	0.80	0.00	1.00	0.00	0.51	0.54	0.33	0.86	0.10	0.54	0.70	0.10	0.36	0.00
11	150	'shelf'	'ice'	0.59	0.15	0.31	0.19	0.20	0.06	0.14	0.15	0.33	0.10	0.70	0.13	0.88	0.18	0.33	0.00	0.15	0.15	0.33	1.00	0.10	1.00	0.70
12	142	'shelf'	'ice'	0.63	0.03	0.45	0.22	0.20	0.08	0.03	0.03	0.45	0.00	0.30	0.00	1.00	0.23	0.45	0.00	0.03	0.03	0.45	1.00	0.00	0.00	0.30
13	1700	'slope'	'-'	0.08	0.75	0.54	0.75	0.67	0.04	0.78	0.75	0.78	0.50	0.20	1.00	0.00	0.78	0.75	0.25	0.78	0.04	0.75	0.78	0.00	0.50	0.20
14	551	'depression'	'ice'	0.29	0.47	0.42	0.67	0.63	0.16	0.47	0.47	0.77	0.60	0.10	0.88	0.12	0.47	0.47	0.16	0.47	0.16	0.47	0.60	0.10	0.60	0.10
15	1993	'slope'	'-'	0.01	0.85	0.51	0.85	0.75	0.11	0.87	0.86	0.86	0.60	0.10	0.00	1.00	0.87	0.86	0.11	0.86	0.11	0.86	0.70	0.10	0.60	0.10
16	1608	'slope'	'-'	0.00	0.78	0.41	0.77	0.63	0.03	0.81	0.78	0.80	0.70	0.20	0.71	0.29	0.81	0.80	0.00	0.78	0.03	0.80	0.78	0.00	0.70	0.20
17	1273	'slope'	'-'	0.00	0.75	0.45	0.74	0.58	0.02	0.77	0.75	0.78	0.90	0.20	0.86	0.14	0.77	0.78	0.25	0.77	0.02	0.75	0.78	0.10	0.90	0.00
18	214	'shelf'	'-'	0.00	0.70	0.42	0.68	0.58	0.05	0.72	0.70	0.72	0.90	0.40	0.86	0.14	0.72	0.72	0.25	0.72	0.05	0.70	0.72	0.10	0.90	0.09
19	1547	'slope'	'-'	0.00	0.55	0.30	0.52	0.30	0.10	0.55	0.55	0.55	0.20	0.00	0.14	0.86	0.55	0.55	0.30	0.55	0.10	0.55	0.55	0.00	0.20	0.00
20	236	'shelf'	'ice'	0.21	0.55	0.51	0.71	0.66	0.03	0.55	0.55	0.55	1.00	0.10	0.78	0.22	0.55	0.55	0.30	0.55	0.03	0.55	0.90	0.50	1.00	0.36

4 kHz

Station	Depth	Bathy Type	Ice	Ice Conc	Wind R2	Wave R2	WW R2	Char R2	Fric Vel R2	U10N R2	Waveage R2	max U10 + SWH R2	U10 + SWH (a)	U10 + SWH (b)	U10 + SWH (α)	U10 + SWH (α-1)	max U10N + SWH R2	U10N + SWH (a)	U10N + SWH (b)	U10N + SWH (α)	U10N + SWH (α-1)	max U10N + WW R2	U10N + WW (a)	U10N + WW (b)	U10N + WW (α)	U10N + WW (α-1)
1	175	'shelf'	'-'	0.00	0.77	0.46	0.74	0.71	0.02	0.78	0.77	0.77	1.00	0.10	0.91	0.09	0.78	0.00	0.20	1.00	0.00	1.00	0.10	0.10	1.00	0.00
4	1558	'slope'	'-'	0.00	0.75	0.43	0.76	0.67	0.04	0.80	0.75	0.77	0.70	0.20	0.78	0.22	0.80	0.20	0.20	0.83	0.17	1.00	0.10	0.10	0.91	0.09
5	1831	'slope'	'-'	0.00	0.73	0.40	0.72	0.62	0.02	0.73	0.73	0.73	0.80	0.10	0.89	0.11	0.76	0.10	0.10	0.91	0.09	1.00	0.00	0.00	1.00	0.00
6	1790	'slope'	'-'	0.00	0.83	0.41	0.83	0.71	0.05	0.85	0.83	0.84	0.40	0.10	0.80	0.20	0.85	0.10	0.10	0.86	0.14	0.60	0.10	0.10	0.86	0.14
8	420	'shelf'	'-'	0.00	0.75	0.47	0.75	0.70	0.04	0.76	0.75	0.75	0.90	0.10	0.90	0.10	0.77	0.00	0.00	1.00	0.00	0.40	0.00	0.00	1.00	0.00
10	110	'shelf'	'ice'	0.14	0.45	0.38	0.38	0.41	0.00	0.44	0.41	0.53	0.80	0.00	0.10	0.00	0.70	0.10	0.88	1.00	0.00	0.80	0.00	0.00	1.00	0.00
11	150	'shelf'	'ice'	0.59	0.15	0.34	0.19	0.26	0.06	0.15	0.14	0.34	0.00	0.10	1.00	1.00	0.50	0.10	0.00	1.00	0.64	0.40	0.70	0.70	0.36	0.64
12	142	'shelf'	'ice'	0.63	0.03	0.46	0.25	0.21	0.07	0.03	0.03	0.46	0.00	0.90	1.00	1.00	0.18	0.88	0.00	1.00	0.00	0.80	0.00	0.00	1.00	0.00
13	1700	'slope'	'-'	0.08	0.75	0.54	0.74	0.66	0.04	0.77	0.74	0.78	0.50	0.20	0.17	0.29	0.25	0.25	0.25	1.00	0.00	0.76	0.00	0.00	1.00	0.00
14	551	'depression'	'ice'	0.29	0.46	0.42	0.67	0.63	0.16	0.45	0.44	0.76	1.00	0.20	0.29	0.16	0.45	0.20	0.20	0.85	0.11	0.85	0.00	0.00	0.91	0.09
15	1993	'slope'	'ice'	0.01	0.85	0.49	0.85	0.75	0.11	0.86	0.85	0.85	0.70	0.10	0.13	0.11	0.86	0.20	0.20	0.85	0.15	0.78	0.50	0.50	0.90	0.10
16	1608	'slope'	'ice'	0.00	0.78	0.42	0.77	0.62	0.03	0.81	0.78	0.80	1.00	0.30	0.17	0.03	0.80	0.30	0.30	1.00	0.00	0.78	0.00	0.00	1.00	0.00
17	1273	'slope'	'-'	0.00	0.76	0.44	0.74	0.59	0.02	0.78	0.76	0.79	0.70	0.30	0.29	0.02	0.79	0.10	0.10	0.91	0.09	0.76	0.10	0.10	0.91	0.09
18	214	'shelf'	'-'	0.00	0.75	0.43	0.74	0.63	0.03	0.78	0.75	0.77	0.70	0.30	0.70	0.70	0.78	0.10	0.10	0.89	0.11	0.78	0.10	0.10	0.83	0.17
19	1547	'slope'	'-'	0.00	0.54	0.30	0.52	0.41	0.09	0.55	0.54	0.54	0.70	0.00	0.70	1.00	0.54	0.00	0.00	0.75	0.25	0.55	0.00	0.00	1.00	0.00
20	236	'shelf'	'ice'	0.21	0.54	0.50	0.70	0.65	0.04	0.54	0.54	0.75	1.00	0.30	0.77	0.23	0.82	0.20	0.00	0.82	0.18	0.75	0.50	0.50	0.64	0.36

References

Addlington, R.H. (1963). Acoustic Reflection Losses at the Sea Surface Measured with Explosive Sources. Journal of the Acoustical Society of America, 35:1834

Axelrod, E.H., Schoomer, B.A., & Winkle, W.A.V. (1965). Vertical Directionality of Ambient Noise in the Deep Ocean at a Site near Bermuda. Journal of the Acoustical Society of America, 37, 77–83.

Barclay, D.R., & Buckingham, M.J. (2013). Depth dependence of wind-driven, broadband ambient noise in the Philippine Sea. The Journal of the Acoustical Society of America. 133(1):62–71.

Bass, S.J., & Hay, A.E. (1997). Ambient noise in the natural surf zone: Wave-breaking frequencies. IEEE journal of oceanic engineering. 22(3):411–424.

Boyer, T.P., Baranova, O.K., Coleman, C., Garcia, H.E., Grodsky, A., Locarnini, R.A., Mishonov, A.V., Paver, C.R., Reagan, J.R., Seidov, D., Smolyar, I.V., Weathers, K., & Zweng, M.M. (2018): World Ocean Database 2018. A.V. Mishonov, Technical Ed., NOAA Atlas NESDIS 87.

Breemer, J. (1989). Soviet Submarines – Design, Development, and Tactics. Janes Information Group.

Buckingham, M.J. (2005). Compressional and Shear Wave Properties of Marine Sediments: Comparisons between Theory and Data. The Journal of the Acoustical Society of America, 117(1), 137-152.

Buckingham, M.J. (1991). On Acoustic Transmission in Ocean-Surface Waveguides. Philosophical Transactions of the Royal Society of London. Series A: Physical and Engineering Sciences. 335:513–555.

Cameron, G.D.M., & Best, M.A. (1986). Quaternary Geology of the Continental Margin of Eastern Canada: Map 1711A. Energy, Mines, and Resources Canada.

Canadian Armed Forces Maritime Warfare Centre. 2016. Canadian Forces Controlled Document 106 – Anti-Submarine Warfare. Royal Canadian Navy, Canada.

Carey, W.M., & Evans, R.B. (2011). Ocean Ambient Noise: Measurement and Theory. Springer Science & Business Media.

Chapman, N.R., & Price, A. (2011). Low Frequency Deep Ocean Ambient Noise Trend in the Northeast Pacific Ocean. The Journal of the Acoustical Society of America. 129(5): 161-165.

Canada Energy Regulator (CER). (2022). Significant or Commercial Discovery https://www.cer-rec.gc.ca/en/about/north-offshore/significant-commercial-discovery.html

Crouch, W.W., & Burt, P.J. (1972). The Logarithmic Dependence of Surface-Generated Ambient-Sea-Noise Spectrum Level on Wind Speed. The Journal of the Acoustical Society of America, 51(3B), 1066–1072.

Cook, B.E. (2002). Uses of Spatial Audio in Sonar. General Dynamics Canada. 4-13, 18-19.

Dawe, R.L. (1997). Detection Threshold Modelling Explained. Aeronautical and Maritime Research Laboratory. Department of Defense, Commonwealth of Australia.

Deane, G.B., & Stokes, M.D. (2002). Scale dependence of bubble creation mechanisms in breaking waves. Nature. 418:839-844.

Delarue, J., Kowarski, K.A., Maxner, E.E., MacDonnell, J.T., & Martin, S.B. (2018). Acoustic Monitoring Along Canada's East Coast: August 2015 to July 2017. Environmental Studies Research Funds Report Number 215. Dartmouth, Canada.

Department of Fisheries and Oceans (DFO). (2017). American Lobster – Lobster Fishing Area 3 – 14C. https://www.dfo-mpo.gc.ca/fisheries-peches/ifmp-gmp/lobster-homard/area-zone-3-14c-eng.html#toc9

Director General METOC. (1995). Military Oceanography Manual. Royal Canadian Navy, Canada. 94.

Discovery of Sound in the Sea. (2021). WOTAN: Wind Observations Through Ambient Noise.

ERA5. (2022). ERA5 Climate Data Store: Hourly Data on Single Levels From 1959 to Present.

Erbe, C. (2011). JASCO Pocket Handbook, 3rd Edition. JASCO Applied Sciences

Farmer, D.M., & Lemon, D.D. (1984). The Influence of Bubbles on Ambient Noise in the Ocean at High Wind Speeds. Journal of Physical Oceanography. 14(11):1762–1778.

Farmer, D.M., & Vagle, S. (1988). On the Determination of Breaking Surface Wave Distributions Using Ambient Sound. Journal of Geophysical Research. 93, 3591-3600.

Furduev, A.V. (1966). Undersurface Cavitation as a Source of Noise in the Ocean. Proceedings of the USSR Academy of Sciences. Izvestyia Atmospheric and Oceanic Physics., 5:523

Foreign Broadcast Information Service. (1992). Three Days on the Typhoon Submarine. Arms Control – JPRS Report. 16-20.

GEBCO Bathymetric Compilation Group 2021 (2021). The GEBCO 2021 Grid - a continuous terrain model of the global oceans and land. https://www.gebco.net/

Gorbachev, V.N. (1994). The Ability of Submarines to Defend Themselves Against Naval Operations in Coastal Waters. Paper from American-Russian Conference on Anti-Submarine Weaponry in Coastal Waters.

Han, J., Shuai, L., Zhongpeng, W., Mingwei, Z., & Jin, B. (2020). Study on the Measurement of Sound Attenuation Coefficient in Bubble Wake by Pool. Science and Technology on Underwater Test and Control Laboratory. E3S Web of Conferences 206, 03013.

Headquarters Naval Material Command. (1969). Physics of Sound in the Sea. Department of the Navy, United States.

Herstein, P.D. (1984). The Effect of Hydrophone Configuration on the Directivity Index of a Line Array. Naval Underwater Systems Center, New London, CT.

Ingenito, F., & Wolf, S.N. (1989). Site dependence of wind-dominated ambient noise in shallow water. The Journal of the Acoustical Society of America. 85(1):141–145.

Jensen, F.B., Kuperman, W.A., Porter M.B., & Schmidt, H. (2011). Computational ocean acoustics. Springer Science & Business Media.

Kewley, D.J., Browning, D.G., & Carey, W.M. (1990). Low-frequency wind generated noise source levels. The Journal of the Acoustical Society of America, 88(4), 1894–1902.

Knudsen, V. O., Alford, R.S., & Emling, J.W. (1948). Underwater Ambient Noise. Journal of Marine Research. 7:410.

Kuperman, W.A., & Ferla, M.C. (1985). A shallow water experiment to determine the source spectrum level of wind-generated noise. The Journal of the Acoustical Society of America. 77(6):2067–2073.

Lin, S., & Sheng J. (2020). Revisiting Dependences of the Drag Coefficient at the Sea Surface on Wind Speed and Sea State. Continental Shelf Research.

McDonald, M.A., Hildebrand, J.A., & Wiggins, S.M. (2006). Increases in deep ocean ambient noise in the Northeast Pacific west of San Nicolas Island, California. The Journal of the Acoustical Society of America. 120(2): 711–718.

Merchant, N., Fristrup, K., Johnson, M., Tyack, P., Witt, M., Blondel, P., & Parks, S. (2014). Measuring acoustic habitats. Methods in Ecology and Evolution. 6. 10.1111/2041-210X.12330.

Miasnikov, E. (1994). Can Russian Strategic Submarines Survive at Sea? The Fundamental Limits of Passive Acoustics. Science and Global Security 4: 213-251.

Miasnikov, E. (1995). What is Known About the Character of Noise Created by Submarines? The Future of Russia's Strategic Nuclear Forces. Center For Arms Control, Energy, and Environmental Studies. Moscow Technical Physical Institute.

Morris, G.B. (1978). Depth Dependence of Ambient Noise in the Northeastern Pacific Ocean. The Journal of the Acoustical Society of America. 64: 581–590.

National Research Council (US) Committee on Potential Impacts of Ambient Noise in the Ocean on Marine Mammals. (2003). Introduction. Ocean Noise and Marine Mammals. Academies Press (US).

Miksis-Olds, J.L., & Nichols, S.M. (2016). Is low frequency ocean sound increasing globally? The Journal of the Acoustical Society of America. 139(1):501–511.

Osler, J.C. (1994). A Geo-Acoustic and Oceanographic Description of Several Shallow Water Experimental Sites on the Scotian Shelf. Defense Research Establishment Atlantic.

Payne, C. (2010). Principles of Naval Weapons Systems. United States Naval Institute Blue and Gold Professional Library.

Pennington, N.J., & Weller, R.A. (1986). FASINEX Frontal Air-Sea Interaction Experiment (January-June 1986): summaries for FASINEX mooring cruises; phase one: R/V KNORR Cruise 119, phase three: RV/KNORR Cruise 123. Woods Hole Oceanographic Institution.

Piggott, C.L. (1965). Ambient Sea Noise at Noise Frequencies in Shallow Water of the Scotian Shelf. The Journal of the Acoustical Society of America. 36:2152.

Porter, M.B. (2011). The BELLHOP Manual and User's Guide.

Prosperetti, A. (1988). Bubble-Related Ambient Noise in the Ocean. The Journal of the Acoustical Society of America 84.3: 1042–1054.

Robinson, C. (2020). Modelling the Coastal Ambient Noise Field in Time, Frequency, and Space. Dalhousie University.

Schmidt, H., & Kuperman, W.A. (1988). Estimation of Surface Noise Source Level From Low Frequency Seismoacoustic Ambient Noise Measurements. The Journal of the Acoustical Society of America. 84: 2153-2162.

Shooter, J.A., & Gentry, M.L. (1981). Wind generated noise in the Parece Vela Basin. Journal of the Acoustical Society of America, 70, 1757-1761.

Stoecker, S.W. (1983). Life Aboard a Soviet Destroyer and a Soviet Submarine. The Rand Corporation.

Urick, R., & Kuperman, W.A. (1984). Ambient noise in the sea. Undersea Warfare Technology Office, Naval Sea Systems Command. Department of the Navy, United States.

Urick, R., & Saxton, H.L. (1947). Surface Reflection of Short Supersonic Pulses in the Ocean. Journal of the Acoustical Society of America, 19:8.

Urick, R. (1983). Principles of Underwater Sound. Peninsula Publishing.

Vagle, S., Large, W.G., & Farmer, D.M. (1990). An Evaluation of the WOTAN Technique of Inferring Oceanic Winds from Underwater Ambient Sound. Journal of Atmospheric and Oceanic Technology 7.

Vego, M. (1983). Submarines in Soviet ASW Doctrine and Tactics. Naval War College Review 36(2).

Wenz, G.M. (1962). Acoustic ambient noise in the ocean: Spectra and sources. The Journal of the Acoustical Society of America, 34(12), 1936-1956.

Wilson, J.H. (1983). Wind Generated Noise Modeling. The Journal of the Acoustical Society of America. 73:211-216.